2010

1-Alkyl-3-Methylimidazolium bis(trifluoromethylsulfonyl)imide Based Ionic Liquids: A Study of Their Physical and Electrochemical Properties

Charles William Dutton
Wright State University

1-ALKYL-3-METHYLIMIDAZOLIUM BIS(TRIFLUOROMETHYLSULFONYL)IMIDE BASED IONIC LIQUIDS: A STUDY OF THEIR PHYSICAL AND ELECTROCHEMICAL PROPERTIES

A thesis submitted in partial fulfillment

of the requirements of the degree of

Master of Science

By

Charles William Dutton

B.S. Wright State University, 2007

2010

Wright State University

WRIGHT STATE UNIVERSITY

SCHOOL OF GRADUATE STUDIES

June 9, 2010

I HEREBY RECOMMEND THAT THE THESIS PREPARED UNDER MY SUPERVISION BY Charles William Dutton ENTITLED 1-Alkyl-3-Methylimidazolium bis(trifluoromethyl-sulfonyl)imide Based Ionic Liquids: A Study of Their Physical and Electrochemical Properties BE ACCEPTED IN PARTIAL FULFILLMENT OF THE REQUIREMENTS FOR THE DEGREE OF Master of Science.

Vladimir Katovic, Ph.D.
Thesis Director

Kenneth Turnbull, Ph.D.
Department Chair

Committee on Final Examination

Vladimir Katovic, Ph.D.

William A. Feld, Ph.D.

David A. Grossie, Ph.D.

John A. Bantle, Ph.D.
Vice President for Research and
Graduate Studies and Interim Dean of
Graduate Studies

ABSTRACT

Dutton, Charles William. M.S., Department of Chemistry, Wright State University, 2010. 1-Alkyl-3-Methylimidazolium bis(trifluoromethyl-sulfonyl)imide Based Ionic Liquids: A Study of Their Physical and Electrochemical Properties.

Ionic liquids are of interest because of their electrochemical and thermal properties and their possible use as electrolytes in batteries. In this work five ionic liquids were synthesized. They consisted of a 1-alkyl-3-methylimidazolium (RMI^+) cation, where the alkyl group was ethyl, propyl, butyl, pentyl, or hexyl, and a bis(tri-fluoromethylsulfonyl)imide (NTf_2^-)anion. The decomposition temperatures, melting points, conductivities, viscosities, densities, absorption and desorption of water, diffusion coefficients, and electrochemical properties were studied. It was found that these ionic liquids were thermally stable up to ~310 ˚C, and that $EMINTf_2$ had a melting point at -18.26 ˚C. Conductivities decreased with increasing alkyl chain length on the imidazolium cation. The densities decreased with increasing chain length and with increasing temperature. Viscosities decreased with increasing temperature but increased with increasing alkyl chain length. Ionic liquids with longer alkyl chains absorbed less water from the atmosphere. The diffusion coefficient of ferrocene in ionic liquids decreased with increasing alkyl chain length. Electrochemical windows increased with increasing chain length, but decreased with an increase in water content. Comparisons of physicochemical and electrochemical properties of $RMINTf_2$

ionic liquids were made with previously studied and analogous ionic liquids containing (RMI^+) cation and the bis(pentafluoroethylsulfonyl)imide ($Beti^-$) anion.

TABLE OF CONTENTS

Page

LIST OF FIGURES

Figure Page

LIST OF TABLES

DEDICATION

To my wife, Lisa. Thank you for your patience.

ACKNOWLEDGEMENTS

I would like to thank Dr. Katovic for his guidance and patience as my advisor. I especially want to thank him for the many group meetings over coffee. They were appreciated. I am thankful to have been your student.

I also want to thank Dr. Katovic's research group: Jen Decerbo, Ashley Topper, Ed Kennedy, Jodie Shoaf, Charles Woods, Kenny Whigham, Amanda Lear, Sandra Felix-Balderama, Matt Jacobs and Tracey Harris. It was fun working with all of you.

I would like to thank Dr. Mike May and Dr. Beth Paul for being sounding boards on the weekends. I learned a lot about perspectives of science and chemistry from both of you.

I would like to thank Dr. Fossum for the instruction and use of the differential scanning calorimeter.

Finally I would like to thank Dr. Feld and Dr. Grossie for their assistance in helping me successfully complete my thesis

I. INTRODUCTON

The term “ionic liquid” generally refers to salts in their liquid state. In recent years the term “ionic liquid” often refers to salts that remain liquid below 100 ^{o}C and are composed of an organic cation and an inorganic anion.[1,2] Room-temperature ionic liquids (RTILs) are, as their name suggests, liquid at room temperature. These substances are of great interest because of their very favorable physical, chemical, and electrochemical properties. They typically have very low vapor pressures and fairly large electrochemical windows. Many ionic liquids have a large liquid temperature range; remaining liquid below water’s freezing point and are thermally stable above 300 ^{o}C. Applications of these liquids range from use as reusable solvents for various reactions (organic, enzymatic) and for use as solvents in electrochemistry and in electrical storage units such as in batteries, fuel cells, and capacitors. Over the past 20 years, interest in ionic liquids has grown significantly. In fact, the number of yearly publications on ionic liquids has grown exponentially since the late 1990s.[1] There is an increasing amount of research being conducted on ionic liquids’ properties and possible practical uses, and the number of possible ionic liquids to explore is essentially limitless

Molten Salts

The precursors to modern ionic liquids are the melts of inorganic salts, such as sodium chloride and potassium chloride, which melt at 801 and 776 ^{o}C, respectively. The term that is used for these generally high-temperature kinds of liquids is molten salts. Molten salts have use because of their thermal stability; generally they do not thermally degrade and are nonvolatile. Because of their large electrochemical windows and extremely high conductivity, they have been used in thermal batteries.[3] Molten salts are often used as nonaqueous solvents. The behavior of liquid water, with its bonding and clathrate formations, is still difficult to understand completely. Kinetics in pure molten salts is also much faster than in aqueous solutions. Theories that work on salts as solutes, because this is a situation of high dilution, cannot normally be applied to situations that occur in biology, geology and industry, where the aqueous solutions are used.[4] Simple, unsolvated anions and cations in their liquid state, such as they occur in molten salts, are much simpler systems for studying physical properties of dissolved species. For example, Davy and Faraday used molten metal halides to verify the Laws of Electrolysis.[4]

Typical drawbacks of molten salts are that they need very high temperatures to operate. This makes their use costly in terms of energy consumption. Molten salts also typically possess corrosive behavior. Mixtures of two molten salts, or melts, have lower melting temperatures than their component salts. These are often used at their eutectic mixtures. Examples are given in Table 1.

Table 1. Eutectic melts of various salts and their melting points[4]

Melt	m.p. (°C)
$KCl:NaCl:AlCl_3$	89
$LiCl:KCl:NaCl:AlCl_3$	61
$AlBr_3:RbBr$	83
$NaNO_3:NH_4NO_3:LiNO_3$	80.5
$LiNO_3:NH_4NO_3$	90
$LiNO_2:KNO_2$	99
$Ca(NO_3)_2 \cdot 4H_2O:CaCl_2 \cdot H_2O$	<15

Ionic Liquids

The term "ionic liquid" is used to describe salts that melt below 100 ˚C, or salts with a melting temperature below that of water.[1] Ethylammonium nitrate, which has a melting point at 12 °C, is considered by some to be the first known RTIL. It was discovered by Paul Walden in 1914.[5] Ethanolammonium nitrate, which begins to melts at 52 °C, was known as early as 1888.

Another documented substance recognized as an ionic liquid were the salts with the heptachlorodialuminate anions.[6] They are known as "red oil" and often appear during $AlCl_3$ catalyzed Friedal-Crafts reactions. First observed in the mid-19th century, "red oil" appears to contain an aromatic intermediate cation and an unregenerated catalyst anion combining into a separate phase. The actual structure was not determined until

NMR spectroscopy became available (Figure 1). Numerous variations of these "red oil" salts have been documented.

There are other variations of ionic liquids which were known about in the 20th century, but these were generally unrelated in discovery and use.

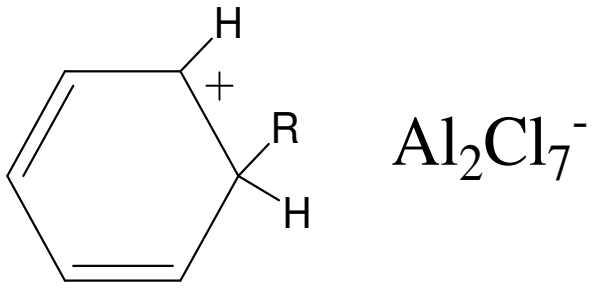

Figure 1. Generic structure of "Red Oil"

Chloroaluminates

It was the research into haloaluminates, specifically chloroaluminate molten salts, that led to today's explosion in interest in ionic liquids. Research in this area was spearheaded by Major (Dr.) Lowell A. King.[1] King was a researcher at the U.S. Air Force Acadamy in the 1960s and his original goal was to find a replacement for the LiCl-KCl melt electrolyte in thermal batteries. The LiCl-KCl mixture has a eutectic melting temperature at 355 ^{o}C. This high temperature was causing internal battery problems. The chloroaluminates, which are composed of alkali salts and aluminum chloride, are molten salts which have relatively low melting temperatures compared to other melts.

The NaCl- $AlCl_3$ melt in particular has a melting point at 107 ^oC when mixed at the eutectic, and has been used as electrolyte in thermal batteries.[1,6]

Chloroaluminates are also of interest because of their acid/base "tunability". The chemical properties, and their use, can be changed depending on the NaCl:$AlCl_3$ ratio. One could make the liquid more acidic, neutral, or basic by altering the following equilibrium:[1]

$$Cl^- + AlCl_3 \rightarrow [AlCl_4]^- + AlCl_3 \rightarrow [AlCl_7]^-$$

Researchers at the Air Force academy, while searching for a new electrolyte to be used with an aluminum anode, found (1948 patent in the aluminum electroplating field) that $AlCl_3$ with 1-ethylpyridinium halide gives a liquid salt 1-ethylpyridinium$^+$ AlCl4$^-$.[1] In 1951, Frank H. Hurley and Thomas P. Wier Jr. of The Rice Institute in Houston, Texas, had reported that $AlCl_3$ / ethylpyridinium bromide (EtPyBr) forms melts at various temperatures depending on composition. They found eutectic melts at the approximately 1:2 and 2:1 composition ratios. These had melting points of 45 ^oC and -40 ^oC respectively.[7] However, alkylpyridinium cations are relatively easy to reduce. The alkylpyridinium cation is shown in Figure 4.

The Dialkylimidazolium Cation

In the search to find a cation that is not as easily reduced as alkylpyridinium ion, the imidazolium salts come into the picture. Although the imidazolium iodide salts were

known in Germany in the 1880s, imidazolium cations came into modern focus thanks to a new computational method (in the late 1970s), Modified Neglect of Differential Overlap (MNDO). This method helped avoid the longer, more painstaking *ab initio* methods of calculations and narrowed down large numbers of possible molecules of interest to a few in a faster, more cost effective way. In 1979, John S. Wilkes and Charles Hussey estimated that the energy of the highest occupied molecular orbital (HOMO) would correspond to the oxidation potential of a molecule, and that the lowest occupied molecular orbital (LUMO) energy would correspond to the reduction potential. This method eventually directed them to the 1,3-dialkylimidazolium cation which was predicted to have a 0.9 V more negative reduction potential than the alkylpyridinium cation.[6,8] An example of a 1,3 dialkyimidazolium cation is shown in Figure 2.

Ionic liquids such as Ethylmethylimidazolium tetrachloroaluminate, [EMIM]Cl-$AlCl_3$, among others, were found to be useful as electrolytes in batteries and as solvents in organic reactions such Friedal-Crafts chemistry.[1]

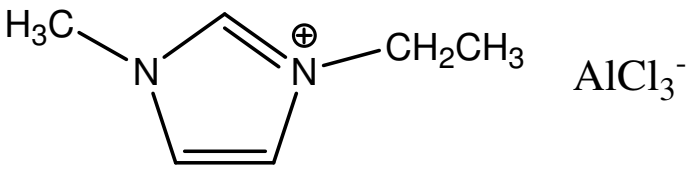

Figure 2. Ethylmethylimidazolium tetrachloroaluminate, [EMIM]Cl-$AlCl_3$

Water Stable Anions

A disadvantage of using chloroaluminates as an anion is its reactivity with water. In 1990 Mike Zaworotko, while on sabbatical leave from The University of St. Mary's, Halifax, began investigating combining dialkylimidazolium cations with water stable anions. This work was done at the U.S. Air Force Academy and his simple idea led to imidazolium based ionic liquids paired with anions which included tetrafluoroborate, hexafluorophosphate, nitrate, sulfate, and acetate salts. In the following years Joan Fuller continued this idea by trying new anions. She also varied the cation by trying different mono- and tri-alkylimidazoliums.[1] One could easily suggest varying the length and structure of the alkyl groups on the cations. Thus, the possible number of room-temperature ionic liquids to be investigated has grown indefinitely, with estimates however, that there could be around 10^{18} possilbe ionic liquids.[2] See the following figures for examples of cations and anions used to make ionic liquids.

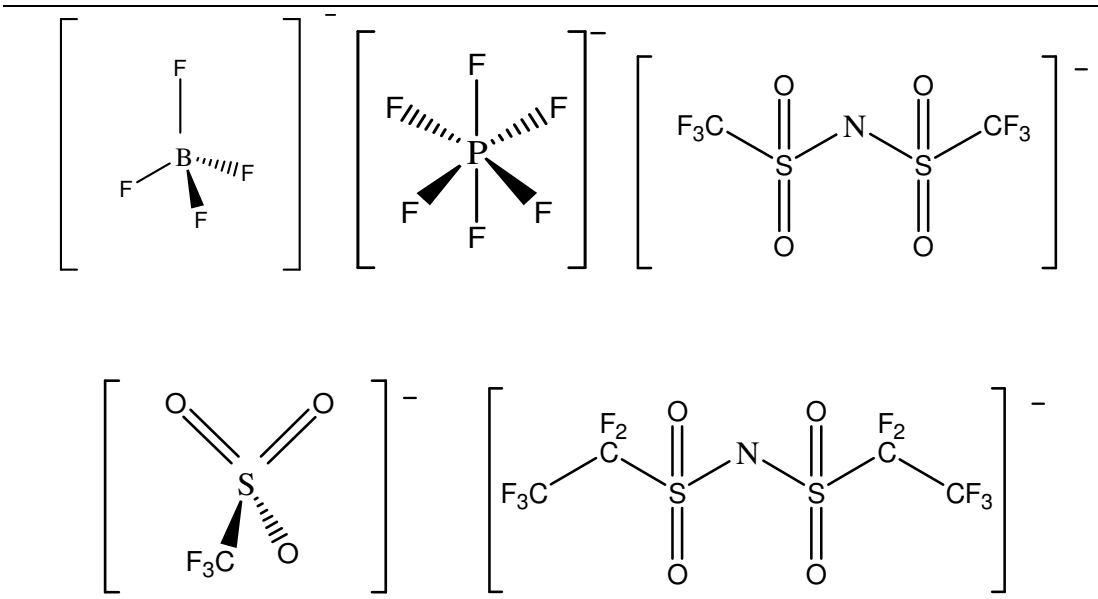

Figure 3. Typical anions used to form ionic liquids

First Row: Tetrafluoroborate, hexafluorophosphate, bis(trifluoromethanesulfonyl)-imide (NTf_2

)Second Row: Trifluoromethane sulffonate (triflate), bis(pentafluoroethanesulfonyl)-imide (Beti)

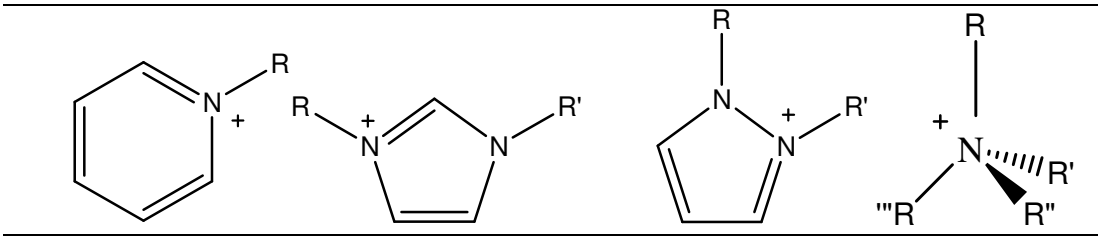

Figure 4. Typical cations used to form ionic liquids

Left to Right: Pyridinium (Pyr), Imidazolium (Im), pyrazolium, ammonium

Properties of 1-Alkyl-3-Methylimidazolium Based Ionic Liquids

Thermal Properties

Typical ionic liquids melt below 100 ˚C and some as low as -100 ˚C.[1] The melting point of a salt is determined by at least two principles; how the molecules are arranged into

a crystal lattice and any disordering mechanisms available to the molecules.[9] The electrostatic forces of the ions dictate that each ion is surrounded by ions of the opposite charge. In the case of sodium chloride, NaCl, there is a simple solution that is shown in the Figure 5.

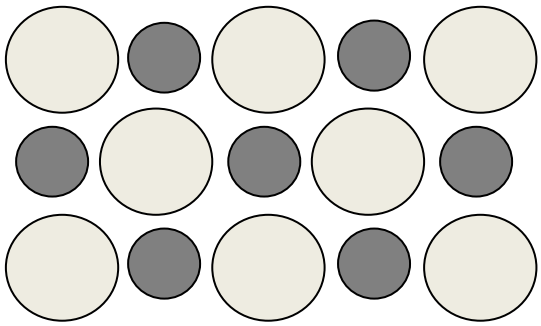

Figure 5. Representation of the crystal structure of NaCl. The larger spheres representing the chloride anions and the smaller spheres representing the sodium cations.

Not all molecules can form a simple lattice structure easily. Complexities arise due to steric effects and repulsive or attractive forces such as hydrogen bonding and Coulumbic forces. Each of these have effects on the lattice energy. In the case of 1,3-alkylimidazolium ionic liquids, a more asymmetrical cation makes orderly stacking more difficult. Longer alkyl chains increase the portion of the molecule that is uncharged. This can result in layers in the crystal structure, with the alkyl chains interdigitating and the charged portions of the molecules clustering together.[9] As an example a schematic can be seen in Figure 6.

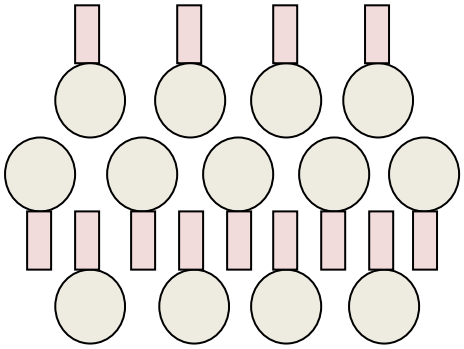

Figure 6. Simple schematic of layers that form in ionic liquids. The rectangles represent the lipid-like alkyl chains, and the circles represent the charged cation-anion clusters.

The electrostatic, or Coulombic attraction between the ions follow the equation:

$$E_c = \frac{M\, Z^+\, Z^-}{4\pi\varepsilon_\circ r}$$

It can be seen that the ion charges (Z^+,Z^-) affect ion attraction, and that a charge ratio of 1:1 between cation and anion is desirable for low melting points. Those ions which are bulky, or effectively increase ion separation, r, also help reduce the melting point. M is the Madelung constant and ε_o is the electric constant.

Experimentally determining melting points of ionic liquids sometimes can be difficult. A common method for the determination of the melting point of ionic liquids is differential scanning calorimetry (DSC). As has been previously shown, the thermal behavior of ionic liquids is somewhat complex. When cooling from the liquid state very often ionic liquids supercool and form a glass, making it difficult to find the freezing/melting point. Glass transition states, T_g, for 1,3-alkylimidazolium ionic liquids

are between -70 to -90 °C. Because data collected on cooling represent kinetic complexities, thermal transition data should be collected upon reheating.[1]

Imidazolium ionic liquids are generally nonvolatile. At high temperatures, a typical inorganic molten salt will vaporize in the form of ion pairs. The ions in ionic liquids however, cannot form as tightly bound pairs, and thus they tend to remain in their liquid state until they reach a temperature that induces thermal decomposition. Being organic, 1,3-alkylimidazolium based ionic liquids typically decompose via pyrolysis, and this is believed to begin at 250 ^{o}C.[1]

Density and Viscosity

Ionic liquids are fluids which behave in a Newtonian manner with viscosities like those of oils.[5] Factors which affect viscosity include impurities, temperature, alkyl chain length, alkyl chain branching, hydrogen bonding and Van der Waals forces. An interesting point is that increasing alkyl chain length on the imidazolium cation does not always increase viscosity. This could be because alkyl groups disrupt hydrogen bonding. On the anion, using fluorinated compounds helps delocalize the negative charge and thus reduce hydrogen bonding with the cation.[10]

The density of ionic liquids is generally the most stable physical property when compared at different temperatures and levels of impurities.[1] Imidazolium based ionic liquids generally have densities between one and two gm/cm^3. Densities

decrease with increasing alkyl chain length on the imidazolium cation.[2,5] Increasing the mass of the anion increases the density.[1]

Electrochemical Properties

The electrochemical properties of ionic liquids are of primary interest because of their possible uses in electrochemical systems such as batteries, fuel cells, capacitors and solar cells. Because of their wide electrochemical window and ability to solvate metal complexes, they are also used as solvents for metal complex studies.[1]

Typical electrochemical windows for ionic liquids range from 3-6 volts. When considering an electrochemical window, the cation and the anion are the limiting factors. The type of working electrode used in measuring the electrochemical window is also important when considering the points at which oxidation or reduction occurs. Platinum and glassy carbon electrodes typically give cathodic and anodic potentials that differ by a fraction of a volt. The widths of the windows, however, remain the same. Platinum is also more sensitive to water impurity, and will show this in a typical cyclic voltammogram. Glassy carbon electrode shows no background current due to trace water.[1] Other impurities, such as trace chlorides that were not removed during ionic liquid synthesis, can significantly affect the observed oxidation current. Electrochemical windows of pertinent ionic liquids on glassy carbon and platinum electrodes are listed in Table 2. These are values for neat or nearly neat materials. Impurities such as increasing amounts of water reduce the electrochemical window.

For a RTIL, the oxidation potential is determined by the anion and the reduction potential is determined by the cation. Ideally, a good RTIL can be cycled between the two potentials without any degradation effects.

Table 2. Electrochemical windows for various ionic liquids.

Ionic Liquid	Total Window (volts)	Source
$EMPBF_4$	4.1	11
$EMIBF_4$	4.2	11
$EMPCF_3SO_3$	4.3	11
$BMIPF_6$	5.0	12
EMIBeti	4.2	13
PMIBeti	4.5	13
BMIBeti	4.5	13
PnMIBeti	4.6	13
HMIBeti	4.7	13

Conductivities of RTILs are typically in the the range of 1 – 20 mS/cm at room temperature, less than typical aqueous electrolyte. This is due to the fact that the ions are large, and may pair up or aggregate. Walden Plot data has shown that ionic liquid conductivity is strongly affected by viscosity.[1] Thus any reduction in viscosity helps increase the conductivity. Ionic liquid density, formula weight, and the radius of the cation and anion are also inherent factors. Impurities have been shown to greatly affect viscosity. Water in particular, even in small amounts, has a great effect on conductivity.[14]

Transport Properties

The diffusion coefficient can be greatly affected by dissolved gases such as CO_2 and argon. Nitrogen does not appear to have any significant effect on the physical properties of ionic liquids.[15] Most mobile charge in imidazolium based ionic liquids is believed to be carried by the cations.[16] One can see factors that affect diffusion, D, from the Stokes-Einstein equation.

$$D = \frac{kT}{c\pi\eta r}$$

Where k is Boltzman's constant, T is absolute temperature, c is a constant, η is viscosity, and r is hydrodynamic radius of the species. For dialkylimidazolium cation hydrodynamic radius is smaller than the anionic for both the BF_4 and NTf_2 anions.[16] It was demonstrated by Akihiro Noda et al, that the cations diffuse easier than the mentioned anions. This is shown in Figure 7.

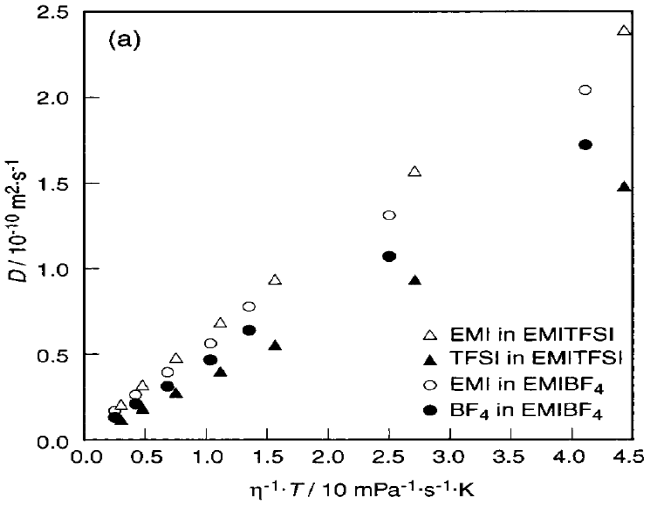

Figure 7. Plot reported by Akihiro Noda et al. showing that the EMI cation has a higher diffusion coefficient than the BF_4^- or NTf_2^- anion (TFSI in the chart).

Other factors that may affect the dialkylimidazium's diffusion ability is its planar structure and the anions pairing ability. NTf_2^- forms more ion pairs with the dialkylimidazolium cation than BF_4^-. These in turn dilute the ion concentration, which reduces Coulumbic interactions between the ions and their environment. This is believed to reduce the viscosity, and thus increase the ionic diffusion coefficient. Unfortunately, the ionic pairs and aggregates do not contribute to conduction, and therefore the ionic conductivity is negatively impacted.

Solvent Interactions

It is apparent that ionic liquids could be considered polar molecules. Measuring the polarity, or dielectric constant, of ionic liquids is difficult due to the fact they are salts.[1] There are both anions and cations present and each interacts with several neighbors. An ionic liquid can therefore be similar to an aqueous solvent or an organic solvent. Being rather cumbersome ions, ionic liquids are also weakly coordinating. Properties such as hydrophobicity or lipophilicity can be altered by changing out cation or anion or altering alkyl chain lengths.

It has been proposed that water absorbed from the atmosphere coordinates mainly with the anion in imidazolium based ionic liquids. Spectral studies using Fourier-transform infrared spectroscopy (FTIR) have led to the conclusion that the anions hydrogen bond with the water in an anion– H-O-H –anion manner.[17] The cations do play some factor in water coordination but not as significant. Changing the alkyl group

on the cation can cause an ionic liquid to change from being soluble in water to insoluble.[5]

The unique solvent properties of ionic liquids and the fact they can be used in biphasic systems make them candidates for extractions, electrochemical studies of complexes, analytical techniques such as chromatography, and for solvents in synthesis reactions. One interesting example reported by Hiroyuki Ohno et al. is the use of an ionic liquid to extract cytochrome c, a redox reactive heme protein, from an aqueous solution. The ionic liquid was poured on top of the aqueous solution containing the protein, resulting in a two phase system with the water phase on the bottom. The system was then cooled to 20 °C from 25 °C, where the system became a single phase. Reheating the system to 25 °C resulted in the ionic liquid on the bottom, water on the top, and the cytohrome c nearly entirely in the ionic liquid. This was done without stirring, and there was little risk of denaturing the protein.[18] Experiments like these suggest the use of ionic liquids for the use of extracting enzyme products from the same solution as the enzymes and reactants, harvesting the desired product and leaving the enzymes for future use.

The properties of ionic liquids can be used to sequester heavy metals from water. If the ionic liquid is designed to separate into a separate phase from the water, the heavy metals will be extracted and the water will be cleaned of these pollutants.[19] Thus it can be seen that RTILs have numerous possible uses.

Batteries

In this age of seeking out renewable energy sources, one such option is the use of rechargeable batteries. Lithium-ion batteries are popular candidates for energy storage. A simple schematic of a lithium-ion battery is shown in Figure 8.

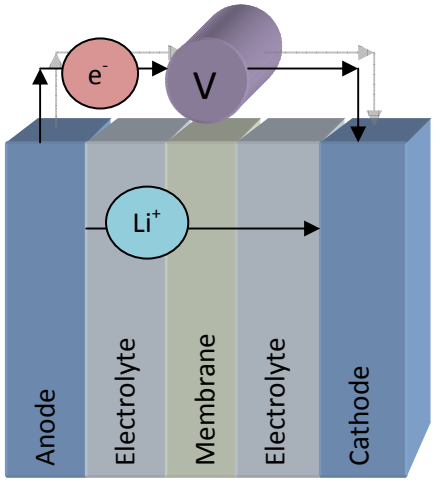

Figure 8. Simple schematic of a lithium-ion battery.

A lithium ion battery uses intercalated lithium instead of solid lithium, and most importantly is a secondary cell. During cell discharge lithium ions travel out of the anode and are deposited in the cathode. Typically a carbon structure is used as the cathode or anode to support the lithium atoms or ions. These intercalating materials nullify the problems that were associated with using lithium metal in the battery. It is the supporting electrolyte which the lithium ions travel through that are another

limiting factor of battery capacity. Imidazolim based ionic liquids are considered strong candidates for being used in lithium-ion batteries as the electrolyte.[20]

Water cannot be used in the electrolyte solution since lithium will react to form lithium hydroxide and hydrogen gas. These conditions will occasionally lead to explosions and therefore a solvent with a wider electrochemical window is used. A general example of a solvent would be a mixture of various organic carbonates. In the 1990s, compounds such as propylene carbonate, diethyl carbonate, ethylene carbonate, and γ–butyrolacetone were used as electrolytes in lithium-ion batteries. In 2000, fluorobenzene was experimented with as an electrolyte. Other fluorinated compounds followed. The high resistivities of fluorinated compounds have made them important elements in the design of lithium ion batteries. The most common electrolytes include $LiPF_6$, $LiBF_4$, Li bis-pentafluoroethanesulfonyl imide and lithium bis-trifluoromethansesulfonyl imide.[21] The anions in these compounds are also poorly coordinating. Still, due to their low thermal stability, low flash point, and high volatility there is potential for battery swelling or even ignition.[22] Imidazolium based ionic liquids have high thermal and electrochemical stabilities, are non-volatile and nonflammable.

II. EXPERIMENTAL

Materials

Lithium bis(trifluoromethanesulfonyl)-imide was obtained from 3M Corporation and used as received. N-methylimidazole (99+%) was purchased from Aldrich Chemical Company, Inc. and was distilled under vacuum at 100 mmHg at 100 ˚C for further purification. 1-Chloroethane gas (99.7%), 1-chloropropane (98%), 1-chlorobutane (anhydrous, 99.5%), 1-chloropentane (99%), and 1-chlorohexane (99%) were also purchased from Aldrich Chemical Company. Acetonitrile-d_3, 100% was purchased from Alfa Aesar, (Stock # 42266, Lot # L08T029) and used as received. The viscosity standard used to calibrate the viscometers was a Certified Viscosity Reference Standard, N100 (lot #08301), which was obtained from Canon Instrument Company.

Instrumentation and Characterization

Nuclear Magnetic Resonance Spectroscopy

Nuclear magnetic resonance (NMR) spectra were obtained using a Bruker 300 MHz NMR**.** Both ^{1}H and ^{13}C carbon spectra were collected at 16 scans and 500 scans respectively. The samples were run using 40 to 60 mg of sample in deuterated acetonitrile as a solvent. Trace amounts of acetonitrile are seen in the carbon NMR spectra. Acetonitrile carbon peaks are typically a singlet at δ 118.26 and a septuplet at δ 1.79.[25] NMR tubes were purchased from Ace® Glass Inc., and had a 5

millimeter diameter and were seven inches long. The spectra are shown in the appendix.

Infrared Spectroscopy

Infrared Spectra (IR) were obtained using a Mattson Genesis II FT-IR spectrometer (model number 960M0000). The software used to interpret spectra was Omnic Version 7.3 (Thermo Electron Corporation). Samples were scanned 16 times and were background subtracted. The resolution was 4 cm^{-1}. Liquid samples were pressed between two NaCl plates. A 0.05 mm Teflon® spacer was used obtain a consistent path length. The spacer width was confirmed by observing the etalons which arose when no sample was pressed between the plates with the spacer.

Determination of Water

A Denver Instruments Coulometric Karl Fischer Titrator, Model 260 was used for measuring the water content of ionic liquids in parts per million. Calibration was done using Hydranal Water Standards from Sigma-Aldrich. Concentrations of 1000 ppm (1.00 mg H_2O per gram at 20 ˚C) and 100 ppm (0.10 mg H_2O per gram) were used, Lot #s 81440 and 72850 respectively. Sample sizes ranged from 30-50 µL. Injections of samples were done using a glass syringe with a stainless steel needle and Teflon® plunger. Syringe, plunger, and needle were cleaned with acetonitrile and stored in an oven at 70-80 °C at atmospheric pressure prior to use.

Absorption and Desorption of Water

A polymer glove box was used in studying absorption and desorption of water by ionic liquids at room temperature. An Electro Tech Systems (ETS) Automatic Humidity Controller (Model 514) was used to control the humidity. Drierite and phosphorous pentoxide were used to absorb excess humidity. Sample sizes ranging from 2-10 mL were used. Ionic liquid samples were placed in glass vials inside the glove box at 60% relative humidity (RH). The water content of the ionic liquids was measured at various time intervals. Once saturation of water was achieved, water desorption was studied in the same manner at 6% RH. Samples were not stirred while conducting the absorption and desorption measurements in glove box but were stirred prior to water content measurements.

Determination of Water Saturation Level

Samples of ionic liquids were immersed in 18 MΩ water and stirred for several days or weeks. Sample sizes ranged from 10 – 20 mL. Samples were measured for water content to find saturation level.

Density

The density of ionic liquids was determined using a Guy-Lussac type specific gravity bottle made by Ace® Glass. The milliliter bottle capped with the $7/12 capillary stopper was calibrated using degassed de-ionized water at a system temperature of 24.65 °C. The density of the water at that temperature is 0.99655

g/mL. Through use of an analytical balance the volume of the capped capillary bottle (including the capillary) was found to be 1.467 mL. The density was determined as various temperatures using a stirred water bath which was kept at a constant temperature. The apparatus was allowed to come to thermal equilibrium for 15 minutes before measurements were taken.

Viscosity

The kinematic viscosity of ionic liquids were taken at 20, 30, 40, and 50 ˚C using a Cannon-Fenske Routine 300 glass viscometer with a viscometer constant of 0.3974 mm^2/s^2.

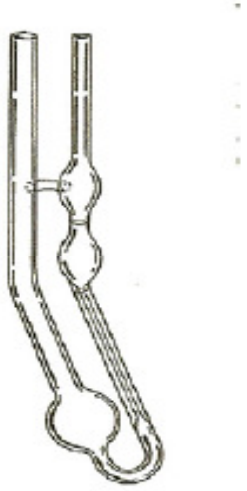

Figure 9. Cannon-Fenske Routine glass viscometer

A stirred water bath kept at a constant temperature was used to keep ionic liquids at a constant temperature for viscosity measurements. The viscometer with ionic liquid inside was immersed in the water bath for at least 15 minutes to allow for thermal

equilibrium before measurements were taken. The viscometer was held in the water bath as long as possible during measurements to avoid cooling when exposed to the air.

The calibration of the viscometer was done using the water bath at 20 ˚C. The Certified Viscosity Reference Standard, N100 (lot #08301), was used. The kinematic viscosity of the reference standard was 315.7 mm^2/sec. The viscometer constant was calculated by dividing the given kinematic viscosity of the reference standard by the time the reference standard oil took to pass two reference points in the viscometer. Measured times and the calculated viscometer constant are given below.

Table 3: Calculation of viscometer constant

Time (sec)	Kinematic viscosity (mm^2/sec)	Calculated Viscometer Constant (mm^2/sec^2)
795.50	315.7	0.3969
795.34	315.7	0.3969
793.28	315.7	0.3980
791.62	315.7	0.3988
796.50	315.7	0.3964
	Average	0.397
	Standard Deviation	±0.001

Kinematic viscosity was calculated by multiplying the measured time by the viscometer constant.

Example: 45.25 sec x 0.3974 mm^2/sec^2 = 17.98 mm^2/sec

The absolute viscosity was then calculated by multiplying the kinematic viscosity by the density.

Thermal Gravimetric Analysis

Thermal gravimetric analysis of the ionic liquids was done using a Perkin Elmer 7 Series Thermal Analysis System. The analysis was done under nitrogen gas from 30 ˚C to 500 ˚C at a heating rate of 10 ˚C /min. Sample sizes ranged from 5-10 mg.

Differential Scanning Calorimetry

Differential Scanning Calorimetry was run on all samples using a Q-200 (TA Instruments). Temperatures were decreased by rate of 5 ˚C per minute to -85 ˚C and allowed to equilibrate for five to ten minutes. The ramp was then set for 10 ˚C per minute to 0.0˚C.

Various methods were also employed in an attempt to find a melting point for most of the RTILs, however, none were successful.

Conductivity

The conductivity of the ionic liquids was measured using an Oakton Conductivity Meter, model WD-35607-10 and glass MI-915 conductivity electrode manufactured by Microelectrodes, Inc. The electrode was inserted into a glass tube where 0.5 – 1.5 mL of ionic was added. The tube was sealed to the electrode using tape. This apparatus was then set into a stirred oil bath where it could come to thermal equilibrium at various temperatures before measurements were taken. Temperatures ranged from 15 – 200 ˚C.

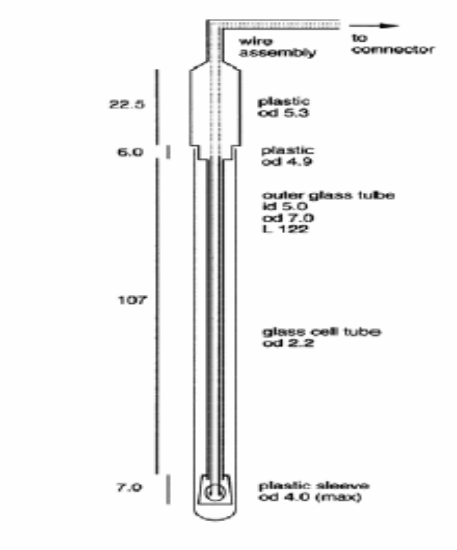

Figure 10. Diagram of conductivity electrode in a glass tube

The cell constant for the electrode was determined using aqueous potassium chloride solution. Concentrations of KCl solutions ranged from 0.01 M to 0.1 M. Each solution

was measured at least three times, with different concentrations being measured at random. The results are shown in Table 4.

Table 4. Conductivity data of KCl standards used for determination of the cell constant

[KCl]	T, Celsius	mS	Kappa (mS/cm)
0.01	22.3	1.947	1.748
0.06	22.3	10.94	6.988
0.04	22.3	7.53	4.892
0.1	22.3	17.34	11.18
0.02	22.3	3.97	2.796
0.08	22.3	14.14	9.084
0.02	22.3	3.97	2.796
0.1	22.4	17.35	11.18
0.04	22.4	7.54	4.892
0.08	22.4	14.16	9.084
0.01	22.3	1.949	1.748
0.06	22.4	10.95	6.988
0.02	22.4	3.96	2.796
0.1	22.4	17.25	11.18
0.04	22.4	7.52	4.892
0.01	22.3	1.948	1.748
0.08	22.4	14.08	9.084
0.06	22.4	10.96	6.988

The conductance, κ (mS/cm) was plotted against the measured conductivity, L (mS). The cell constant, d/a (cm^{-1}), could then be determined from the following linear equation:

$$\kappa = (d/a)L$$

The plot of the Kappa (K) versus measured conductivity for calibration of the conductivity probe are shown in Figure 15. The kappa values were interpolated according to Jones and Prendergast's work.[24]

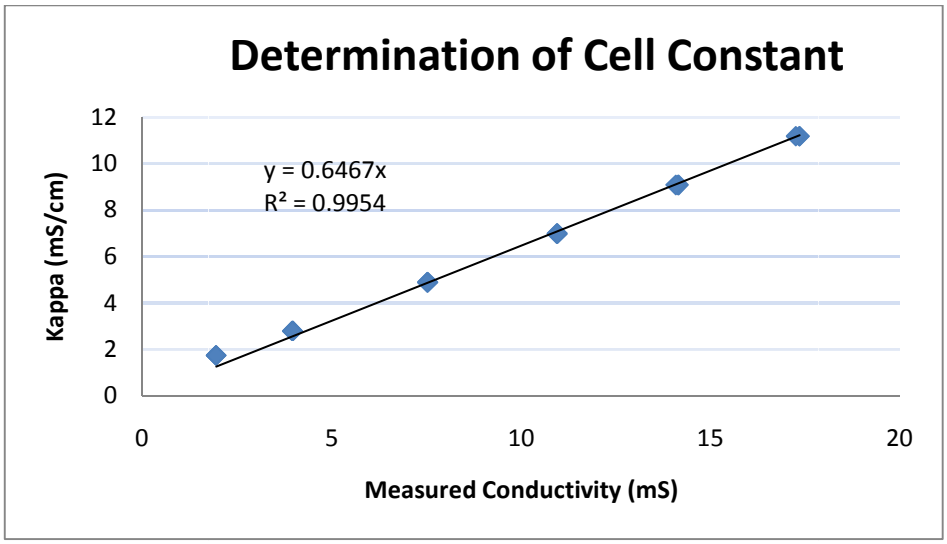

Figure 11. Determination of cell constant

The conductivities of KCl solutions were measured at 22.3 -22.4 ˚C and the cell constant is estimated to be 0.65 cm^{-1}.

Electrochemical Properties

Electrochemical potential windows of ionic liquids were determined using Princeton Applied Research Potentiostat/Galvanostat (Model 173) with a EG&G Parc Universal Programmer (Model 175). An Omnigraphic 2000 recorder by Houston Instruments was used to record the data. About 1-2 mL of ionic liquid was added to a glass conical vial with a plastic screw cap and septum with holes for electrodes (Figure 12). Glassy carbon and platinum electrodes were used as working electrodes. A platinum wire was used as the counter electrode and Ag|AgCl dipped in an ionic liquid was used as a reference electrode. Nitrogen gas was bubbled through the solution immediately prior to analysis and solution was tested for water content. Scan rates used to determine electrochemical windows were 50 mV/sec.

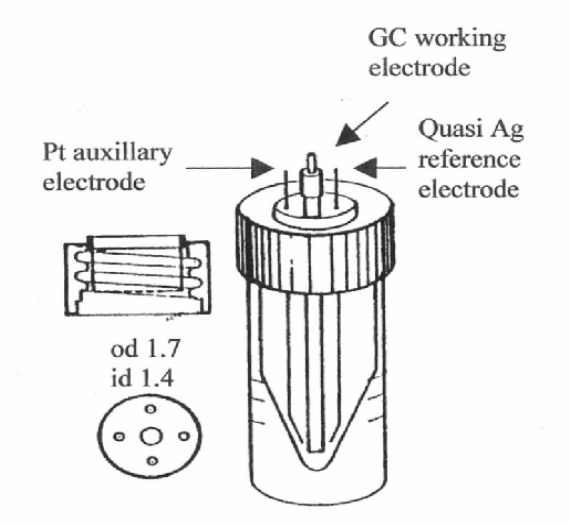

Figure 12. Diagram of cell used for electrochemical measurements

The area of the working electrodes was determined using cyclic voltammetry (CV). A solution of 2.0 x10^{-6} M ferrocene in HPLC grade acetonitrile and 0.10 M *n*-tetrabutylammonium hexafluorophosphate as a supporting electrolyte was used.[25] Cyclic voltammagrams were measured at various scan rates. From the anodic peak heights as a function of $v^{1/2}$ the area of the working electrodes were calculated using the Randel-Sevcik equation:

$$i_{p,a} = (2.687 \times 10^5 \text{ mol}^{-1} \text{ V}^{-1/2}) \, n^{3/2} \, v^{1/2} \, D^{1/2} \, A \, C$$

Where $I_{p,a}$ is the anodic peak hight, n is the number of electrons transferred in the half-reaction, v is the scan rate, D is the diffusion coefficient of the analyte, A is the area of the working electrode, and C is the concentration of the analyte. The constant,

2.687×10^5 mol^{-1} $V^{-1/2}$, is Faraday's constant divided by the universal gas constant, R, and the absolute temperature which is assumed to be 298.15 K.

A cyclic voltammagram of ferrocene in acetonitrile is shown in Figure 18. Glassy carbon electrode was used as a working electrode at 20 ,50, 100, 200 mV/sec scan rates.

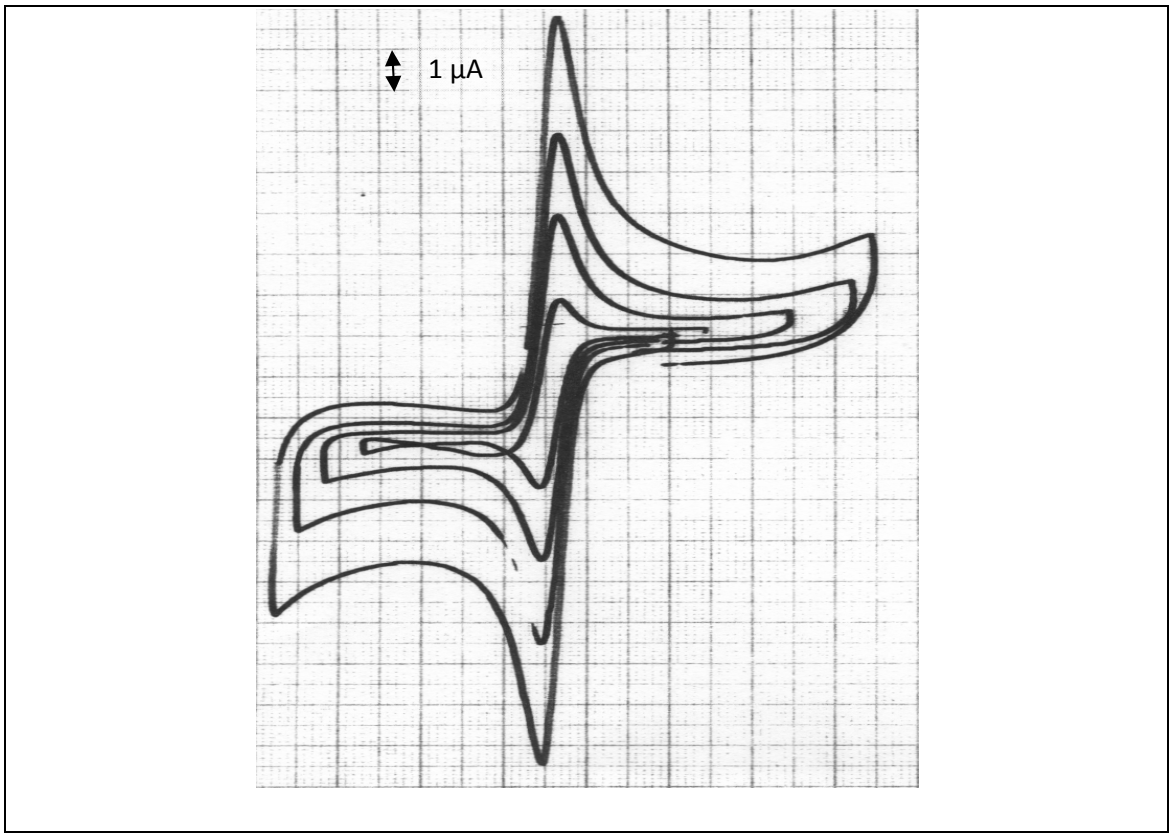

Figure 13. Cyclic voltamogram of ferrocene in acetonitrile obtained at different scan rates using glassy carbon working electrode.

From the cyclic voltammagrams the following data were obtained.

Table 5. CV data for ferrocene in acetronitrile obtained using a glassy carbon electrode.

peak height			scan rate	
(cm)	µA/cm	µA	(V/sec)	$(\text{scan rate})^{1/2}$
6.1	1	6.1	0.2	0.4472
4.2	1	4.2	0.1	0.3162
2.6	1	2.6	0.05	0.2236
0.93	1	0.93	0.02	0.1414

Using the Randel-Sevcik equation as $i_{p,c} = k^* v^{1/2}$, where k is $(2.687 \times 10^5\ \text{mol}^{-1}\ \text{V}^{-1/2})\ n^{3/2}\ D^{1/2}$ A C, the data in the table above can be used to determine k. A plot of the peak height versus the scan rate is shown in Figure 14.

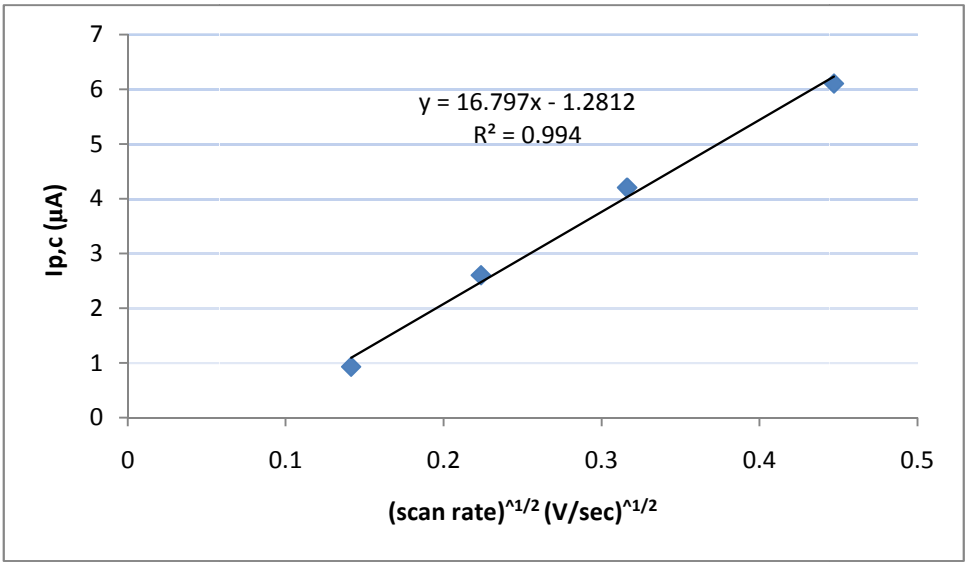

Figure 14. Plot of anodic peak current ($I_{p,a}$) versus the square root of the scan rate when using the glassy carbon electrode in ferrocene solution. (4850 ppm H_2O)

Slope from the graph in Figure 19, k, equals 1.68×10^{-6} A $V^{1/2}$ $sec^{-1/2}$. Since this is equivalent to (2.687×10^{5} mol^{-1} $V^{-1/2}$) $n^{3/2}$ $D^{1/2}$ A C and n, A and C are known, the effective area of the glassy carbon electrode was determined to be 6.66×10^{-3} cm^2. This procedure was repeated using the platinum working electrode and the area was found to be 7.10×10^{-3} cm^2. The CVs of ferrocene in acetronitrile using platinum working electrode as well as the corresponding data and graph can are shown in Figures 15-16 and Table 6.

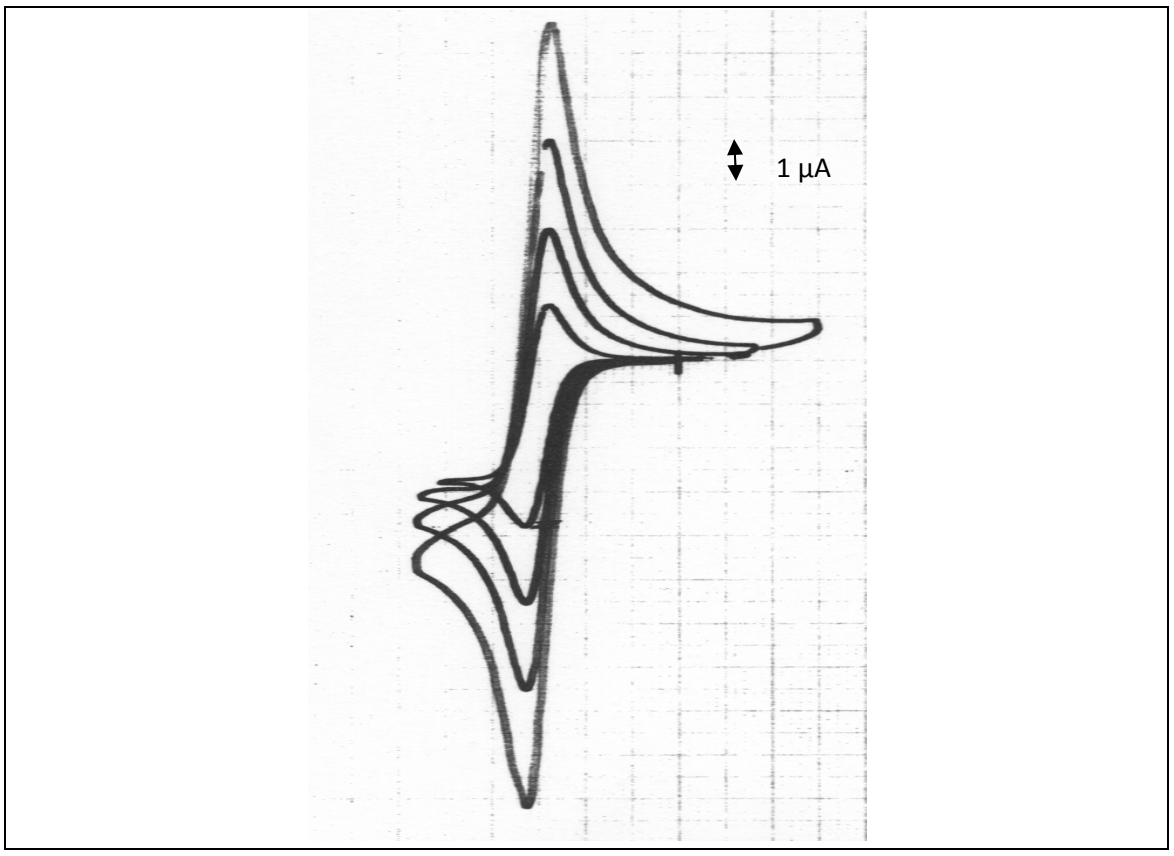

Figure 15. CVs of ferrocene in acetonitrile using a platinum working electrode obtained at different scan rates. The water content was 4860 ppm H_2O and the temperature was 23.9 ˚C.

Table 6. CV data from ferrocene in acetronitrile using a platinum electrode.

peak height (cm)	µA/cm	µA	scan rate (V/sec)	$(\text{scan rate})^{1/2}$
6.75	1	6.75	0.2	0.4472
4.71	1	4.71	0.1	0.3162
2.95	1	2.95	0.05	0.2236
1.27	1	1.27	0.02	0.1414

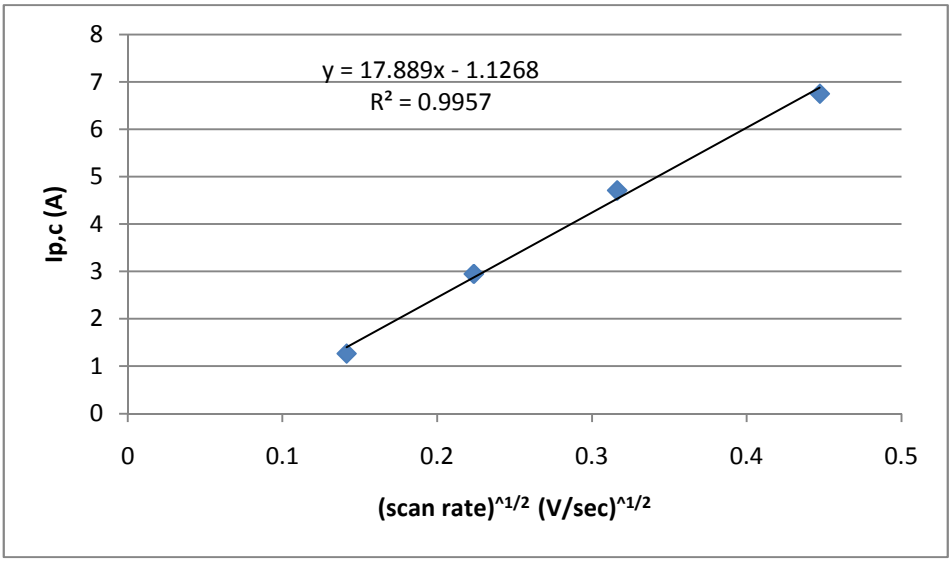

Figure 16. Current as a function of scan rate of ferrocene in acetonitrile using platinum electrode.

Synthesis

Preparation of 1-ethyl-3-methylimidazolium chloride $(EMICl)^-$

1-ethyl-3-methylimidazolium chloride was prepared by reacting 0.609 moles (50.0 g) of N-methylimidazole with 0.610 moles (39.5 g) of 1-chloroethane gas.

First, inside of a nitrogen filled glove bag, a small liquid nitrogen and ethanol bath was placed on top of a scale. Inside the nitrogen bath a safety coated pressure bottle manufactured by Ace® Glass Co. was set. 1-chloroethane gas was fed into the bottle and allowed to condense until a desired weight was attained. Then N-methylimidazole was added so that liquid 1-chloroethane was in excess and the bottle was sealed using a threaded Teflon® stopper. The bottle was then set in a stirred oil bath at 45 °C and covered so no light could affect the reaction. As the reaction proceeded over a period of one to two weeks, the top layer of the two layers in the bottle would diminish. When a change in the top layer was no longer observed the reaction was considered complete. The bottle was the set in a freezer to allow for crystallization. The excess 1-chloroethane was evaporated at room temperature. The crystals of EMICl were then dissolved in acetonitrile and recrystallized with ethyl ether. The ethyl ether was decanted and crystals of EMICl were dried in a vacuum. Yield was around 95%.

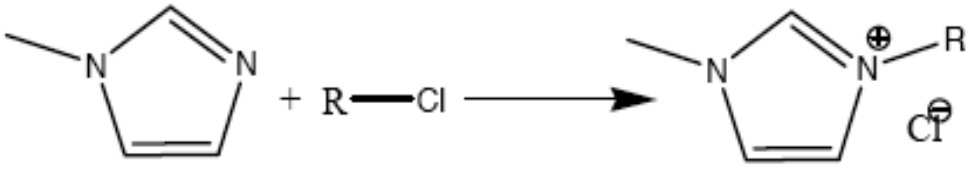

Figure 17. Preparation of 1-ethyl-3-methylimidazolium chloride

Preparation of 1-ethyl-3-methylimidazolium bis(trifluoromethanesulfonyl)-imide ($EMINTf_2$)

1-ethyl-3-methylimidazolium bis(trifluoromethanesulfonyl)-imide was made via an ion exchange reaction (metathesis) using EMICl and Lithium bis(trifluoromethanesulfonyl)-imide. About 30 milliliters of water was used to completely dissolve 0.0653 moles (9.57 g) of EMICl together with 0.0646 moles (18.55 g) of lithium bis(trifluoromethanesulfonyl)-imide inside a round-bottom flask. The solution was set aside to stir with a stirbar for two days. As the reaction proceeded a layer of 1-ethyl-3-methylimidazolium bis(trifluoromethanesulfonyl)-imide formed at the bottom of the flask. When the reaction was complete, the solution was transferred to a glass separatory funnel where the aqueous phase was separated from the heavier ionic liquid phase. Lithium chloride was removed from the ionic liquid by multiple extractions using equal amounts of water. The extraction was repeated 15-20 times until the aqueous solution didn't show presence of chloride ion when reacted with silver nitrate. The $EMINTf_2$ liquid was then placed under vacuum of about 1-10 millitorr to remove residual water. The structure and purity were confirmed using ^{1}H NMR and is shown in Figure 55. Peaks were found a δ 8.43 (1H), 7.39 (2H), 4.19 (2H), 3.84 (3H), 2.18 (water peak), 1.48 (3H). Structure and purity were also confirmed using ^{13}C NMR and is shown in Figure 56. Peaks were found at 135.4, 123.4, 121.7, 44.6, 35.5, 14.2. Solvent peaks from trace amounts of CH_3CN were found at 117.0 and 0.00.

Preparation of 1-propyl-3-methylimidolium chloride (PMICl)

Inside an Ace® threaded pressure bottle 0.621 moles (48.788 g) of 1-chloropropane and 0.615 moles (50.487 g) of N-methylimidazole was mixed. This procedure was performed inside of a nitrogen filled glove bag. The N-methylimidazole was previously distilled under vacuum. The 1-chloropropane was added in an excess of about 1%. After the bottle was sealed it was placed in a 45 ˚C oil bath in a dark hood and stirred for about two weeks. As the reaction progressed, a bottom layer would increase. Once no change in the two phases was observed, the reaction was considered complete. The bottle was then placed in a freezer overnight to crystallize PrMICl from the bottom layer. The top layer was then decanted. Ethyl ether was then added to enhance crystallization.

Preparation of 1-Propyl-3-methylimidazolium bis(trifluoromethanesulfonyl)-imide ($PrMINTf_2$)

1-Propyl-3-methylimidazolium bis(trifluoromethanesulfonyl)-imide was prepared in the same manner as $EMINTf_2$. In a round bottom flask, 0.105 moles (16.799 g) of 1-propyl-3-methylimidazolium chloride was mixed with 0.103 moles (29.50 g) of lithium bis(trifluoromethanesulfonyl)-imide in water for two days. The lithium chloride was then extracted 15-20 times in a separatory funnel. Silver nitrate was used to test the aqueous extract for chlorides. Drying was done under vacuum. The structure and purity were confirmed using ^1H NMR and is shown in Figure 57. Peaks were found a δ 8.41 (1H), 7.384 (1H), 7.355 (1H) 4.11 (2H), 3.84 (3H), 2.16

(water peak), 1.87 (2H) and 0.94 (3H). Structure and purity were also confirmed using ^{13}C NMR and is shown in Figure 58. Peaks were found at 135.6, 123.4, 122.0, 50.8, 35.6, 22.8, and 9.4. Solvent peaks from trace amounts of CH_3CN were found at 117.0 and 0.00.

Preparation of 1-butyl-3-methylimidazolium chloride (BMICl)

Inside an Ace® threaded pressure bottle 0.231 moles (21.345 g) of 1-chlorobutane and 0.233 moles (19.1224 g) of N-methylimidazole was mixed. This procedure was performed inside of a nitrogen filled glove bag. The N-methylimidazole was previously distilled. The 1-chlorobutane was added in an excess of about 1%. After the bottle was sealed it was placed in a 45 ˚C oil bath in a dark hood and stirred for about two weeks. As the reaction progressed, a bottom layer would increase. Once no change in the two phases was observed, the reaction was considered complete. The bottle was then placed in a freezer overnight to crystallize BMICl from the bottom layer. The top layer was then decanted. Ethyl ether was then added and the freezing and decanting was repeated.

Preparation of 1-butyl-3-methylimidazolium bis(trifluoromethanesulfonyl)-imide (BMINTf$_2$)

1-butyl-3-methylimidazolium bis(trifluoromethanesulfonyl)-imide was prepared in the same manner as EMINTf$_2$. In 30 milliliters of water, 0.0518 moles (9.04 g) of 1-butyl-3-methylimidazolium chloride was mixed with 0.0522 moles (15.0 g) of lithium bis(trifluoromethanesulfonyl)-imide. Solution was stirred for two days and the

washed 15-20 times in a separatory funnel. Silver nitrate was used to test the water for chlorides. Drying was done under vacuum. The structure and purity were confirmed using ^{1}H NMR and is shown in Figure 59. Peaks were found a δ 8.42 (1H), 7.37 (2H), 4.14 (2H), 3.84 (3H), 2.17 (water peak), 1.84 (2H) 1.35 (2H) and 0.96 (3H). Structure and purity were also confirmed using ^{13}C NMR and is shown in Figure 60. Peaks were found at 135.6, 123.4, 122.0, 49.05, 35.6, 31.3, 18.67, and 12.32. Solvent peaks from trace amounts of CH_3CN were found at 117.0 and 0.00.

Preparation of 1-pentyl-3-methylimidazolium chloride (PnMICl)

Inside an Ace® threaded pressure bottle 0.444 moles (47.286 g) of 1-chloropentane and 0.435 moles (35.746 g) N-methylimidazole was mixed. This procedure was performed inside of a nitrogen filled glove bag. The N-methylimidazole was previously distilled. The 1-chlorobutane was added in an excess of about 1%. After the bottle was sealed it was placed in a 45 ˚C oil bath in a dark hood and stirred for about two weeks. As the reaction progressed, a bottom layer would grow. Once no change in the two phases was observed, the reaction was considered complete. The bottle was then placed in a freezer overnight to crystallize the bottom layer. The top layer was then decanted. Ethyl ether was then added to enhance crystallization.

Preparation of 1-pentyl-3-methylimidazolium bis(trifluoromethanesulfonyl)-imide ($PnMINTf_2$)

1-pentyl-3-methylimidazolium bis(trifluoromethanesulfonyl)-imide was prepared in the same manner as $EMINTf_2$. In about 150 milliliters of water, 0.566 moles (106.88 g) of 1-pentyl-3-methylimidazolium chloride was mixed with 0.572 moles (164.10 g) of lithium bis(trifluoromethanesulfonyl)-imide. The solution was stirred for two days and then the lithium chloride was extracted with water 15-20 times in a separatory funnel. Silver nitrate was used to test the water for chlorides. Drying was done under vacuum. The structure and purity were confirmed using ^{1}H NMR and is shown in Figure 61. Peaks were found a δ 8.43 (1H), 7.378 (2H), 4.14 (2H), 3.85 (3H), 2.18 (water peak), 1.85 (2H), 1.35 (4H) and 0.92 (3H). Structure and purity were also confirmed using ^{13}C NMR and is shown in Figure 62. Peaks were found at 135.6, 123.40, 122.03, 49.3, 35.57, 29.00, 27.51, 21.4 and 12.78. Solvent peaks from trace amounts of CH_3CN were found at 117.02 and 0.00.

Preparation of 1-hexyl-3-methylimidazolium chloride (HMICl)

Inside an Ace® threaded pressure bottle, 0.313 moles (37.76 g) of 1-chlorohexane and 0.297 moles (24.4 g) N-methylimidazole was mixed. This procedure was performed inside of a nitrogen filled glove bag. The N-methylimidazole was previously distilled. The 1-chlorobutane was added in an excess of about 1%. After the bottle was sealed it was placed in a 45 ˚C oil bath in a dark hood and stirred for about two weeks. As the reaction progressed, a bottom layer would grow. Once no

change in the two phases was observed, the reaction was considered complete. The bottle was then placed in a freezer overnight to crystallize the bottom layer. The top layer was then decanted. Ethyl ether was then added and the freezing and decanting was repeated.

Preparation of 1-hexyl-3-methylimidazolium bis(trifluoromethanesulfonyl)-imide ($HMINTf_2$)

1-hexyl-3-methylimidazolium bis(trifluoromethanesulfonyl)-imide was prepared in the same manner as $EMINTf_2$. In about 100 milliliters of water 0.210 moles (42.52 g) of 1-hexyl-3-methylimidazolium chloride was mixed with 0.212 moles (60.819 g) of lithium bis(trifluoromethanesulfonyl)-imide. The solution was stirred for two days and the excess lithium chloride was extracted from the ionic liquid using water 15-20 times in a separatory funnel. Silver nitrate was used to test the water for chlorides. Drying was done under vacuum. The structure and purity were confirmed using ^{1}H NMR and is shown in Figure 63. Peaks were found a δ 8.41 (1H), 7.388 (1H), 7.351 (1H), 4.135 (2H), 3.842 (3H), 2.167 (water peak), 1.843 (2H), 1.33 (6H), 0.916 (3H). Structure and purity were also confirmed using ^{13}C NMR and is shown in Figure 64. Peaks were found at 135.55, 123.38, 122.01, 49.30, 35.57, 30.47, 29.26, 25.06, 21.80, and 12.90. Solvent peaks from trace amounts of CH_3CN were found at 116.99 and 0.00.

III. RESULTS AND DISCUSSION

In this work the physical, thermal and electrochemical properties of imidazolium type ionic liquids containing (1-alkyl-3-methylimidazolium cation and bis(trifluoromethanesulfonyl)imide anions) were studied as a function of alkyl chain length. Their properties were also compared to the properties of ionic liquids containing the same cation but different anions, viz. $Beti^-$ and BF_4^-. The following ionic liquids were synthesized and characterized:

1-ethyl-3-methylimidazolium bis(trifluoromethanesulfonyl)imide ($EMINTf_2$),

1-propyl-3-methylimidazolium bis(trifluoromethanesulfonyl)imide ($PrMINTf_2$),

1-butyl-3-methylimidazolium bis(trifluoromethanesulfonyl)imide ($BMINTf_2$),

1-pentyl-3-methylimidazolium bis(trifluoromethanesulfonyl)imide ($PnMINTf_2$) and

1-hexyl-3-methylimidazolium bis(trifluoromethanesulfonyl)imide ($HMINTf_2$).

The syntheses involved first the preparation of 1-alkyl-3-methylimidazolium chloride by reaction of N-methylimidazole with an alkyl chloride:

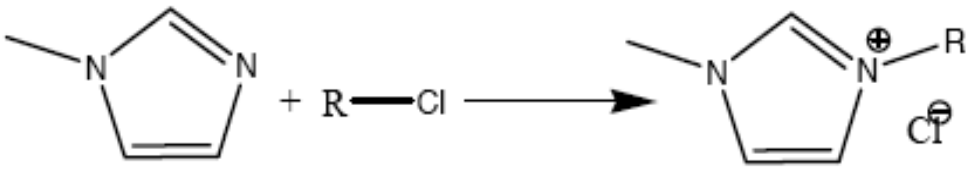

Figure 18. Preparation of 1-alkyl-3-methylimidazolium chloride

The next step in the synthesis involved the replacement of chloride with bis(trifluoromethanesulfonyl)imide anion (NTf_2^-):

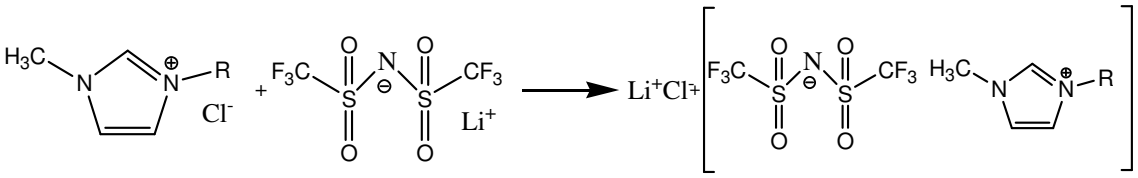

Figure 19. Metathesis reaction to form 1-alkyl-3-methylimidazolium bis(trifluoromethanesulfonyl)imide.

Physical and electrochemical properties of these ionic liquids containing NTf_2^- anion were compared to the properties of ionic liquids containing the same cation but larger anion, bis(pentafluoroethylsulfonyl)imide ($Beti^-$). It was presumed that the ionic liquid containing smaller NTf_2^- anion will have higher conductivity and lower viscosity.

Thermal Properties

The thermal properties of ionic liquids 1-alkyl-3-methylimidazolium bis(trifluoromethanesulfonyl)imide, $RMINTf_2$, were studied by differential scanning calorimetry (DSC), and thermal gravimetric analysis (TGA). Differential scanning calorimetry (DSC) was used to determine the melting point or glass transition temperatures (T_g) of the ionic liquids. Thermal gravimetric analysis (TGA) provided information on the thermal stability and decomposition temperatures of ionic liquids.

The decomposition temperatures of $RMINTf_2$ ionic liquids are given in Table 7. For comparison Table 7 also shows the decomposition temperatures of analogous ionic liquids containing the $Beti^-$ anion. The TGA curves for the ionic liquids containing NTf_2^- anions are given in the Appendix and a typical TGA curve of $PrMINTf_2$ is shown in Figure 20.

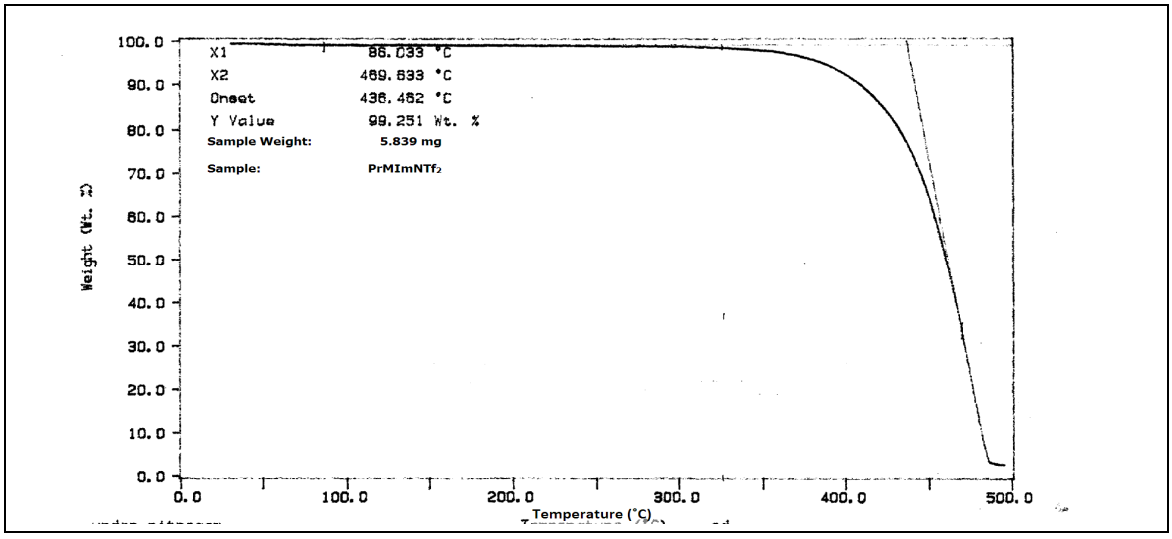

Figure 20. TGA decomposition curve for $PrMINTf_2$

Table 7. Comparison of decomposition temperatures of various ionic liquids containing NTf_2^- and $Beti^-$ anion.

Ionic Liquid	T_{start}	T_{onset}
$EMINTf_2$	326	443
EMIBeti	325	420
$PrMINTf_2$	324	444
PrMIBeti	326	410
$BMINTf_2$	322	428
BMIBeti	314	410
$PnMINTf_2$	338	425
PnMIBeti	318	425
$HMINTf_2$	311	406
HMIBeti	321	405

The TGA curves for other $RMINTf_2$ ionic liquids are shown in the appendix. Table 8 gives the values of the onset temperatures obtained with standard deviation when TGA measurements were repeated several times.

Table 8. TGA onset temperatures (°C) obtained for various ionic liquids containing the NTf_2^- anion

Ionic Liquid:	$EMINTf_2$	$PrMINTf_2$	$BMINTf_2$	$PnMINTf_2$	$HMINTf_2$
	444.814	437.039	432.303	423.475	412.748
	439.908	450.714	424.891	425.603	406.078
	443.616	443.618	425.21	417.296	402.652
		452.747		424.517	404.3
		441.381		431.839	
		436.462			
Average	442.7793	443.6602	427.468	424.546	406.4445
Std Dev.	2.557776	6.829011	4.19027	5.196525	4.429085

Table 9. TGA T_{start} temperatures (°C) obtained for the ionic liquids containing the NTf_2^- anion.

Ionic Liquid:	$EMINTf_2$	$PrMINTf_2$	$BMINTf_2$	$PnMINTf_2$	$HMINTf_2$
	319.32	326.25	321.25	340	308.75
	336.7	322.5	311.25	323	315.5
	320.6	310	333.78	347.56	296.512
		325		343.75	325
		324.52		336.25	
		335.65			
Average	325.54	323.987	322.1	338.1	311.44
Std Dev.	9.67	8.25	11.3	9.44	11.978

Plots of T_{start} and T_{onset} temperature versus the alkyl chain length obtained for $RMINTf_2$ ionic liquids are shown in Figure 21 and 22. For comparison Figures 21 and 22 also contain the same data obtained for ionic liquids containing the $Beti^-$ anion.

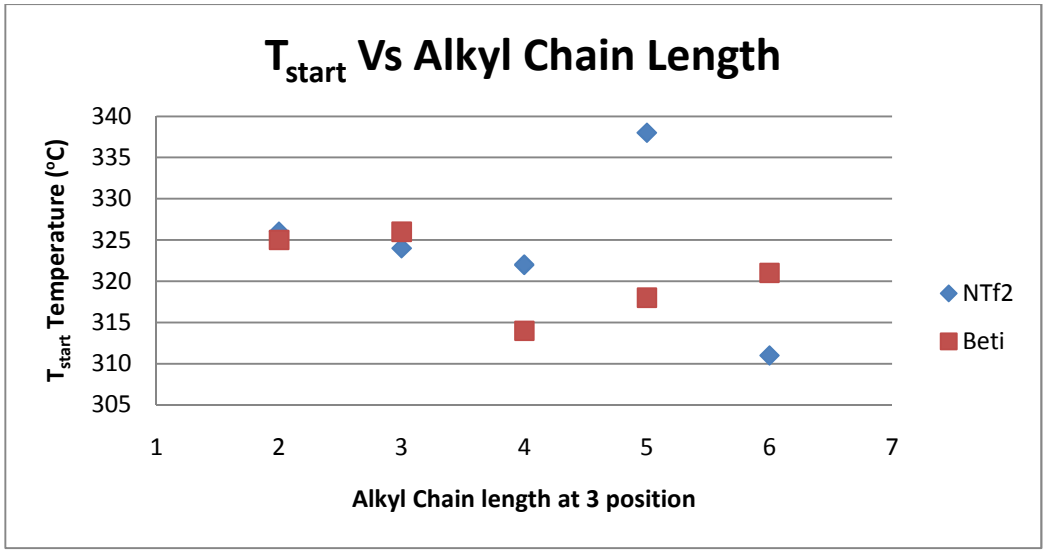

Figure 21. Comparison of the T_{start} values and alkyl chain length for $RMINTf_2$ and RMIBeti ionic liquids.

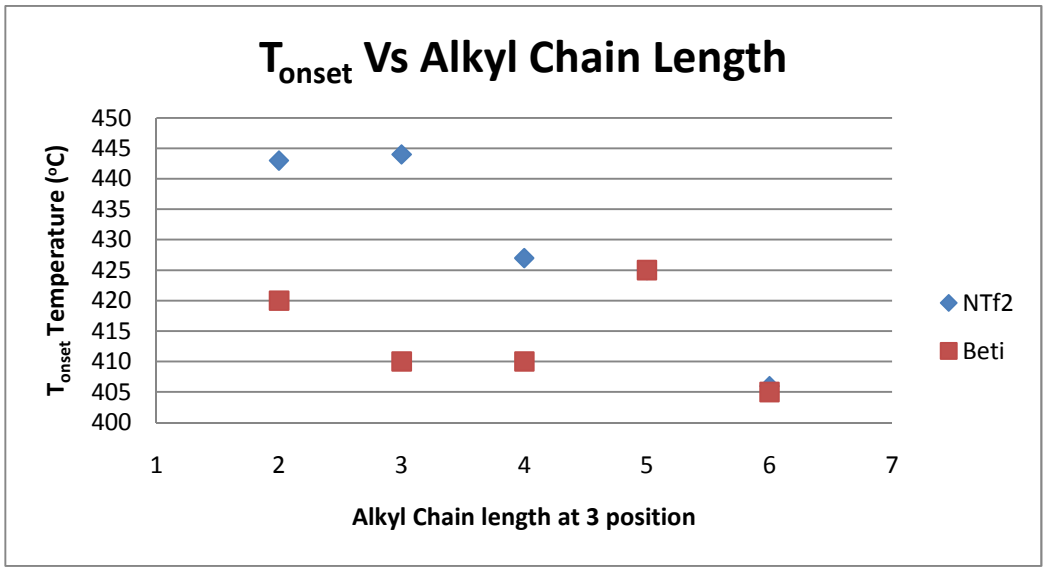

Figure 22. Comparison of the T_{onset} values and alkyl chain length for $RMINTf_2$ and RMIBeti ionic liquids.

From the graphs in Figures 21 and 22 it can be seen that there is a general decrease in thermal stability as the alkyl chain length at the 3-position increases, regardless of the anion. This is more evident in Figure 22 which compares T_{onset} values. Ionic liquids with the NTf_2 anion have somewhat higher T_{onset} temperatures than ionic liquids with the Beti anion. The exception is $PnMINTf_2$, which has the same T_{onset} temperature as PnMIBeti. The plot in Figure 21 shows a downward trend of decreasing T_{start} with increasing alkyl chain length except for $PnMINTf_2$ whose T_{start} value is somewhat higher. As shown in Figure 21 the T_{start} temperatures of ionic liquids containing NTf_2^- and $Beti^-$ anion are very similar.

The differential scanning calorimetry (DSC) curve for $EMINTf_2$ ionic liquid is shown in Figure 23. This ionic liquid has a sharp melting point at around -18.7 ^oC and has an enthalpy of fusion of about 47.8 J/g.

The DSC curve for $PrMINTf_2$ is shown in Figure 24. The DSC curve does not show a sharp melting point. This suggests that ionic liquids with longer R groups form glasses at lower temperatures. Attempts were made using various scan rates and hold times to freeze $PrMINTf_2$ as well as BMINTf2 and $PnMINTf_2$. They all showed possible structural changes around -35 ^oC. $HMINTf_2$ appeared to show a glass transition temperature around -25 ^oC. More DSC scans of these ionic liquids are given in the appendix.

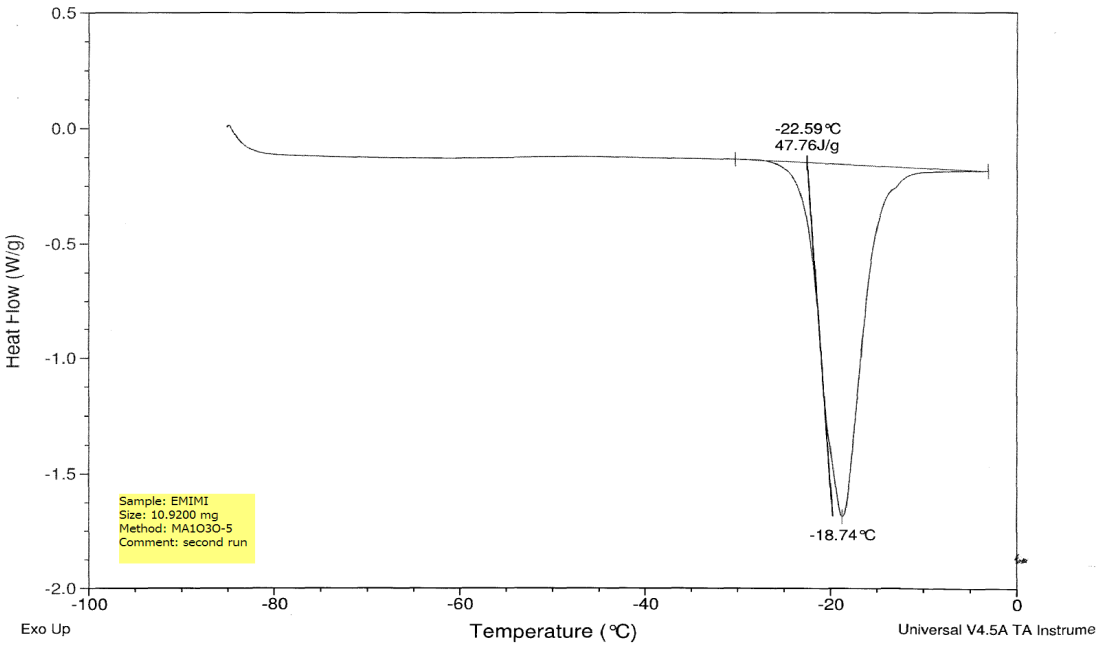

Figure 23. DSC curve for $EMINTf_2$

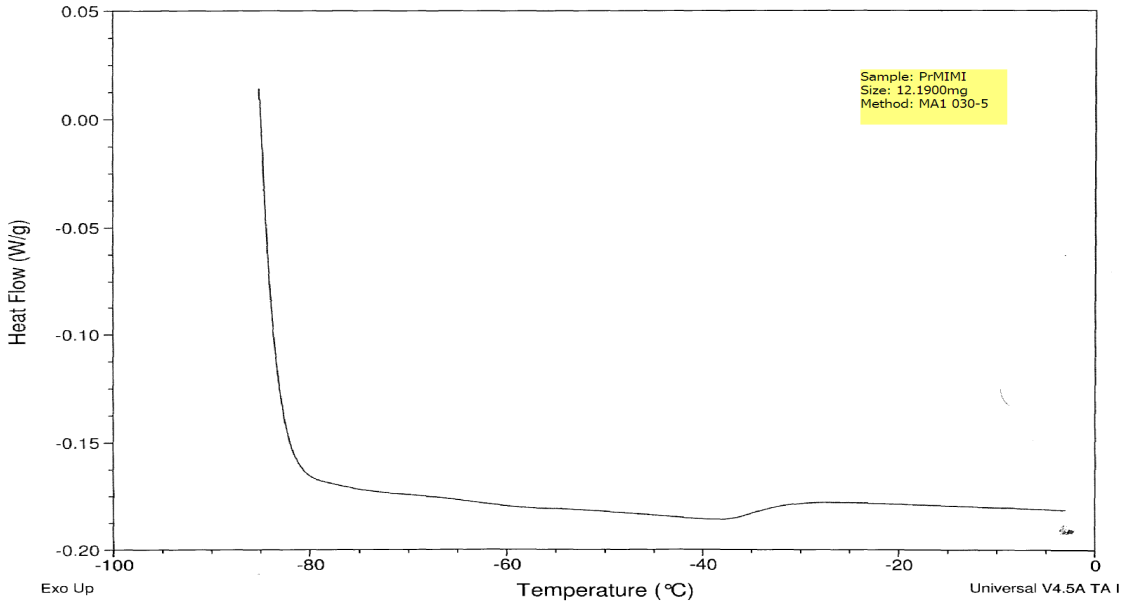

Figure 24. DSC curve for $PrMINTf_2$

Density and Viscosity

The density and viscosity of $RMINTf_2$ ionic liquids as a function of temperature and containing different amounts of water are given in Tables 10 - 24 and Figures 25 - 29.

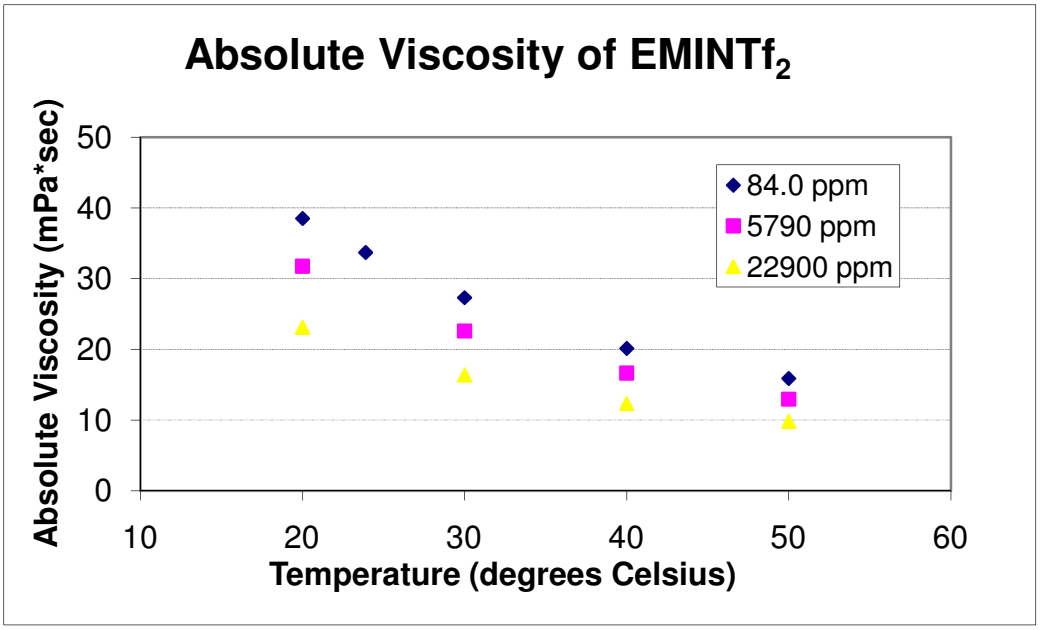

Figure 25. Absolute viscosity as a function of temperature (°C) for $EMINTf_2$ ionic liquid containing different amounts of water

Table 10. Kinematic viscosity of $EMINTf_2$ at various temperatures and water content

Temperature (ºC)	84.0 ppm	5790 ppm	22900 ppm
20	25.085	20.91	15.18
23.9	22.069	------	-------
30	17.95	15.01	10.80
40	13.34	11.12	8.181
50	10.58	8.709	6.543

Table 11. Density (g/mL) of $EMINTf_2$ at various temperatures and water content

Temperature (ºC)	84.0 ppm	5790 ppm	22900 ppm
20	1.536	1.519	1.524
23.9	1.527	------	------
30	1.522	1.505	1.516
40	1.510	1.495	1.504
50	1.502	1.504	1.495

Table 12. Absolute viscosity of $EMINTf_2$ at various temperatures and water content in mPa*sec

Temperature (ºC)	84.0 ppm	5790 ppm	22900 ppm
20	38.52	31.76	23.13
23.9	33.70	------	------
30	27.31	22.59	16.37
40	20.15	16.63	12.31
50	15.88	12.31	9.779

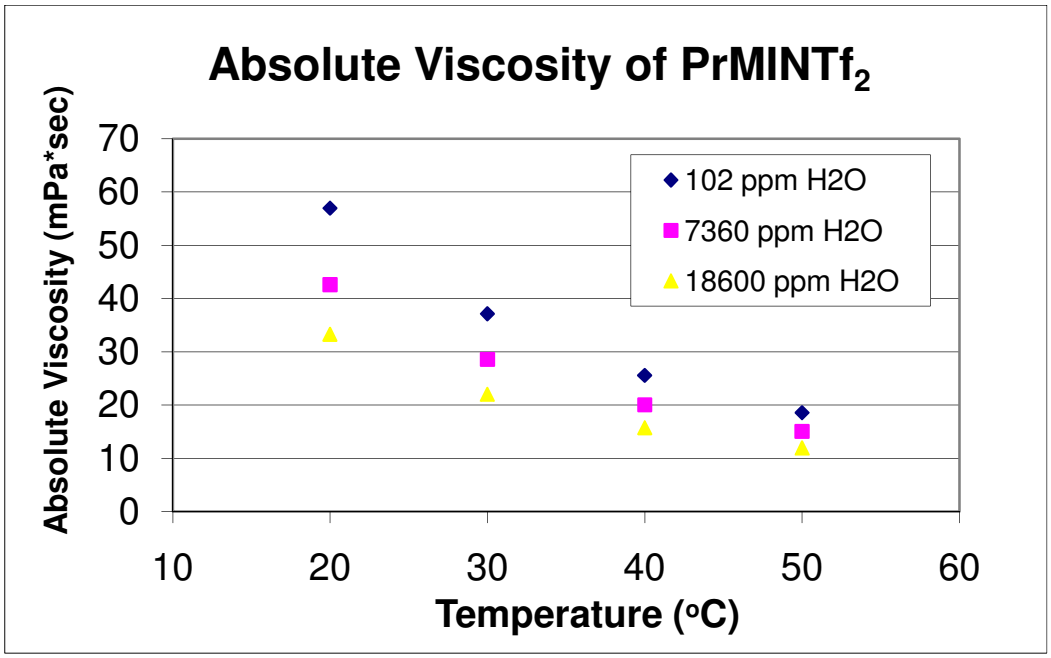

Figure 26. Absolute viscosity as a function of temperature (°C) for $PrMINTf_2$ ionic liquid containing different amounts of water

Table 13. Kinematic viscosity of $PrMINTf_2$ at various temperatures and water content

Temperature (ºC)	102 ppm	7360 ppm	18600 ppm
20	38.16	28.80	22.62
30	25.16	19.46	15.04
40	17.44	13.73	10.85
50	12.75	10.39	8.27

Table 14. Density (g/mL) of $PrMINTf_2$ at various temperatures and water content

Temperature (ºC)	102 ppm	7360 ppm	18600 ppm
20	1.493	1.479	1.473
30	1.477	1.468	1.463
40	1.466	1.458	1.451
50	1.457	1.449	1.442

Table 15. Absolute viscosity of $PrMINTf_2$ at various temperatures and water content in mPa*sec

Temperature (ºC)	102 ppm	7360 ppm	18600 ppm
20	56.98	42.58	33.30
30	37.16	28.57	22.01
40	25.58	20.03	15.74
50	18.57	15.05	11.93

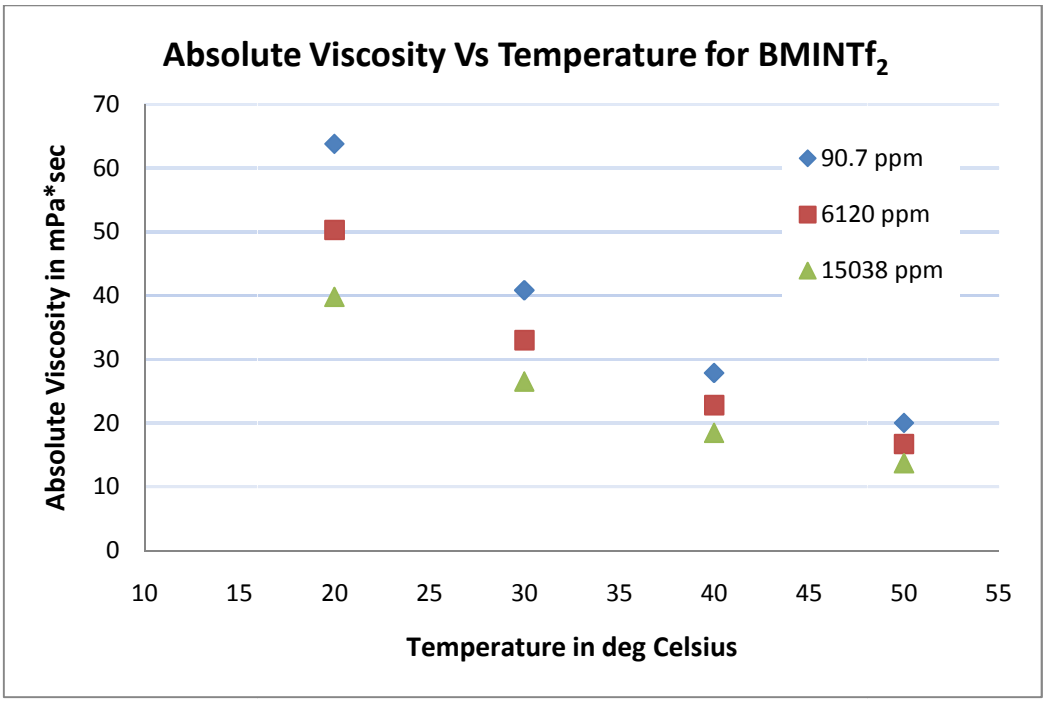

Figure 27. Absolute viscosity as a function of temperature (°C) for $BMINTf_2$ ionic liquid containing different amounts of water

Table 16. Kinematic viscosity of $BMINTf_2$ at various temperatures and water content

Temperature (ºC)	91 ppm	6120 ppm	15038 ppm
20	44.01	34.74	27.83
30	28.39	23.01	18.68
40	19.49	16.04	13.1
50	14.13	11.84	9.79

Table 17. Density (g/mL) of $BMINTf_2$ at various temperatures and water content

Temperature (ºC)	91 ppm	6120 ppm	15038 ppm
20	1.449	1.447	1.430
30	1.438	1.434	1.420
40	1.430	1.421	1.410
50	1.419	1.412	1.401

Table 18. Absolute viscosity of $BMINTf_2$ at various temperatures and water content in mPa*sec

Temperature (ºC)	91 ppm	6120 ppm	15038 ppm
20	63.76	50.28	39.80
30	40.83	32.99	26.52
40	27.86	22.80	18.47
50	20.05	16.72	13.71

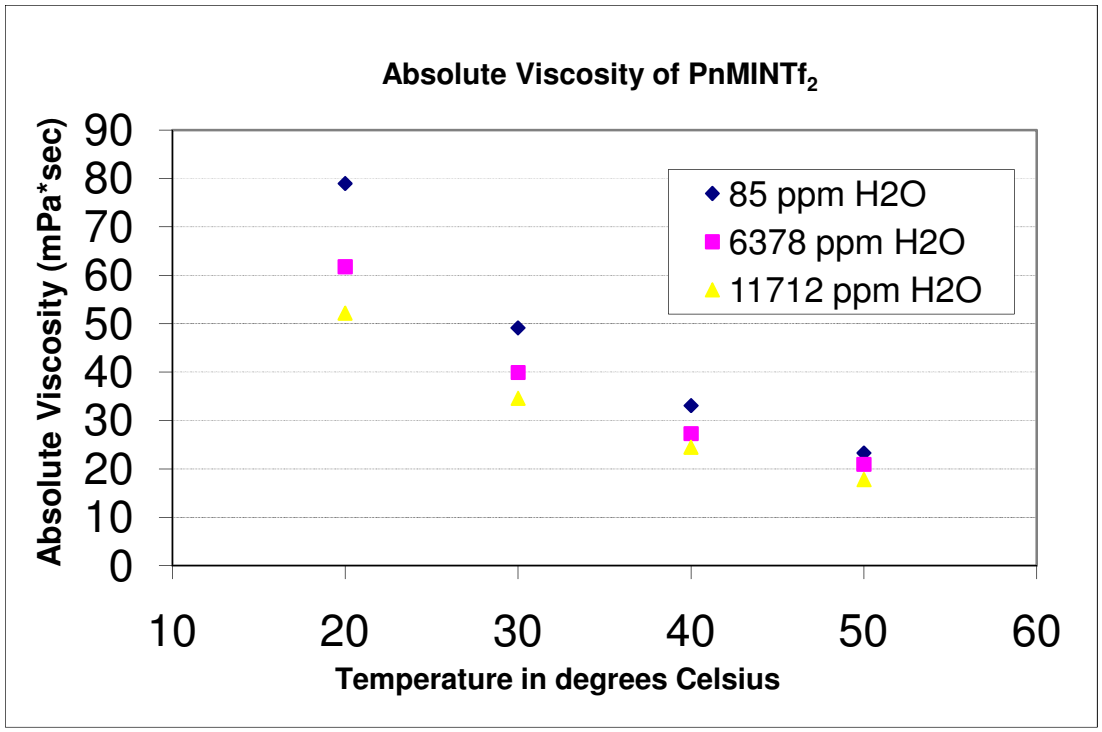

Figure 28. Absolute viscosity as a function of temperature (°C) for $PnMINTf_2$ ionic liquid containing different amounts of water

Table 19. Kinematic viscosity of $PnMINTf_2$ at various temperatures and water content

Temperature (ºC)	85 ppm	6378 ppm	11712 ppm
20	56.08	43.68	37.07
30	35.04	28.45	24.67
40	23.7	19.55	17.57
50	16.8	15.11	12.86

Table 20. Density (g/mL) of $PnMINTf_2$ at various temperatures and water content

Temperature (ºC)	85 ppm	6378 ppm	11712 ppm
20	1.408	1.414	1.4107
30	1.403	1.403	1.400
40	1.396	1.395	1.392
50	1.386	1.385	1.381

Table 21. Absolute viscosity of $PnMINTf_2$ at various temperatures and water content in mPa*sec

Temperature (ºC)	85 ppm	6378 ppm	11712 ppm
20	78.98	61.77	52.16
30	49.18	39.92	34.56
40	33.08	27.27	24.46
50	23.29	20.93	17.76

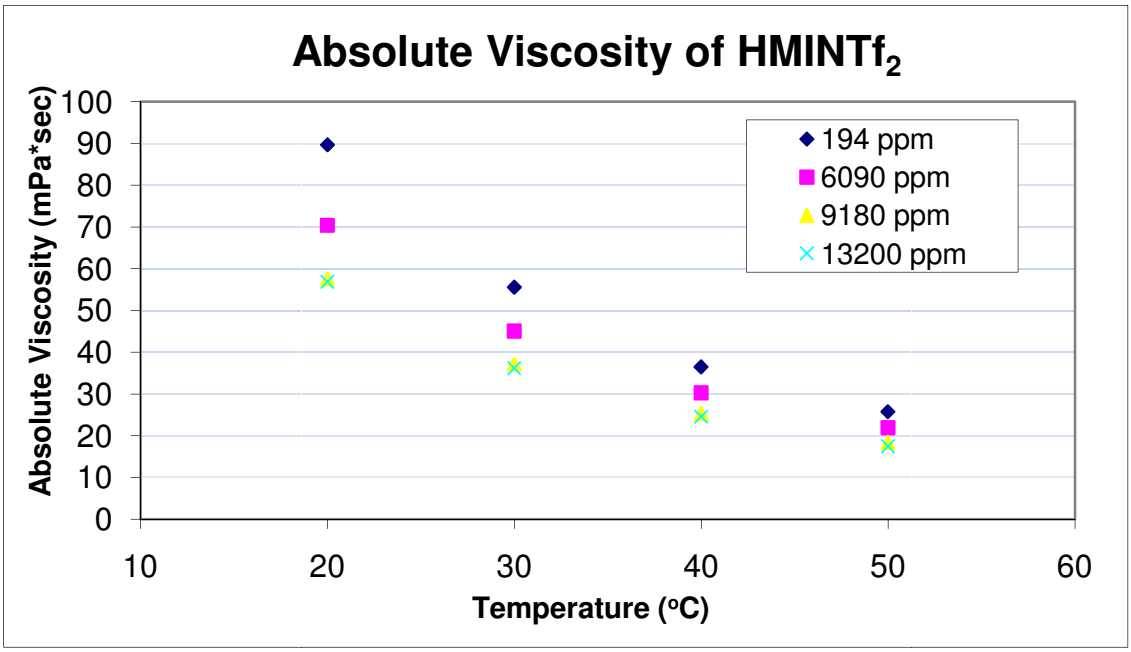

Figure 29. Absolute viscosity as a function of temperature (°C) for $HMINTf_2$ ionic liquid containing different amounts of water

Table 22. Kinematic viscosity of $HMINTf_2$ at various temperatures and water content

Temperature (ºC)	194ppm	6090 ppm	9180 ppm	13200 ppm
20	64.9	51.05	41.81	41.26
30	40.44	32.93	27.22	26.42
40	26.69	22.28	18.67	18.07
50	19	16.21	13.63	12.93

Table 23. Density (g/mL) of $HMINTf_2$ at various temperatures and water content

Temperature (ºC)	194 ppm	6090 ppm	9180 ppm	13200 ppm
20	1.382	1.379	1.377	1.378
30	1.374	1.368	1.368	1.369
40	1.367	1.359	1.356	1.359
50	1.355	1.351	1.347	1.351

Table 24. Absolute Viscosity of $HMINTf_2$ at various temperatures and water content in mPa*sec

Temperature (ºC)	194 ppm	6090 ppm	9180 ppm	13200 ppm
20	89.70	70.41	57.56	56.87
30	55.55	45.06	37.24	36.16
40	36.48	30.29	25.32	24.55
50	25.74	21.90	18.36	17.47

As described in the experimental part the kinematic viscosities were measured using a Cannon-Fenske viscosity meter at constant temperature (20, 30, 40, 50 °C). The values for absolute viscosities (μ) were obtained by multiplying the kinematic viscosity by the density at specific temperatures. The values for kinematic viscosities together with corresponding densities and calculated absolute viscosities at different temperatures are given in Tables 10-24. The absolute viscosity and kinematic viscosity increased with increasing length of R group. As a function of temperature both kinematic and absolute viscosities decrease with temperature (Figure 30). Dependence of absolute viscosity as a function of water content of ionic liquids and temperature for different R groups are shown in Figures 25-29. At each specific temperature the absolute viscosity decreases as the amount of the water in ionic liquid increases. Figure 30 gives a comparison of absolute viscosity of $RMINTf_2$ ionic liquds and the corresponding ionic liquid containing $Beti^-$ anion.

Figure 30 shows that ionic liquids conataining NTf_2^- anion have significantly lower absolute viscosities then RMIBeti ionic liquids. This was expected because the Beti-anion is larger than NTf_2^-. Similar ionic liquids with the same anion but larger alkyl chain length have higher viscosities, due increasing van der Waals forces.

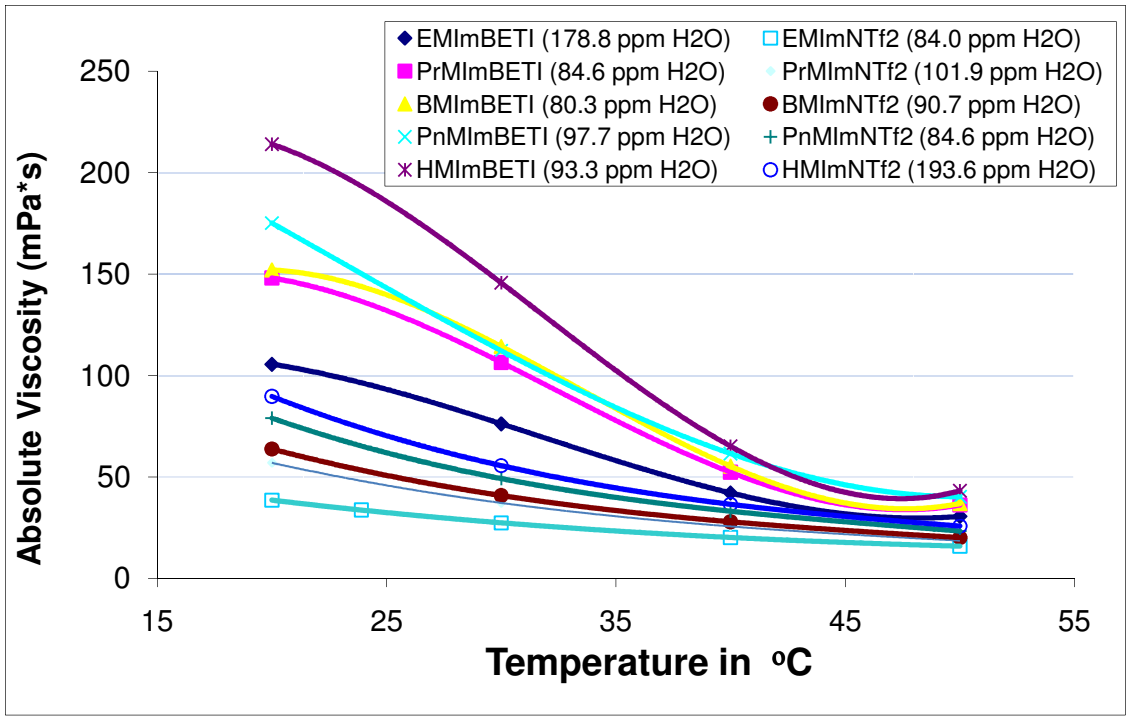

Figure 30. Comparison of absolute viscosities of ionic liquids.

Densities of NTf_2^- anion containing ionic liquids were measured at different temperatures (20, 30, 40, 50 °C). These liquids contained a very small amount of water (80-190 ppm). As described in the experimental part the measurements were done by weighing a known volume of ionic liquid at constant temperature. The data given in Table 25 are shown in Figure 31. It was found that as the alkyl group increases from ethyl to hexyl the densities of ionic liquids decrease. Comparison of densities obtain at different temperatures (Table 25) show that as the temperature increases from 20 to 50 °C the densities of corresponding ionic liquids decrease by about 0.02 g/mL. Figure 31 compares the densities data for $RMINTf_2$ ionic liquids as a function temperature. As the R group increases from ethyl to hexyl the densities decrease. A similar trend is observed for ionic liquids containing the $Beti^-$ anion. For comparison Figure 31 also

contains the density values for ionic liquids containing the $Beti^-$ anion. In general ionic liquids with $Beti^-$ anions show larger densities than ionic liquids containing the NTf_2^- anion. This is expected because RMIBeti ionic liquids contain a larger concentration of fluorinated carbons.

Table 25. Density of RMINTf2 and RMIBeti RTILs with low water content at various temperatures

Temperature	$EMImNTf_2$ (84 ppm H_2O)	$PrMImNTf_2$ (102 ppm H2O)	$BMImNTf_2$ (91 ppm H_2O)	$PnMImNTf_2$ (85ppm H_2O)	$HMImNTf_2$ (194 ppm H_2O)
20 °C	1.536	1.493	1.449	1.408	1.382
30 °C	1.522	1.477	1.438	1.403	1.374
40 °C	1.510	1.466	1.430	1.396	1.367
50 °C	1.502	1.457	1.419	1.386	1.355

Temperature	EMImBETI (179 ppm H_2O)	PrMImBETI (85 ppm H_2O)	BMIBETI (80 ppm H_2O)	PnMIBETI (98 ppm H_2O)	HMIBETI (93 ppm H_2O)
20 °C	1.597	1.555	1.507	1.481	1.445
30 °C	1.589	1.551	1.508	1.480	1.448
40 °C	1.581	1.542	1.499	1.471	1.434
50 °C	1.559	1.521	1.482	1.456	1.428

A comparison of densities of $RMINTf_2$ and RMIBeti ionic liquids is shown in Figure 31.

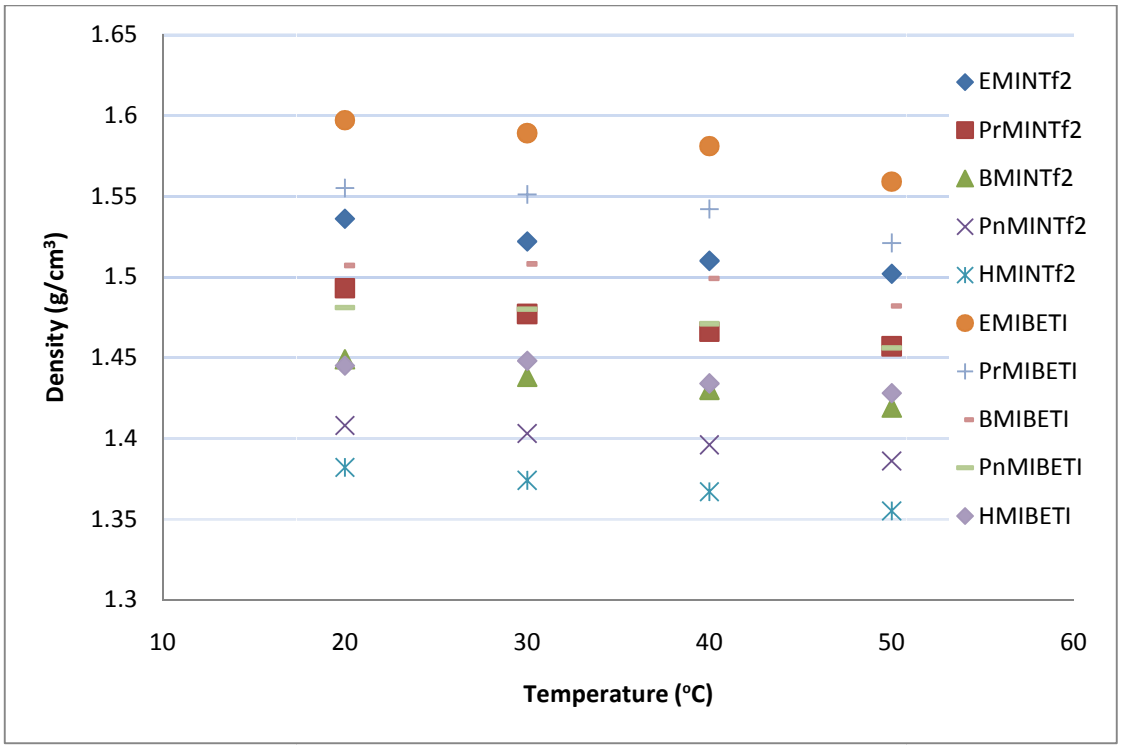

Figure 31. Comparison of the densities of $RMINTf_2$ and RMIBeti ionic liquids.

Figure 31 shows that RMIBeti ionic liquids have higher densities than analogous $RMINTf_2$ ionic liquids. This is expected because the RMIBeti ionic liquids consist of a higher concentration of fluorinated carbons. The figure also shows that an increase in the alkyl chain length decreases the density. This is expected because hydrocarbons are less dense than fluorinated carbons. The longer alkyl chains increase the proportion of hydrocarbons to fluorinated carbons in the ionic liquid's composition. Increasing temperature decreases the density of both RMIBeti and $RMINTf_2$ ionic liquids. This is a typical property of materials and is therefore expected.

Conductivity

The conductivity of $RMINTf_2$ ionic liquids compared to $RMIBF_4$ ionic liquids at different temperatures are shown in Figure 32.

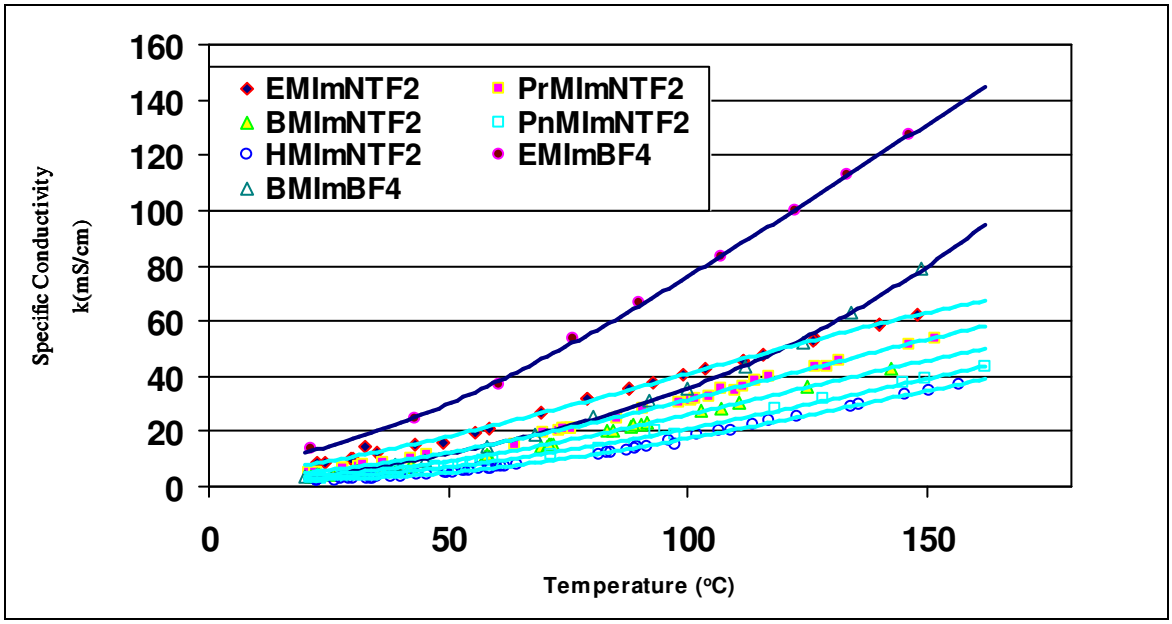

Figure 32. The conductivity of $RMINTf_2$ and $RMIBF_4$ ionic liquids as a function of temperature

It can be seen from Figure 32 that $RMINTf_2$ ionic liquids have lower conductivities than $RMIBF_4$ ionic liquids. The BF_4^- anion is much smaller and more spherical than the NTf_2^- anion and therefore would move with less resistance. It is also shown that ionic liquids with the same anion but shorter alkyl chains have higher conductivities. This is likely due to the lower viscosities of ionic liquids with shorter alkyl chains. As the temperature increases from 20 °C to 150 °C the conductivity increases by a factor of about 10.

The conductivity of RMIBeti ionic liquids compared to the conductivity of $RMIBF_4$ ionic liquids is shown in Figure 33.

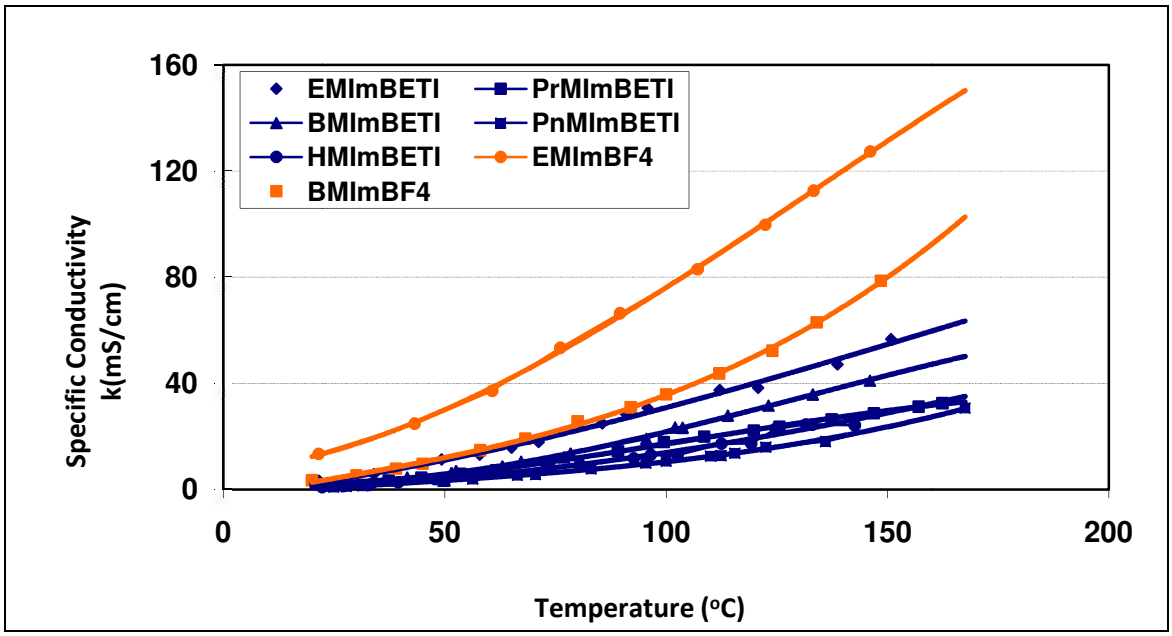

Figure 33. The conductivity of RMIBeti compared to the conductivity of $RMIBF_4$ ionic liquids

It can be seen from Figure 33 that RMIBeti ionic liquids have lower conductivities than $RMIBF_4$ ionic liquids. The BF_4^- anion is much smaller and more spherical than the NTf_2^- anion and therefore would move with less resistance. It is also shown that, generally, RMIBeti ionic liquids with shorter alkyl chains have higher conductivities. This is likely due to the lower viscosities of ionic liquids with shorter alkyl chains.

A comparison of $RMIBF_4$, RMIBeti and $RMINTf_2$ ionic liquids is shown in Figure 34.

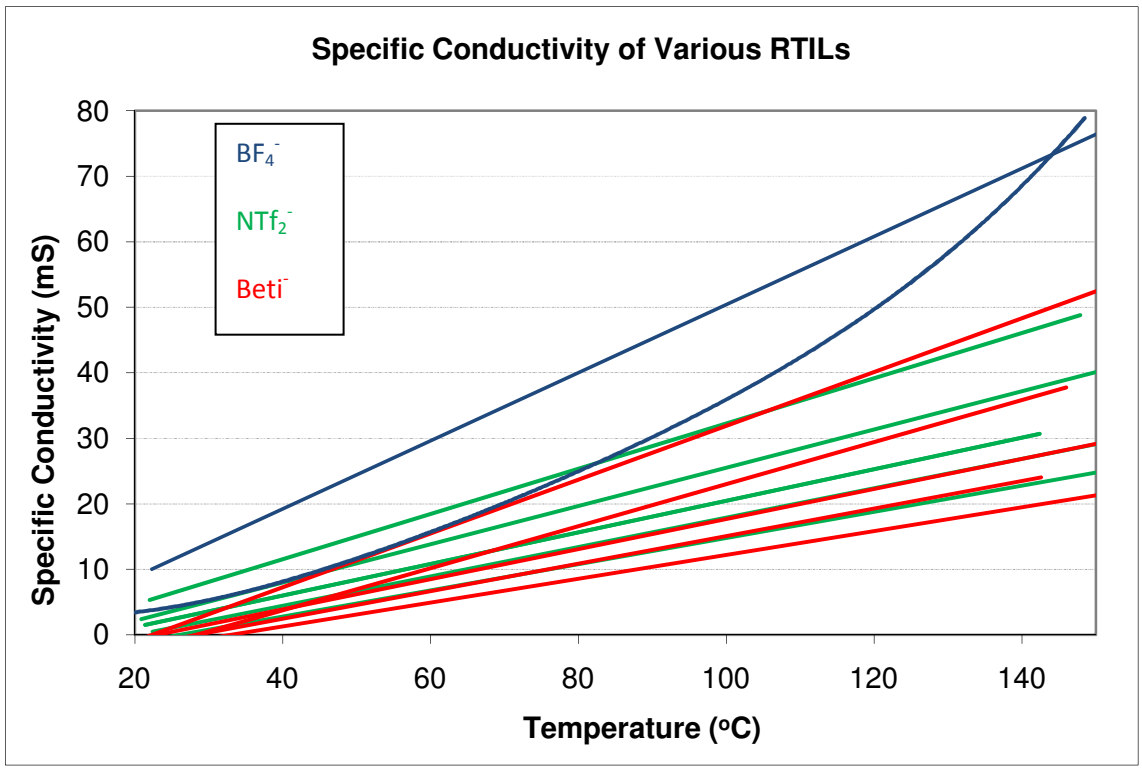

Figure 34. The conductivity of $RMIBF_4$ compared to the conductivity of RMIBeti and $RMINTf_2$ ionic liquids

From Figure 34 it is shown that the conductivities of analogous RMIBeti and $RMINTf_2$ ionic liquids are about the same.

Water Absorption and Desorption by Ionic Liquids

It is very important that the amount of impurities in ionic liquids is minimized because they can alter some chemical and physical properties. The most common impurity is excess of Cl^- which can be easily detected by cyclic voltammetry or by reaction with Ag^+. Sometimes the ionic liquids contain some organic impurities which are yellow or red in color. This discolorization is observed if the glassware used for the synthesis was washed with acetone and/or if the starting material N-methylimidazole was not distilled prior to use.

The other most common impurity in ionic liquids is water which can be absorbed by ionic liquids when exposed to moist air. Although the ionic liquids with alkyl groups containing more than three carbon atoms do not mix with water, they still contain some water (by absorption from moist air). The water absorption and desorption by $RMINTf_2$ ionic liquids containing NTf_2^- anion and different alkyl groups was studied by exposing the ionic liquids to the environment containing 60% and 6% relative humidity at 25 °C. This was done in a controlled atmosphere box. The amount of water was measured at different time intervals by a coulometric Karl-Fisher method. The data are shown in Figures 35 and 36, and in Table 27. More data tables can be found in the Appendix. At the beginning of the exposure ionic liquids absorb water relatively fast and reach a saturation level after about 20,000 minutes. The saturation level is achieved much faster by the ionic liquids containing $Beti^-$ or BF_4^- anions. After exposing water saturated ionic liquids at 60% humidity the humidity was lowered to 6% relative

humidity. The ionic liquids then desorb water to less than 1000 ppm. The water desorption curves for $RMINTf_2$ ionic liquids is given in Table 27 and shown in Figure 36.

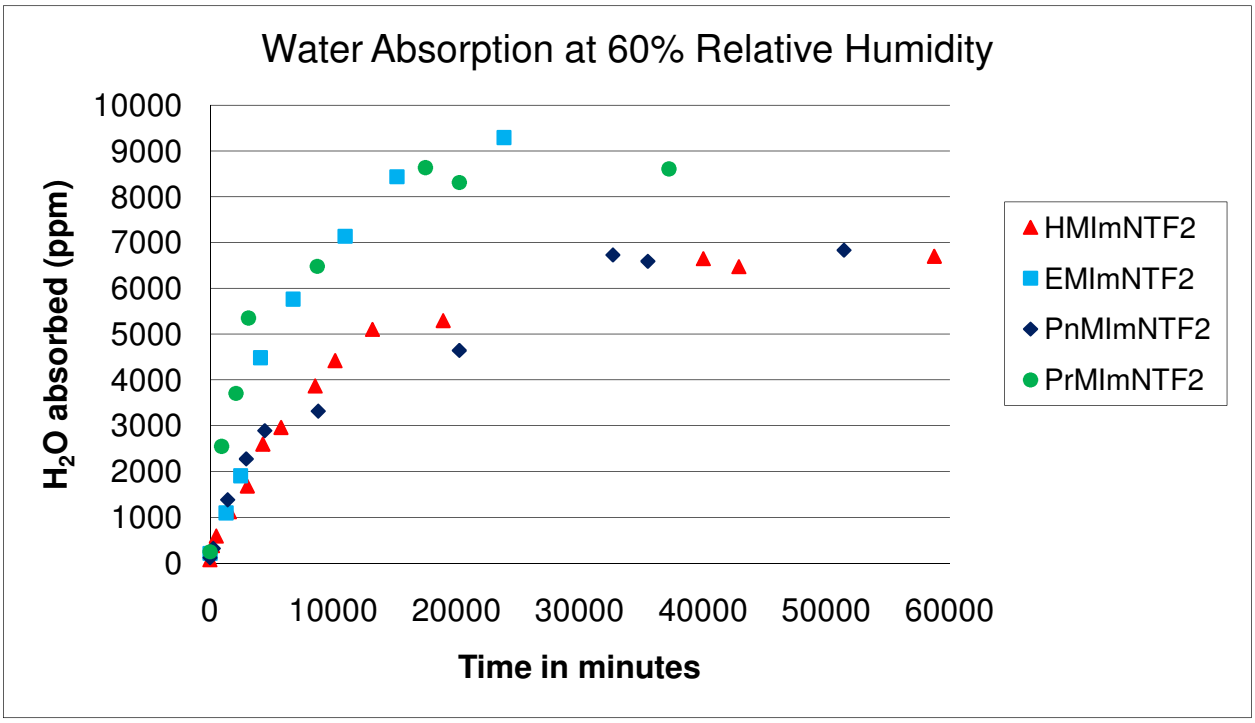

Figure 35. Water absorption by $RMINTf_2$ ionic liquids at 60% relative humidity.

Table 26. Water content (ppm) of $RMINTf_2$ ionic liquids when saturated at room temperature and atmospheric pressure.

Time Expired	$EMINTf_2$	$PrMINTf_2$	$BMINTf_2$	$PnMINTf_2$	$HMINTf_2$
One Month	19900	19500	14800	12200	12400
Four Months	20900	No data	No data	13100	No data

It can be seen from Table 26 that the maximum water absorption is achieved by ionic liquids containing smaller alkyl chain length.

Table 27. Desorption data for $RMINTf_2$ ionic liquids at 6% relative humidity

Time (min)	$EMImNTf_2$	$PrMImNTf_2$	$PnMImNTf_2$	$HmImNTf_2$
0	9290	8610	6830	6700
1129	4210	4110	2640	712
1460	3150	3680	2460	729
2532	1730	2000	1780	434
4067	860	956	897	374
5453	700	712	787	378
6819	623	772	657	353

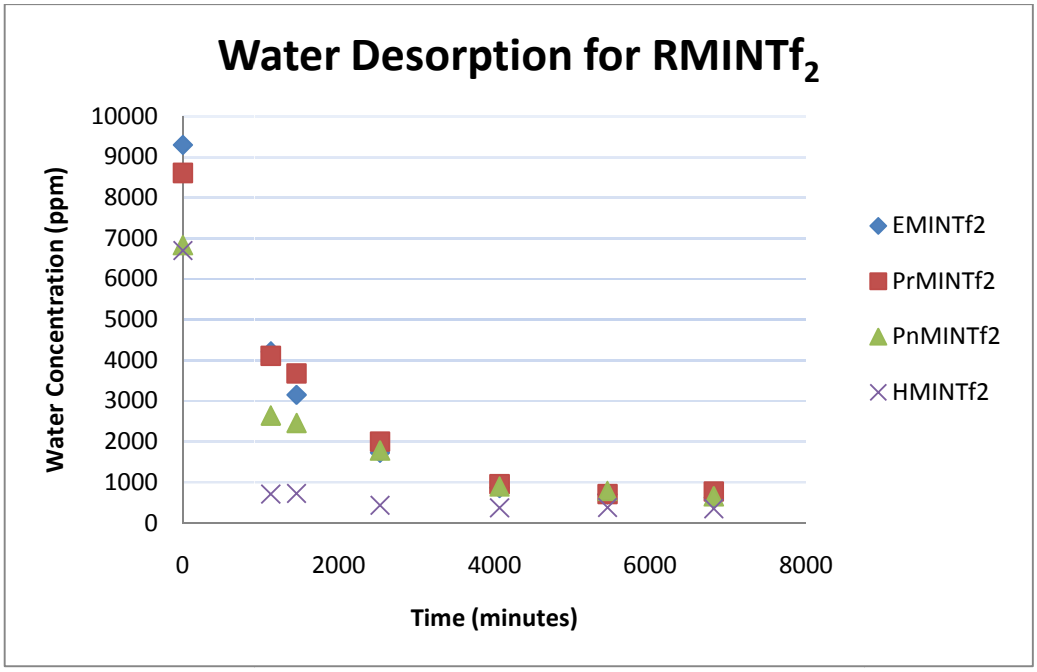

Figure 36. Water desorption curves for $RMINTf_2$ ionic liquids.

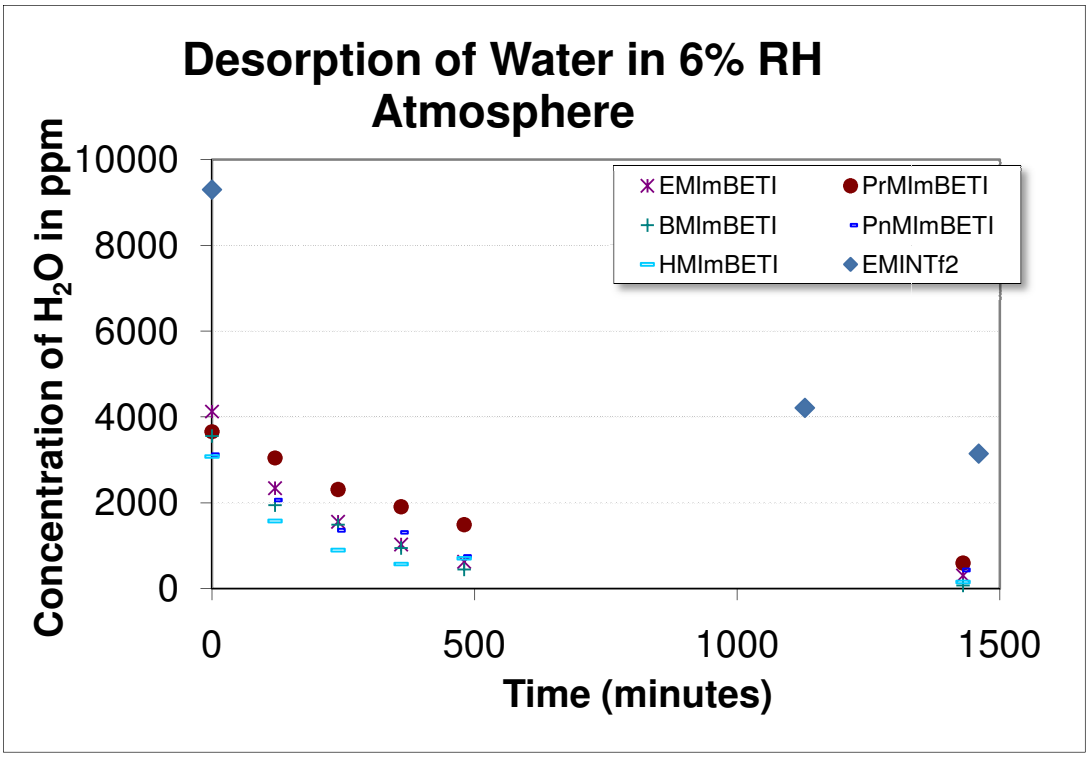

Figure 37. Water desoption curves for RMIBeti$^-$ ionic liquids.[11]

Infrared Spectra of RTILS

The infrared (IR) spectra of $EMINTf_2$ (Figure 40), $PrMINTf_2$ (Figure 42), $PnMINTf_2$ (Figure 44), and $HMINTf_2$ (Figure 46), show that the water IR bands increase in magnitude as the concentration of water increases. At relatively low concentration of water (<200 ppm) no IR bands in the 3300-3700 cm^{-1} range are observed. As the concentration of water increases, from 200 ppm to 5200 ppm, two sharp bands at 3650 cm^{-1} and 3550 cm^{-1} are observed. The same sharp bands are observed for water in the vapor phase. This implies that at the low concentration of water all water molecules are in monomeric form and do not form hydrogen bonds among themselves. As the concentration of water in ionic liquids was further increased, a new broad band at about 3420 cm^{-1}, appeared and increased in size. This broad band is characteristic for

the presence of hydrogen bonds between water molecules. This implies that as the concentration of water is increased the water molecules are close enough to start forming hydrogen bonds. Similar behavior was previously observed for ionic liquids containing BF_4^- and $Beti^-$ anions. The IR spectrum of $BMINTf_2$ containing less than 100 ppm water shows no absorption bands due to the presence of water (Figure 38).

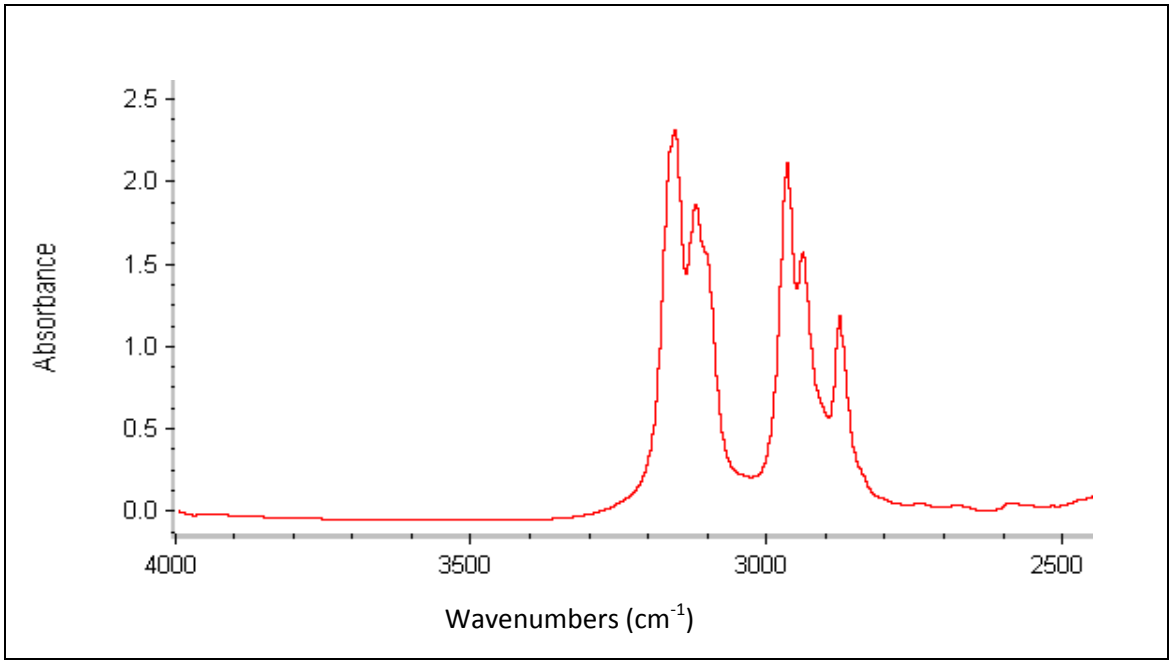

Figure 38. IR spectra for $BMINTf_2$ IL containing less than 200 ppm H_20

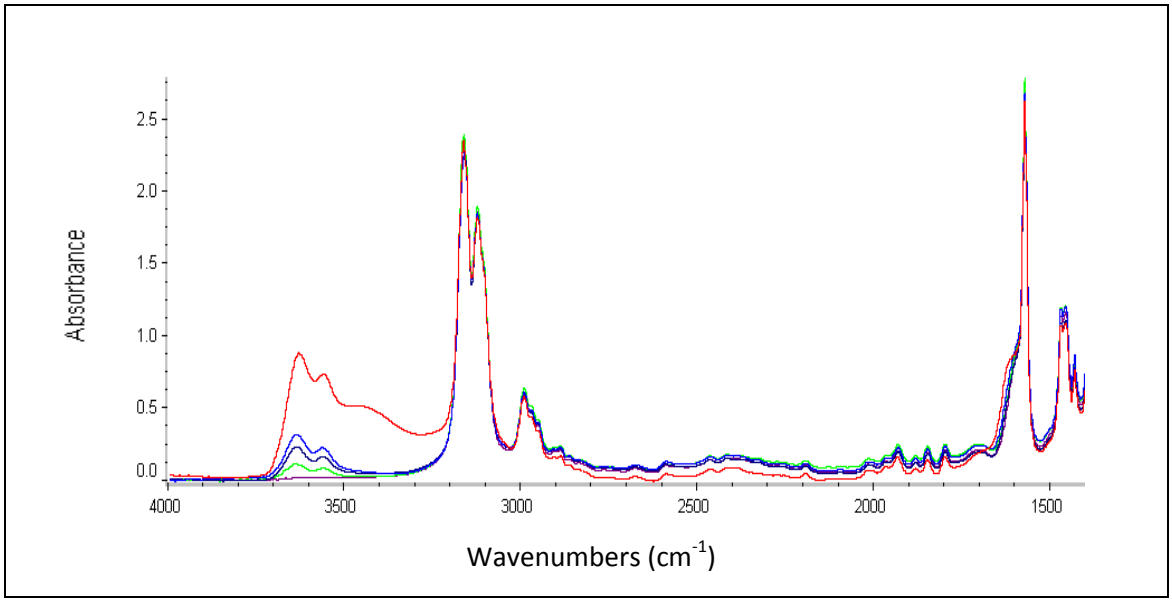

Figure 39. IR spectra for $EMINTf_2$ ILs containing <200, 1600, 4300, 5700 and 22000 ppm H_20

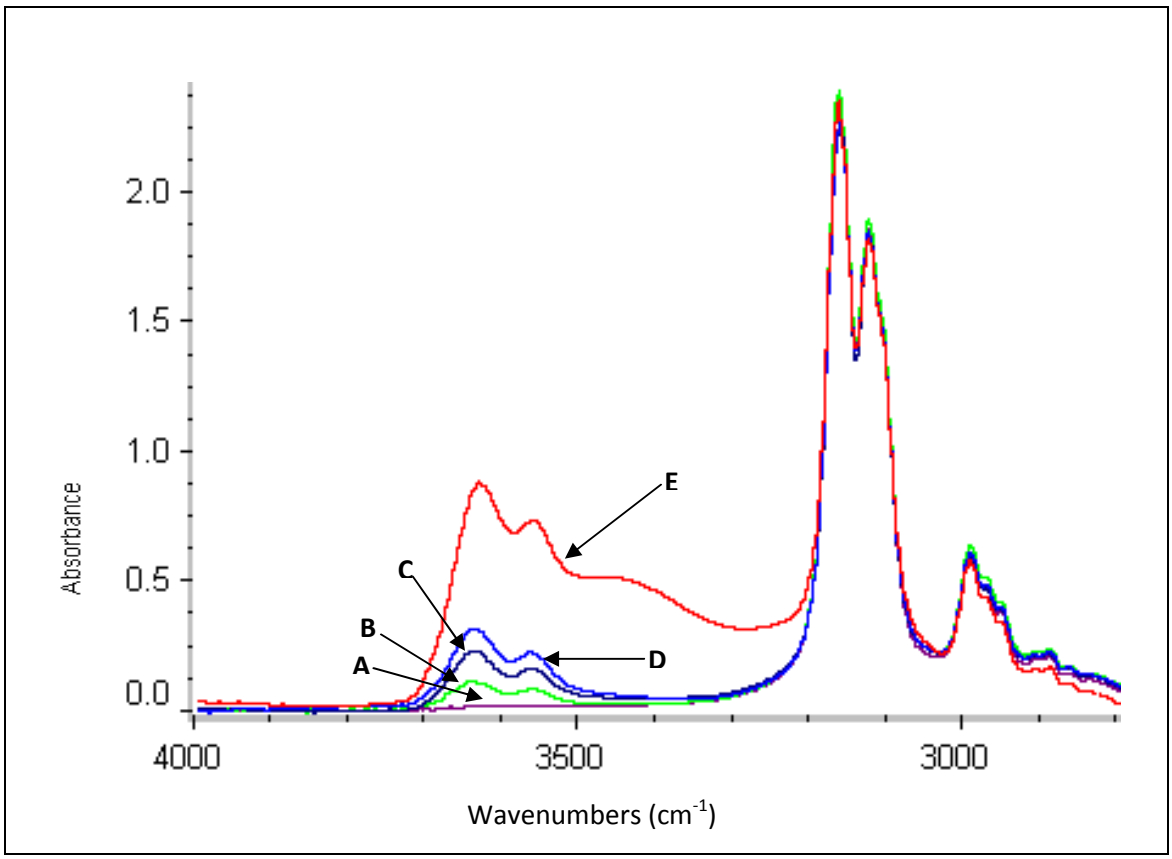

Figure 40. IR spectra for $EMINTf_2$ ILs containing <200 (A), 1600 (B), 4300 (C), 5700 (D) and 22000 (E) ppm H_20

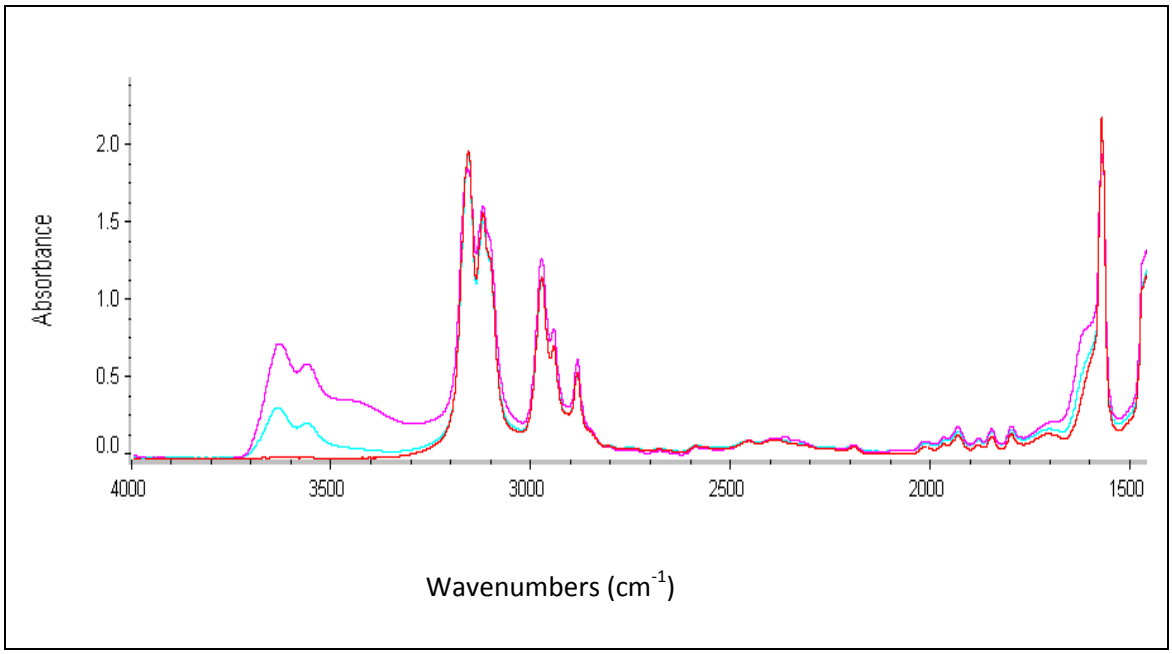

Figure 41. IR spectra for $PrMINTf_2$ ILs containing <200, 7300 and 19000 ppm H_20

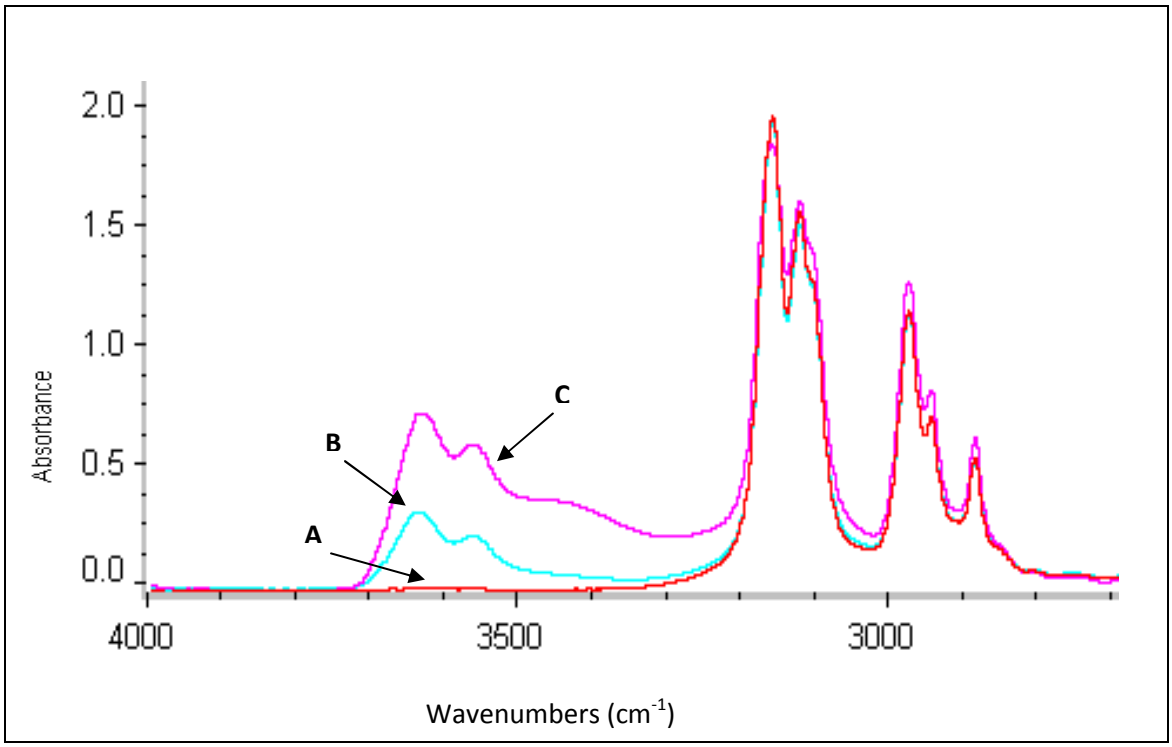

Figure 42. IR spectra for $PrMINTf_2$ ILs containing <200 (A), 7300 (B) and 19000 (C) ppm H_20

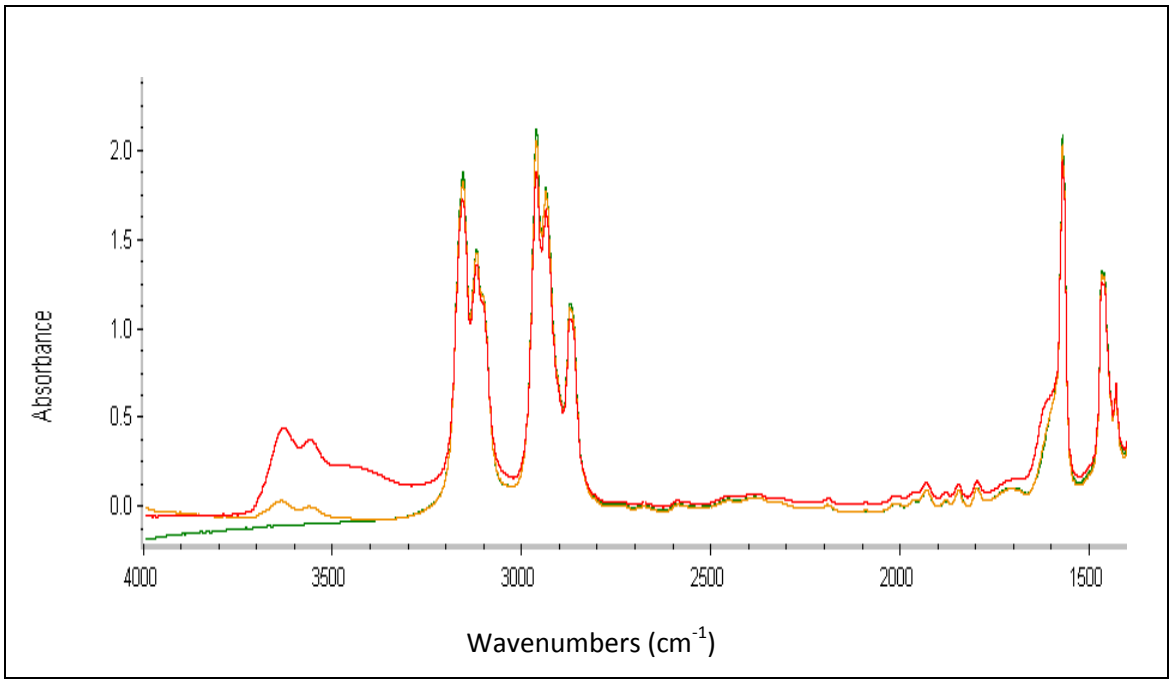

Figure 43. IR spectra for $PnMINTf_2$ ILs containing <200, 2400, and 15500 ppm H_20

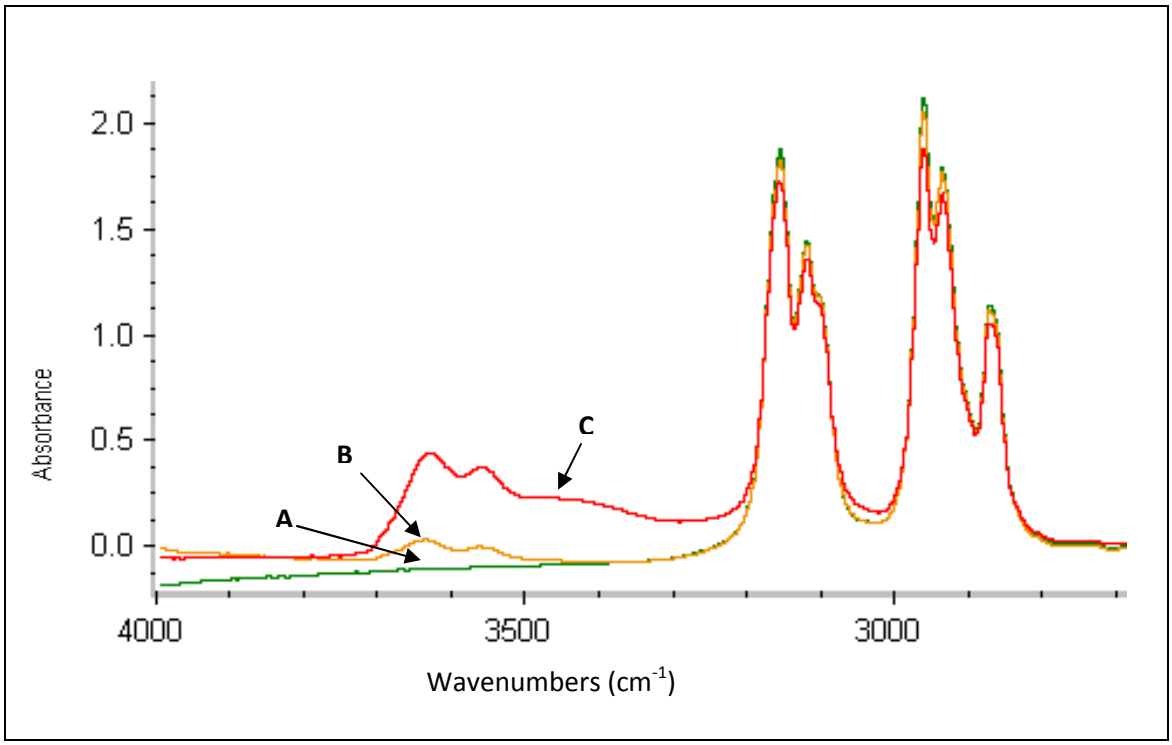

Figure 44. IR spectra for $PnMINTf_2$ ILs containing <200 (A), 2400 (B), and 15500 (C) ppm H_20

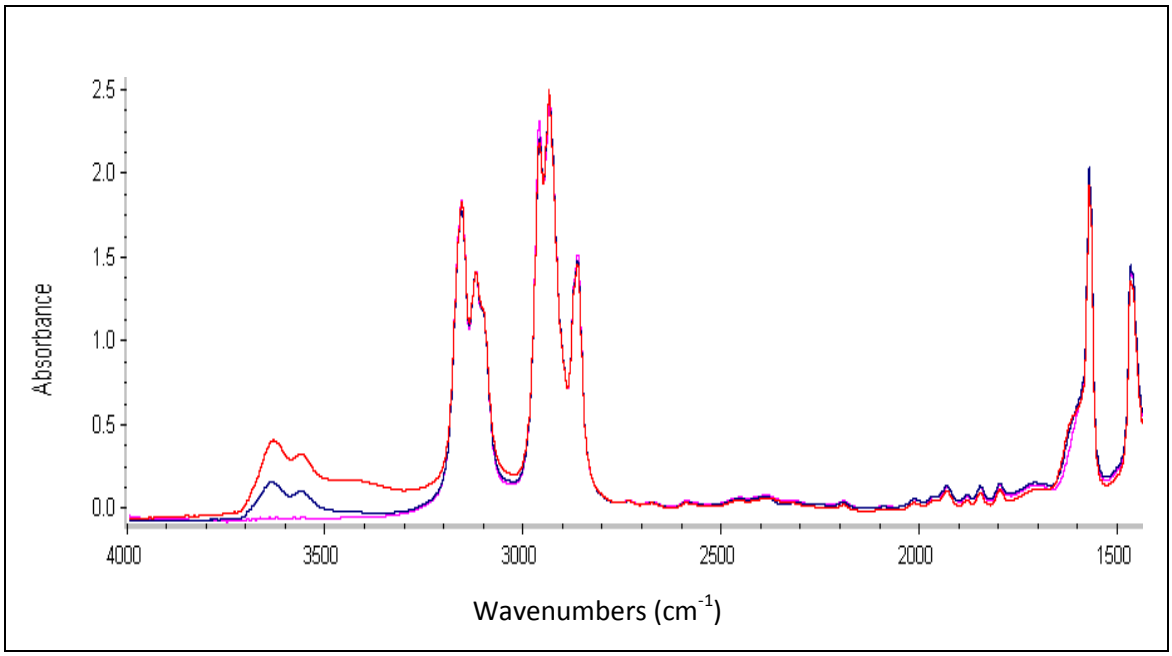

Figure 45. IR spectra for $HMINTf_2$ ILs containing <200, 6000 and 12400 ppm H_20

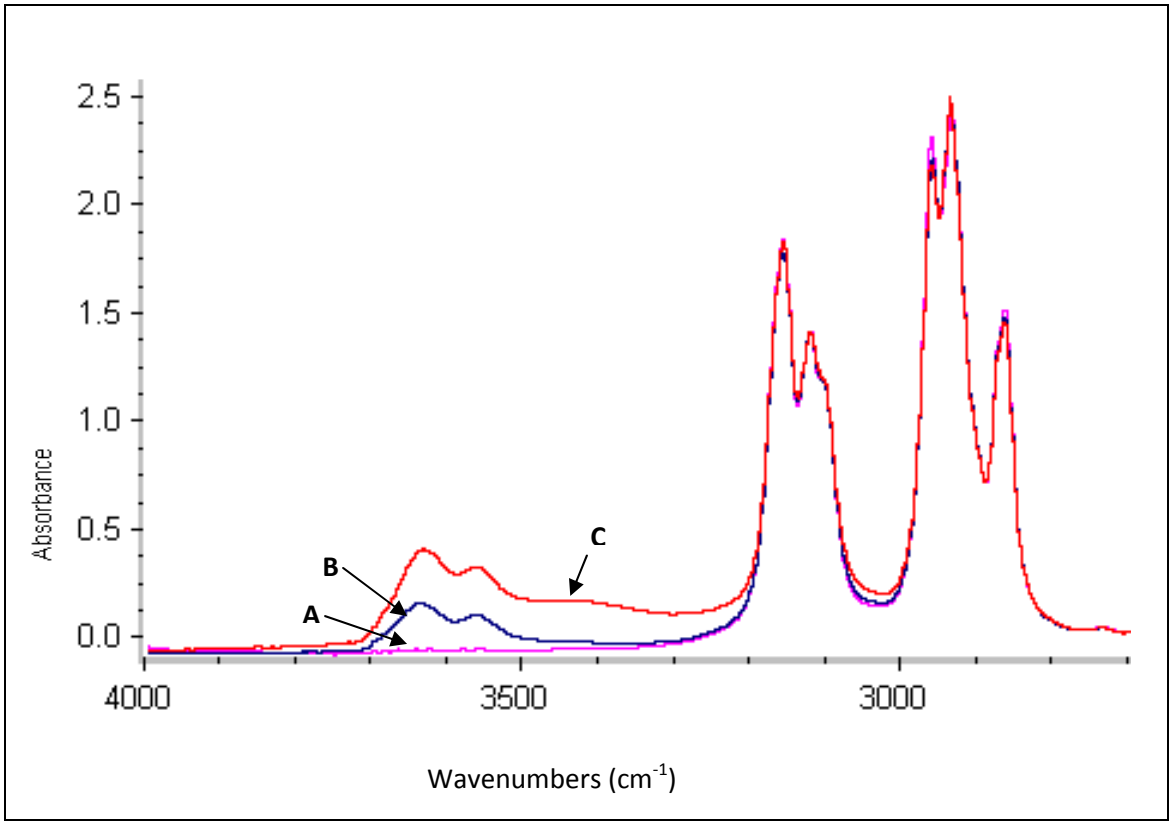

Figure 46. IR spectra for $HMINTf_2$ ILs containing <200 (A), 6000 (B) and 12400 (C) ppm H_20.

Determination of Diffusion Coefficients of Ionic Liquids containing NTf_2^- anions using Cyclic Votammagrams

The cyclic voltammagrams of ferrocene in $PnMINTf_2$ at several scan rates using a platinum electrode is shown in Figure 47. The ferrocene concentration was 47.4 $x10^{-6}$ mol cm^{-3}. The values of anodic peak currents ($I_{p,a}$) as a function of scan rates are shown in Table 28.

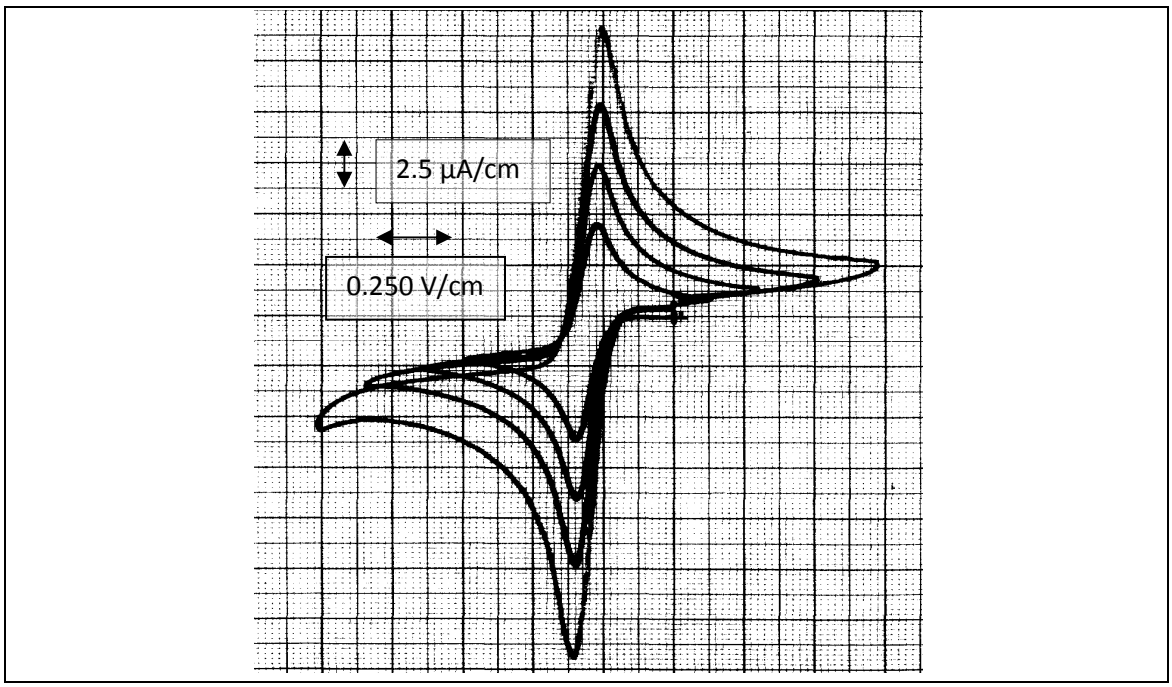

Figure 47. CVs of ferrocene in $PnMImNTf_2$ using a platinum working electrode. The water concentration was measured at 3040 ppm.

Table 28. Peak heights and scan rates for ferrocene in $PnMINTf_2$.

peak height (cm)	µA/cm	µA	scan rate (V/sec)	$(\text{scan rate})^{1/2}$
5.75	2.5	14.375	0.20	0.447
4.25	2.5	10.625	0.10	0.316
3.05	2.5	7.625	0.05	0.224
2.00	2.5	5.000	0.02	0.141

From Table 28 a plot of the peak height (in µA) versus the square root of the scan rate and is shown in Figure 48.

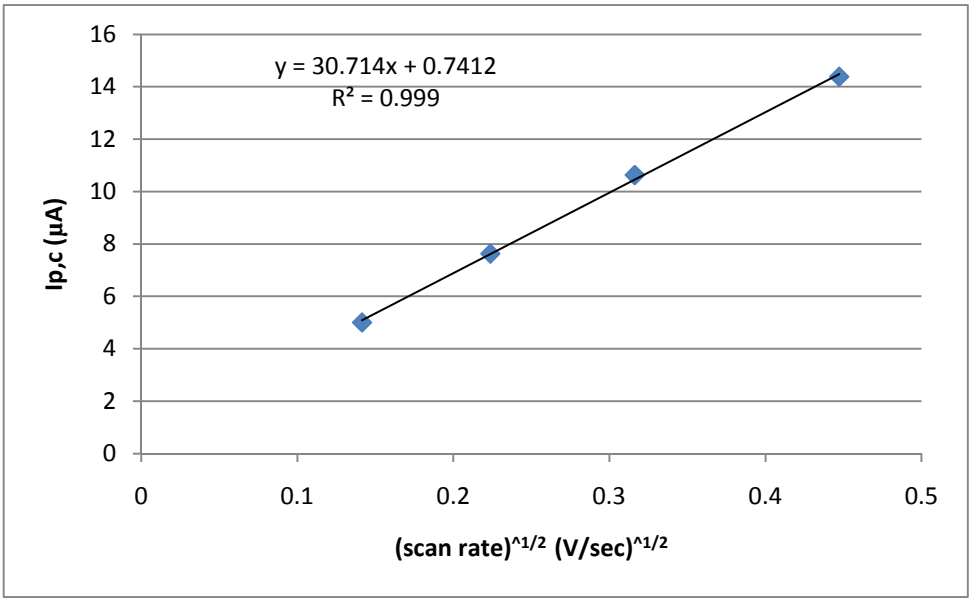

Figure 48. Plot of peak height versus the square root of the scan rate for $PnMINTf_2$ ionic liquid

Using the slope in Figure 48 and using the (Randel-Sevcik) equation, $Ip = (2.687 \times 10^5\ mol^{-1}\ V^{-1/2})\ n^{3/2}\ D^{1/2}\ A\ C$. The diffusion coefficients for different ionic liquids were calculated and are shown in Table 29.

Table 29. Randel-Sevcik data for ferrocene in $PnMINTf_2$.

$n^{3/2}$	$F R^{-1} T^{-1}$	C (mol cm^{-3})	A (cm^2)	k (A $V^{-1/2}$ $sec^{-1/2}$)	$D^{½}$ ($cm^{½}$ $sec^{-1/2}$)
1	$2.69x10^5$	$47.4 x10^{-6}$	7.1 x10-2	30.7 x10-6	$340 x10^{-6}$

Using the Randel-Sevcik equation and the data in Table 29, the diffusion coefficient of ferrocene in $PnMINTf_2$ was calculated to be 1.15×10^{-7} cm sec^{-1}. CV scans and tables of data derived from them for other ionic liquids can be found in the Appendix. A summary of the diffusion coefficient results can be found in Table 30.

Table 30. Diffusion coefficients of ferrocene in ionic liquids determined using cyclic voltammetry.

Ionic Liquid	Working Electrode	Diffusion Coefficient (cm sec^{-1})
$EMINTf_2$	Glassy Carbon	$3.42x10^{-7}$
$EMINTf_2$	Platinum	$2.10x10^{-7}$
$BMINTf_2$	Glassy Carbon	$1.18x10^{-7}$
$BMINTf_2$	Platinum	$8.78x10^{-8}$
$PnMINTf_2$	Glassy Carbon	$9.00x10^{-8}$
$PnMINTf_2$	Platinum	$1.15x10^{-7}$
$HMINTf_2$	Glassy Carbon	$1.16x10^{-7}$
$HMINTf_2$	Platinum	$1.16x10^{-7}$

A plot of the diffusion coefficients as a function of alkyl chain length is shown in Figure 49.

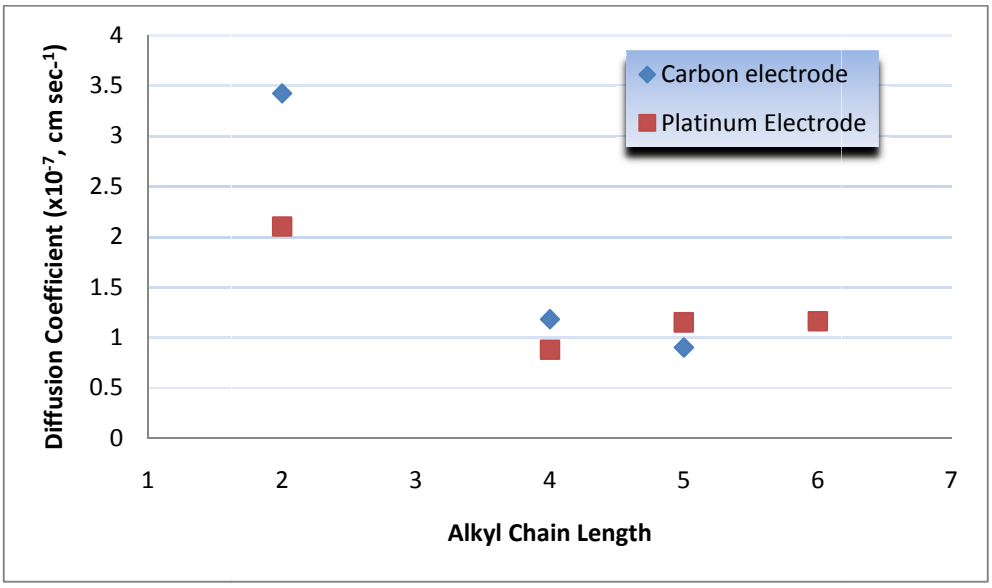

Figure 49. Diffusion coefficient compared to chain length $RMINTf_2$ ionic liquids

Figure 49 shows that the diffusion coefficient changes little as alkyl chain length changes from 4 to 6. $EMINTf_2$ has a higher diffusion coefficient that $BMINTf_2$, $PnMINTf_2$, and $HMINTf_2$. This would be expected because $EMINTf_2$ has a higher conductivity than the other $RMINTf_2$ ionic liquids, and is therefore less resistant to charge movements.

Electrochemistry

Cyclic voltametry was used to obtain the electrochemical windows of various $RMINTf_2$ ionic liquids. The measurements were done using a glassy carbon and platinum working electrodes, silver quasi reference and platinum auxiliary electrodes. The voltammograms are obtained after deaerating the ionic liquids with nitrogen. The cyclic voltammograms (CVs) are shown in Figure 50. As the size of the alkyl group increases from ethyl to hexyl the potential windows increase.

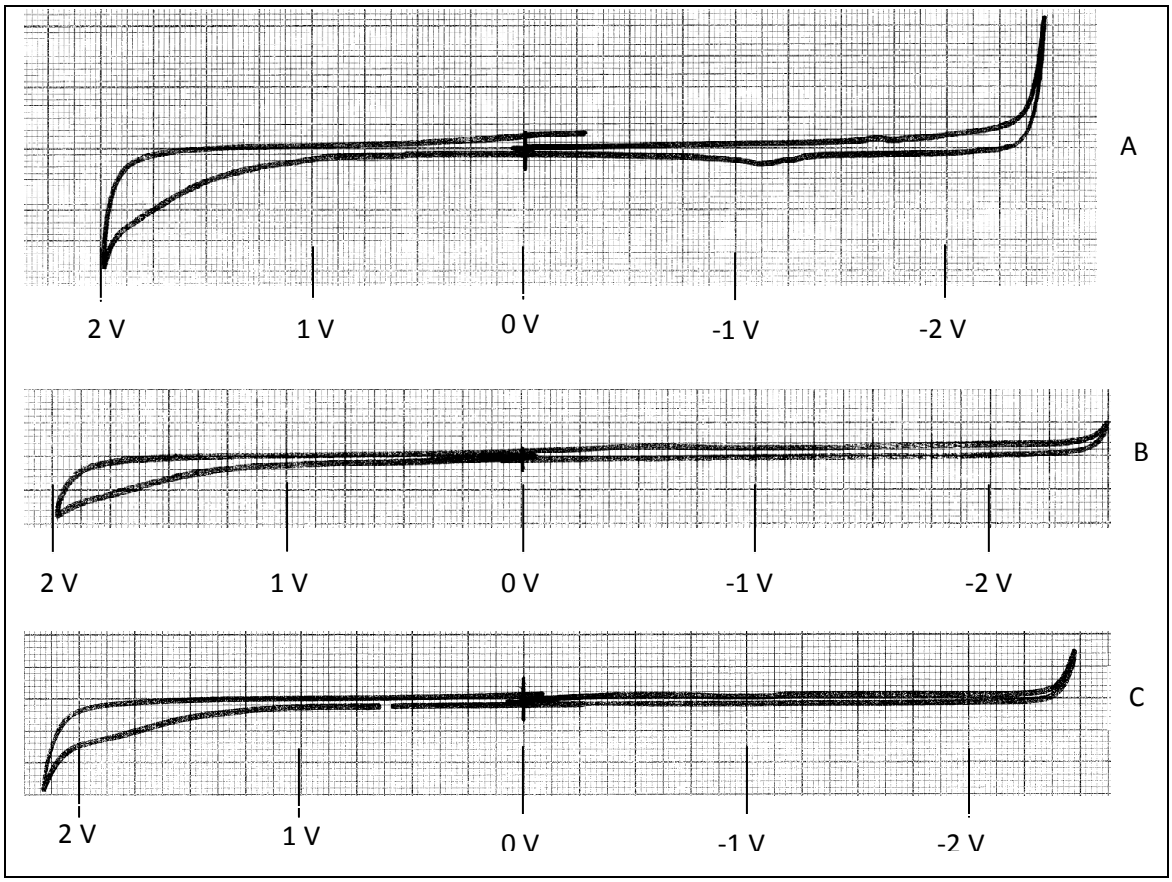

Figure 50. Cyclic voltammograms of ionic liquids, $RMINTf_2$, containing different alkyl groups on a GC working electrode.

A) $EMINTf_2$ (1700 ppm H_2O), B) $PnMINTf_2$ (1070 ppm H_2O), C) $HMINTf_2$ (560 ppm H_2O)

Influence of the amount of water present in ionic liquids on the potential windows is shown in Figures 51-54. The size of the potential window decreases as the concentration of water increases. This is particularly visible when the platinum working electrode is used instead of the glassy carbon electrode.

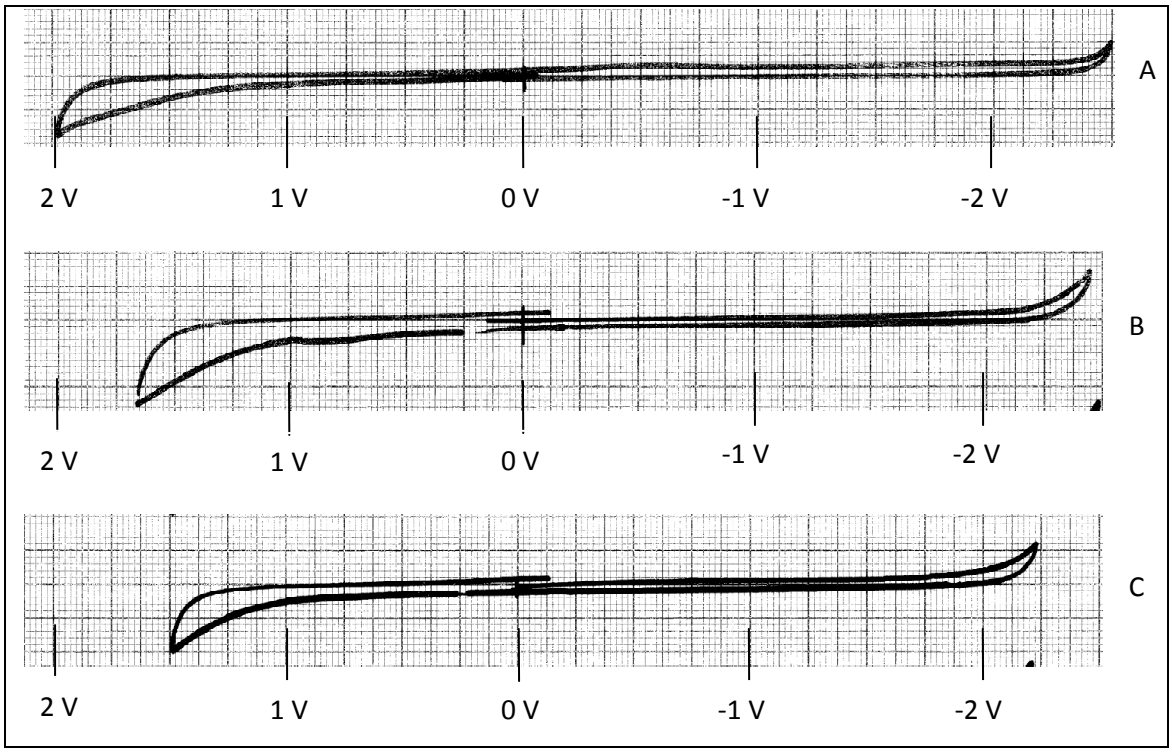

Figure 51. CVs of $PnMINTf_2$ using a GC working electrode. Water concentration: A) 2000 ppm, B) 6130 ppm, C) 11070 ppm

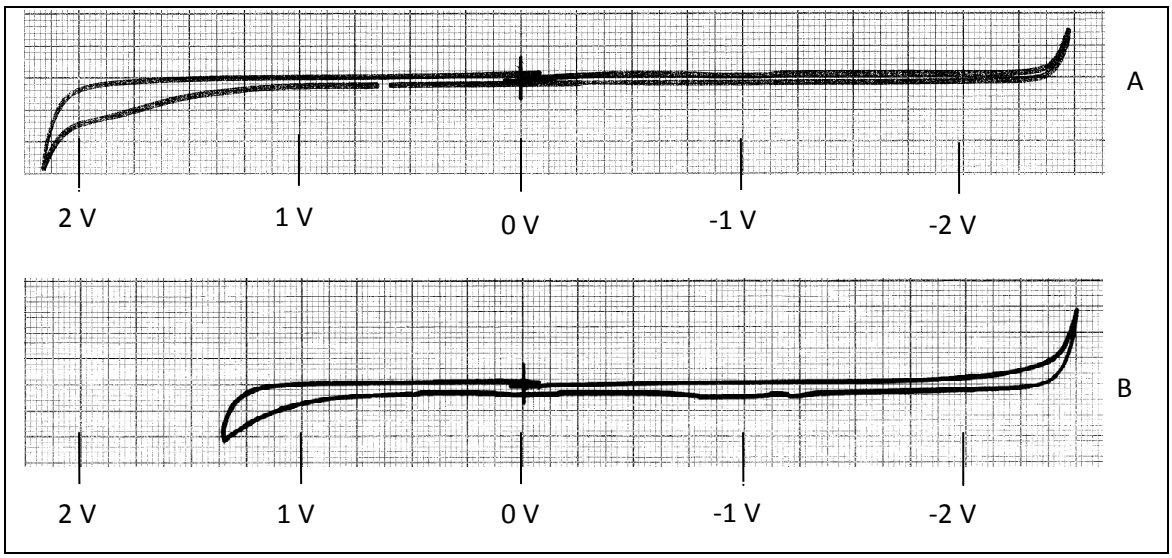

Figure 52. CVs of $HMINTf_2$ ionic liquid using a GC working electrode. Water concentration: A) 560 ppm, B) 7910 ppm.

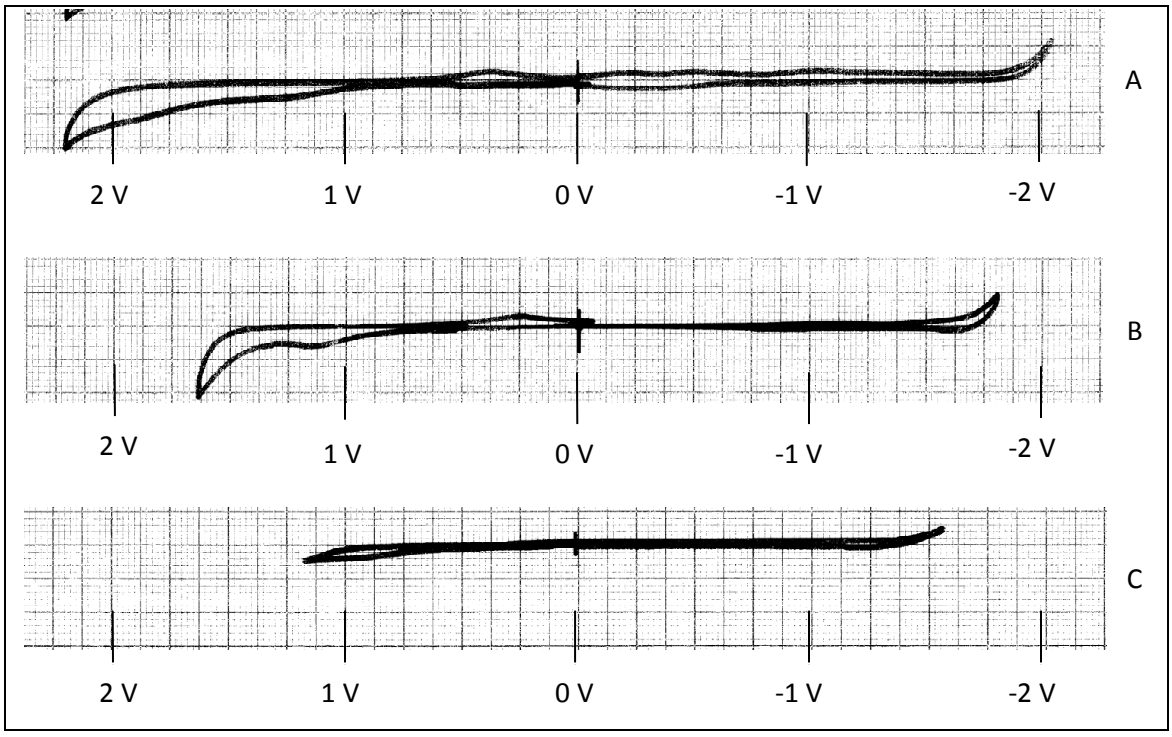

Figure 53. CVs of $PnMINTf_2$ ionic liquid using a platinum working electrode.

Water concentration: A) 1070 ppm, B) 6130 ppm, C) 12000 ppm.

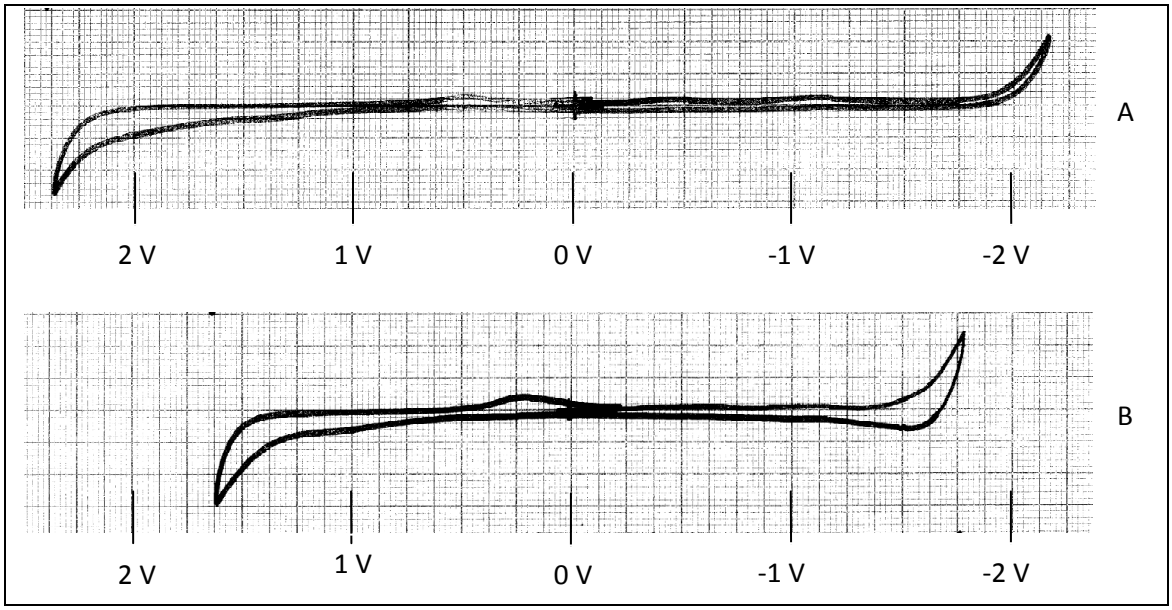

Figure 54. CVs of $HMINTf_2$ ionic liquid using a platinum working electrode.

Water concentration: A) 560 ppm, B) 7910 ppm.

IV. CONCLUSION

Several new imidazolium type ionic liquids, $RMINTf_2$, containing NTf_2^- anions have been synthesized and characterized. Their physical and electrochemical properties were measured and compared to the properties of ionic liquids containing the same cation and different $Beti^-$ anion.

Their thermal properties were studied using TGA and DSC methods. All the ionic liquids containing NTf_2^- anion are thermally stable up to ~310 ˚C. The comparison to the ionic liquids with $Beti^-$ anion containing the same cation demonstrated that the ionic liquids with the NTf_2^- anion are more thermally stable.

The DSC experiment showed that only $EMINTf_2$ shown a sharp melting point at -18.26 ˚C. The ionic liquids with larger R groups ($PrMINTf_2$, $BMINTf_2$, $PnMINTf_2$, $HMINTf_2$) when cooled formed glasses.

The density studies showed that the density decreases with increasing chain length and with temperature. In comparison with corresponding $Beti^-$ ionic liquids, NTf_2^- anion containing ionic liquids have smaller densities.

Water absorption studies showed that NTf_2^- ionic liquids absorbed more water than corresponding $Beti^-$ ionic liquids. Infrared spectra displayed the presence of peaks at 3550 cm^{-1} and 3650 cm^{-1}, which are characteristic to the presence of monomeric water. As the amount of water increases a new broad band at 3420 cm^{-1} appeared and increased in size as the water concentration increased. This clearly demonstrates

that as the concentration of water increased the monomeric water polymerized by forming hydrogen bonds.

Conductivity studies showed that as the length of alkyl groups increased the conductivity decreased. In comparison to $Beti^-$ ionic liquids the NTf_2^- ionic liquids showed larger conductivity.

The cyclic voltammetry studies showed that NTf_2^- ionic liquids have ~4.2 V electrochemical window. However, this window decreases as the amount of water in ionic liquids increases.

V. REFERENCES

1. Wassersheid, P.; Welton, R. (Editors), *Ionic Liquids in Synthesis 2nd Ed*.; Wiley-VCH: Weinheim, Germany, 2007.

2. Koel, Mihkel Ed., *Ionic Liquids in Chemical Analysis*. CRC Press New York, 2009.

3. Guidotti, Ronald A., Masset, Patrick. Journal of Power Sources 161, **2006,** 1443.

4. Lovering, David G., Gale, Rogert J. Eds. *Molten Salt Techniques Volume One*; Plenum Press: New York and London

5 Marsh, K.N.; Boxall, J.A.; Lichtenthaler R. *Fluid Phase Equilibria*, 219, **2004**, 93.

6 Wilkes, John S. *Green Chemistry*, **2002**, 4, 73-80.

7. Hurley, F. H.; Wier, T. P. *J. Electrochem. Soc.* **1951**, *98*, 203

8. J.S. Wilkes, J.A. Levisky, R.A. Wilson, C.L. Hussey, *Inorg. Chem*. 21, **1982**, 1263.

9. Henderson, Wesley A., et al. *Linking Together Ion Structure, Crystal Packing and Salt Thermal Properties*. PRiME 2008 Meeting, The Electrochemical Society Abs 2958

10. Bonhôte, P., Dias A.P., Papageorgiou N., Kalyanasundaram K., Grätzel, M. *Inorg. Chem* **1996**, 35, 1168.

11. Dyar, H. A., *The synthesis, electrochemical and thermal characterization of 1-ethyl-3-methylimidazolium and 1-ethyl-2-methylpyrazolium based room temperature ionic liquids*, M.S. Thesis, **1999**, Wright State University.

12. Popp, B. V., *Imidazolium and pyrazolium based room temperature ionic liquids: Studies of physical, thermal and electrochemical properties*, M.S. Thesis, **2002**, Wright State University.

13. Decerbo, J. N., *1-alkyl-3-methylimidazolium bis(pentafluoroethylsulfonyl)imide based ionic liquids: A study of their physical and electrochemical properties,* M.S. Thesis, **2008**, Wright State University.

14. Widegren, J. A., Saurer, E. M., Marsh, K.N., Magee, J.W. *J. Chem. Thermodynamics* 37, **2005**, 569.

15. Barrose-Antle, L. E., Aldous, L., Hardacre, C., Bond, A. M., Compton, R. G. *J. Phys. Chem C*. **2009**, 113, 7750.

16. Ohno, H. *Electrochemical Aspects of Ionic Liquids*; Wiley Interscience. Hoboken, N.J., 2005.

17. Cammarata, L., Kazarian, S. G., Salter, P.A., Welton, T. *Phys. Chem. Chem. Phys.* **2001**, 3, 5192.

18. Ohno, H., Fukumoto, K., Kohno, Y., *Unique phase behavior of ionic liquid/water mixture*. PRiME 2008 Meeting, The Electrochemical Society. Abs 2960.

19. Chang, K. *With a Splash of Salt, Industry May Reap Environmental Advantages*. New York Times D2, April 24, **2001**.

20. Garcia, B. Lavallée, S., Perron, G., Michot, C., Armand, M., *Electrochimica Acta* 49, **2004**, 4583.

21. Yoshio, M., Brodd R. J., Kozawa A., Eds. *Lithium Ion Batteries Science and Technology*. Springer. New York. 2009.

22. Giroud N.M, Rouault H., Chainet E., Poignet J.C., *Physicochemical study of ionic liquids' structure and influence of the lithium salt associated*. PRiME 2008 Meeting, *The Electrochemical Society*. Abs 0026

23. Silverstein, R. M., Webster, F. X., Kiemle, D. J., *Spectrometric Identification of Organic Compound,s 7th ed.*; John Wiley and Sons, Inc: Hoboken, N.J., 2005.

24. Jones, G., Prendergast, M. J.; *J. Am. Chem. Soc.* **1937**, *59* (4), 731.

25. Tsierkezos, Nikos G.; *J Solution Chem*. **2007**, 36, 289.

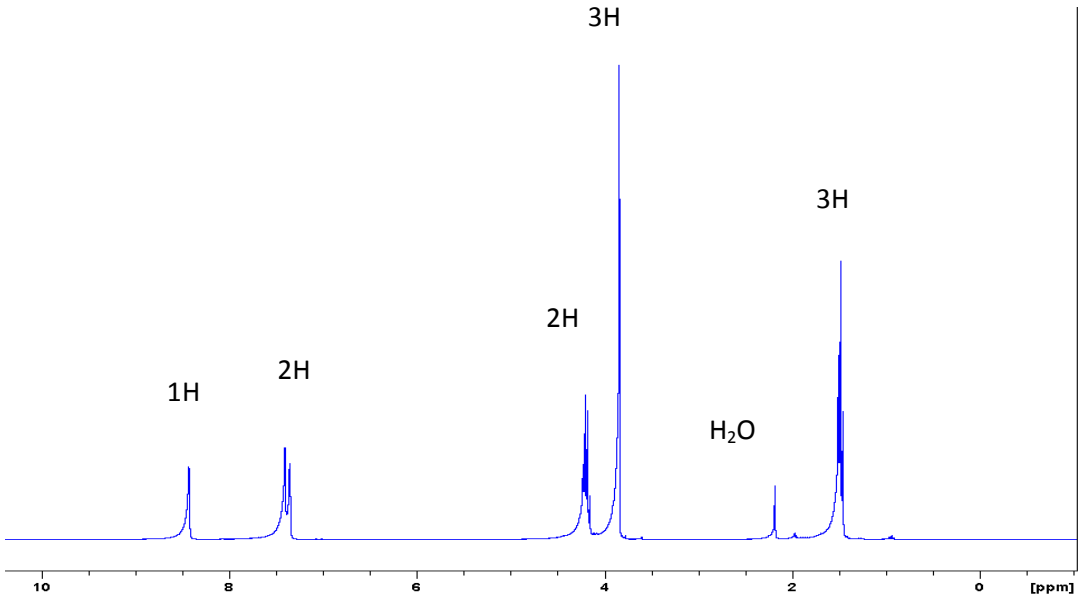

Figure 55. The proton NMR spectrum for $EMINTf_2$

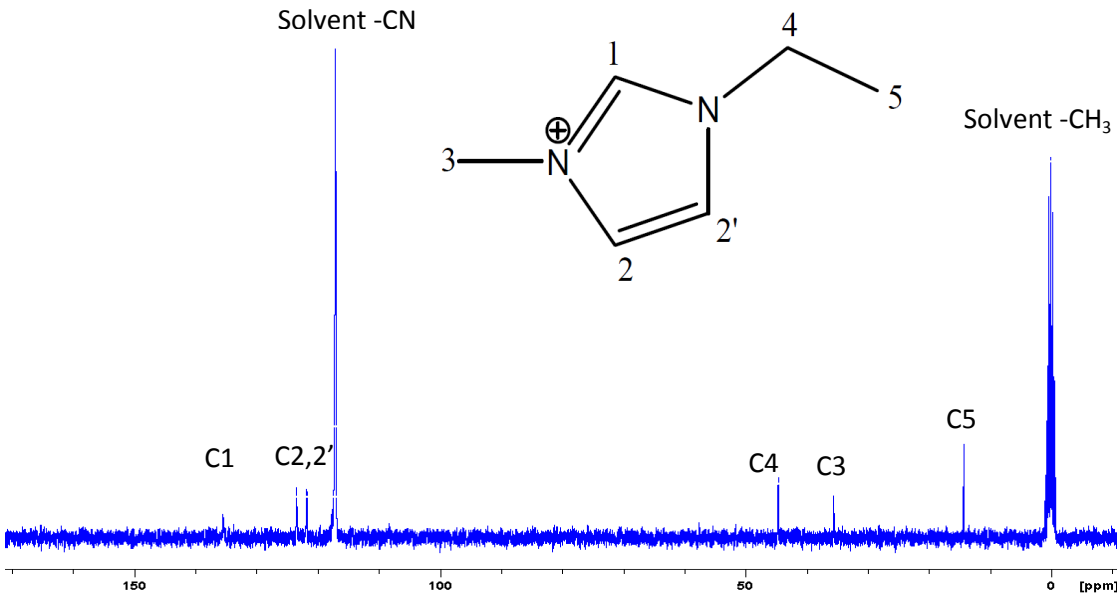

Figure 56. The carbon NMR spectrum for $EMINTf_2$

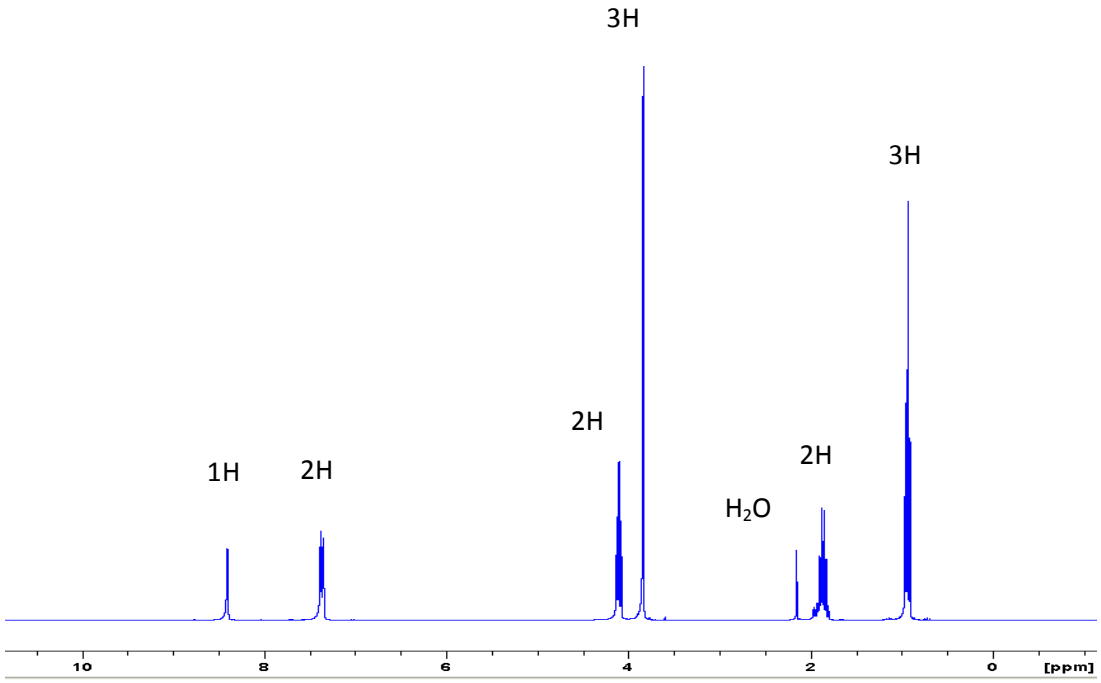

Figure 57. The proton NMR spectrum for $PrMINTf_2$

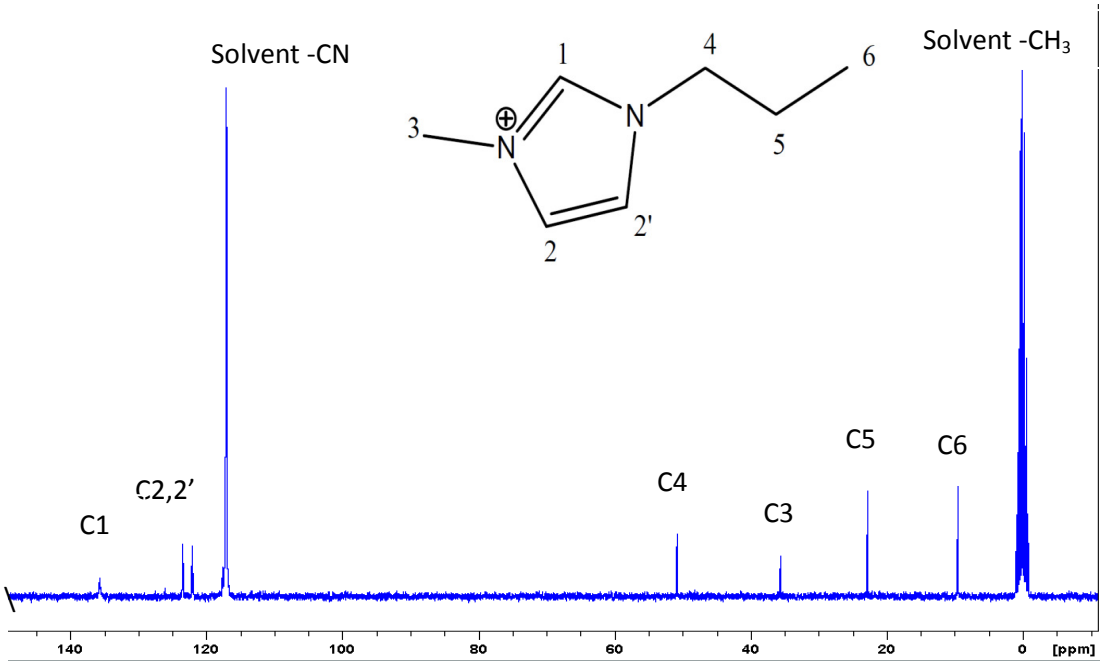

Figure 58. The carbon NMR spectrum for $PrMINTf_2$

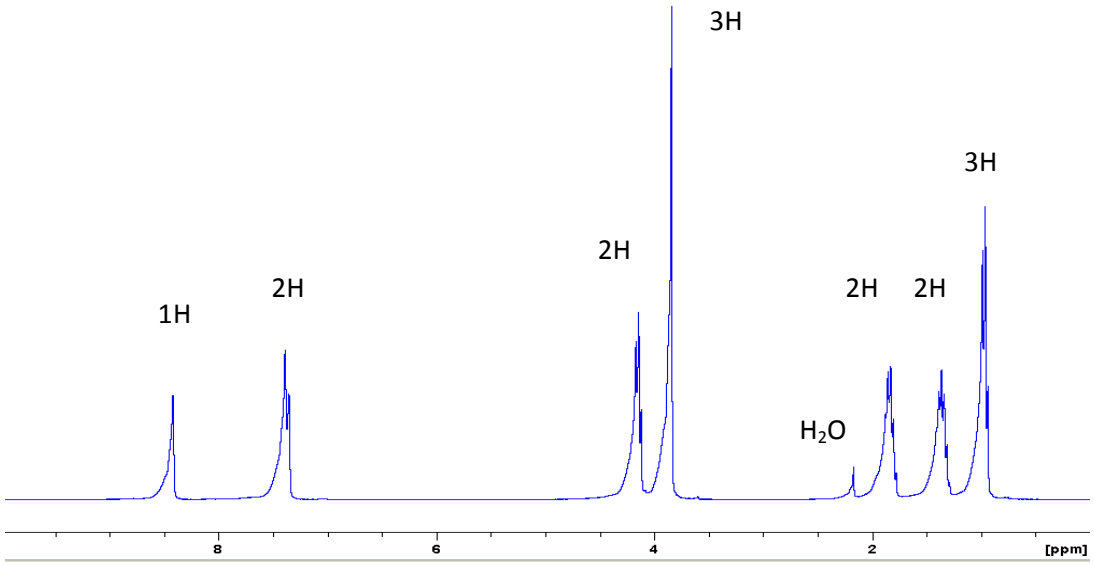

Figure 59. The proton NMR spectrum for $BMINTf_2$

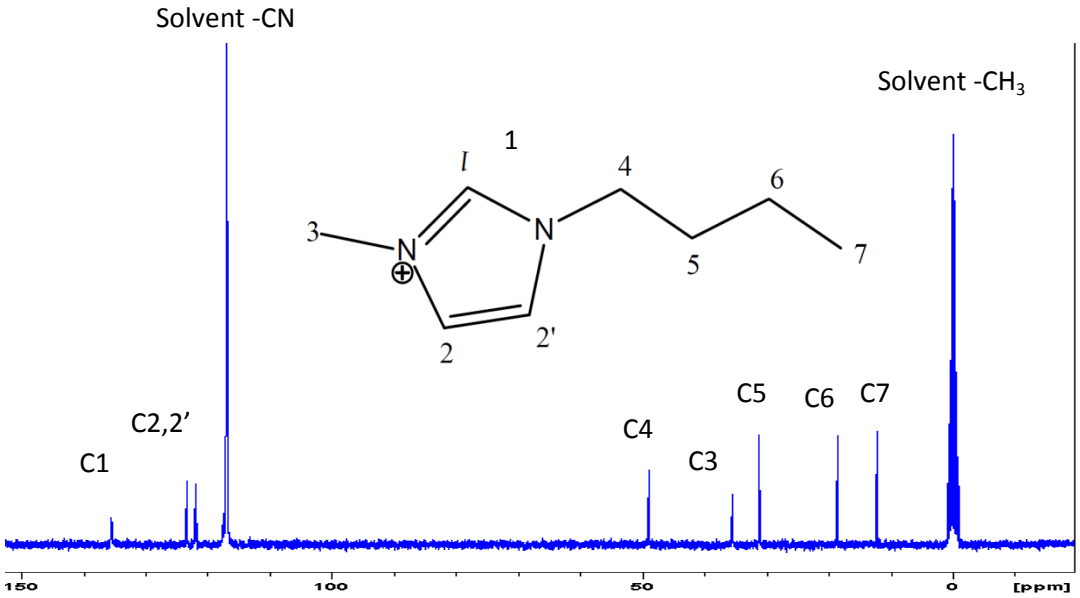

Figure 60. The carbon NMR spectrum for $BMINTf_2$

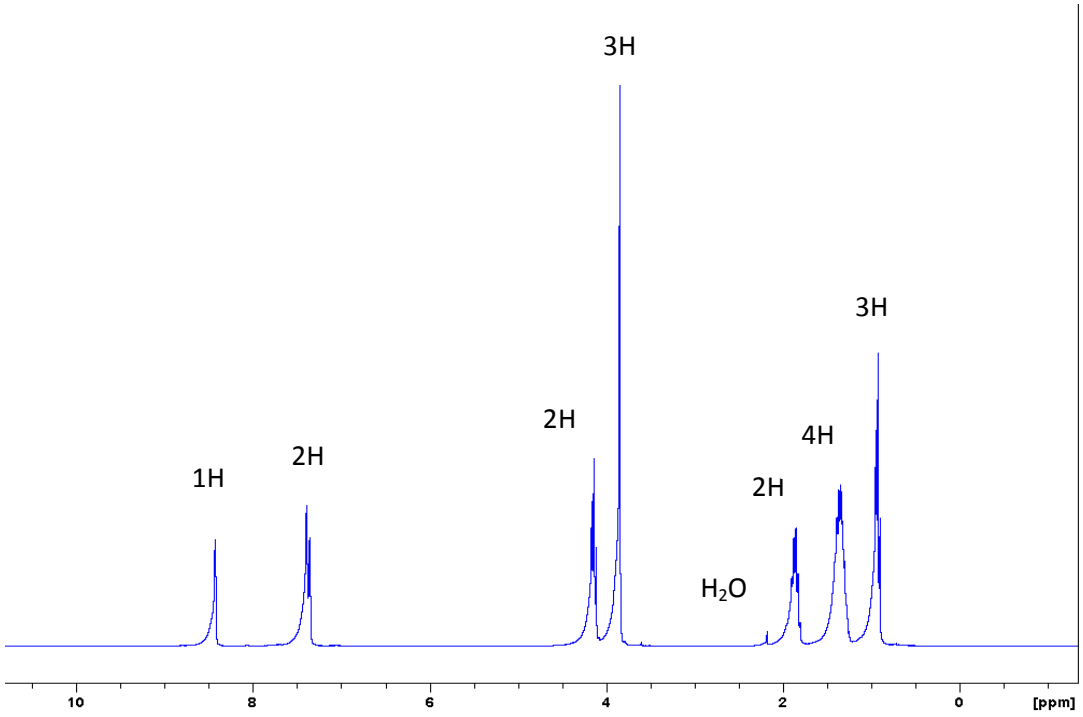

Figure 61. The proton NMR spectrum for $PnMINTf_2$

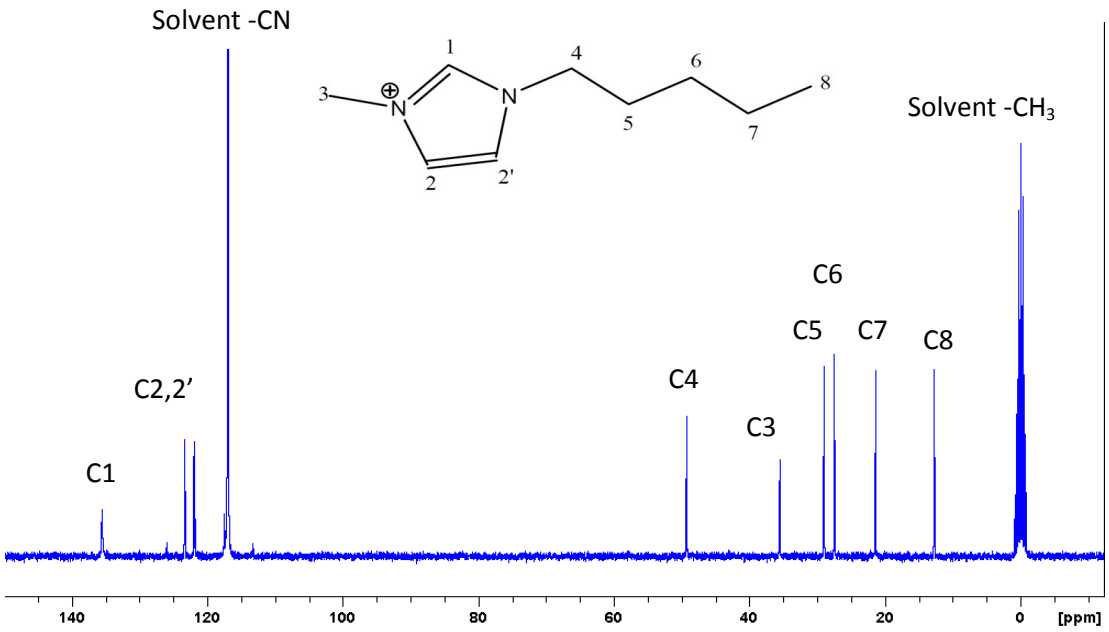

Figure 62. The carbon NMR spectrum for $PnMINTf_2$

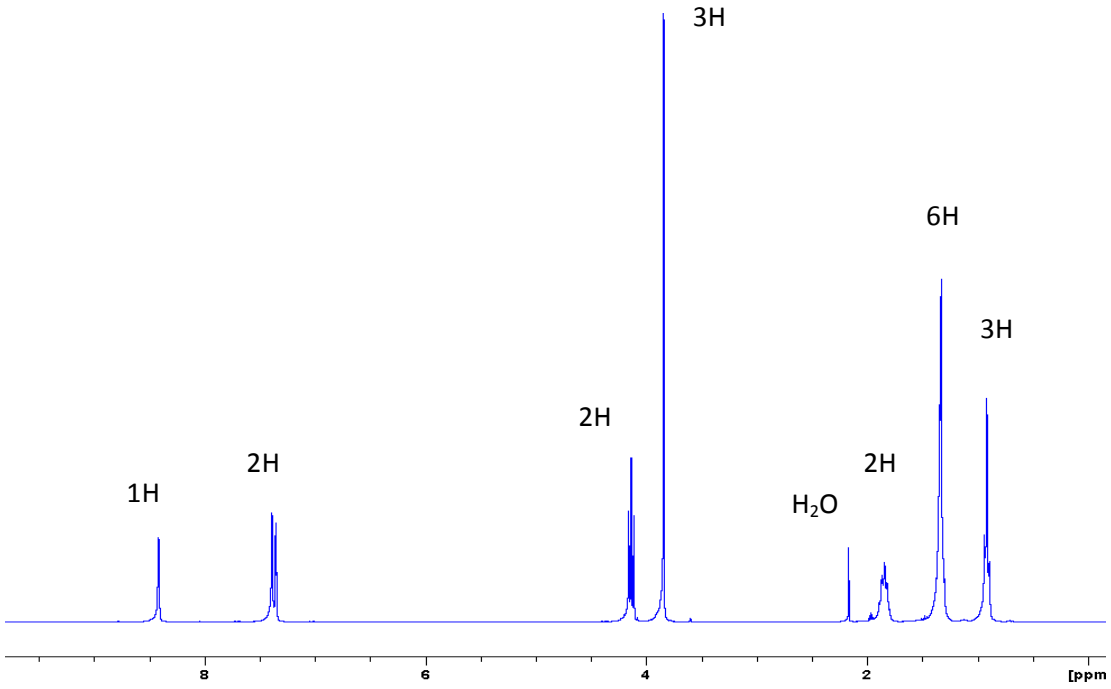

Figure 63. The proton NMR spectrum for $HMINTf_2$

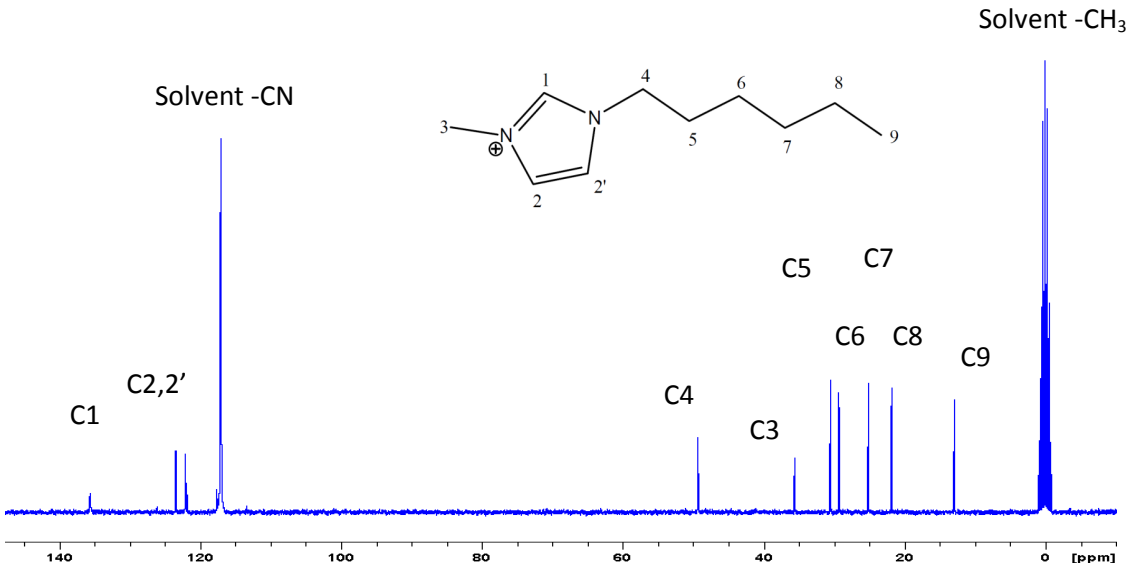

Figure 64. The carbon NMR spectrum for $HMINTf_2$

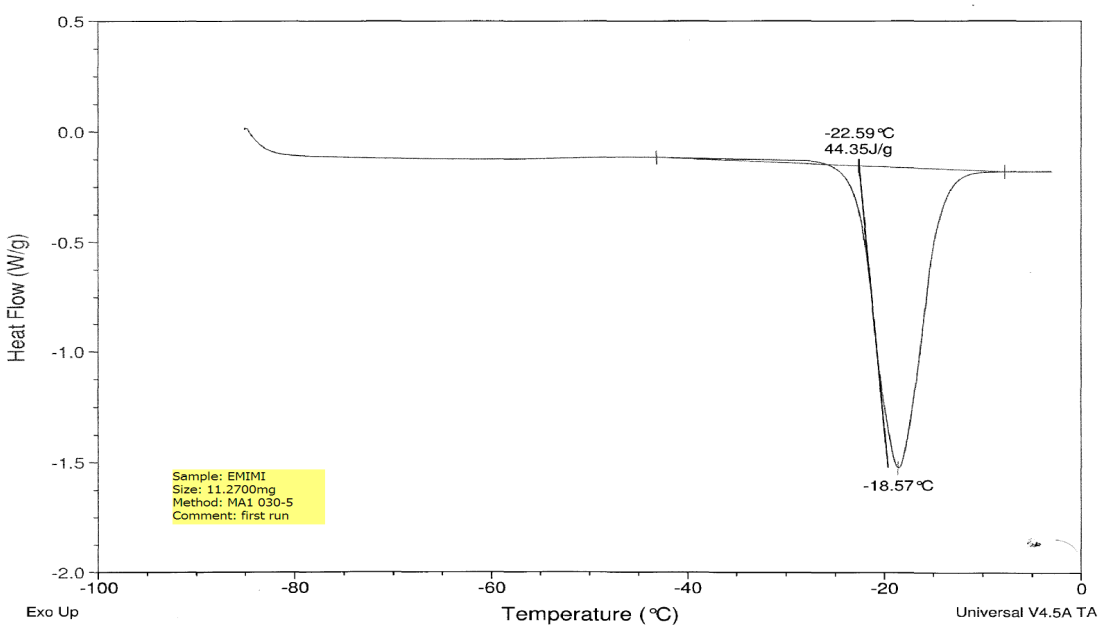

Figure 65. The DSC scan for $EMINTf_2$ ionic liquid.

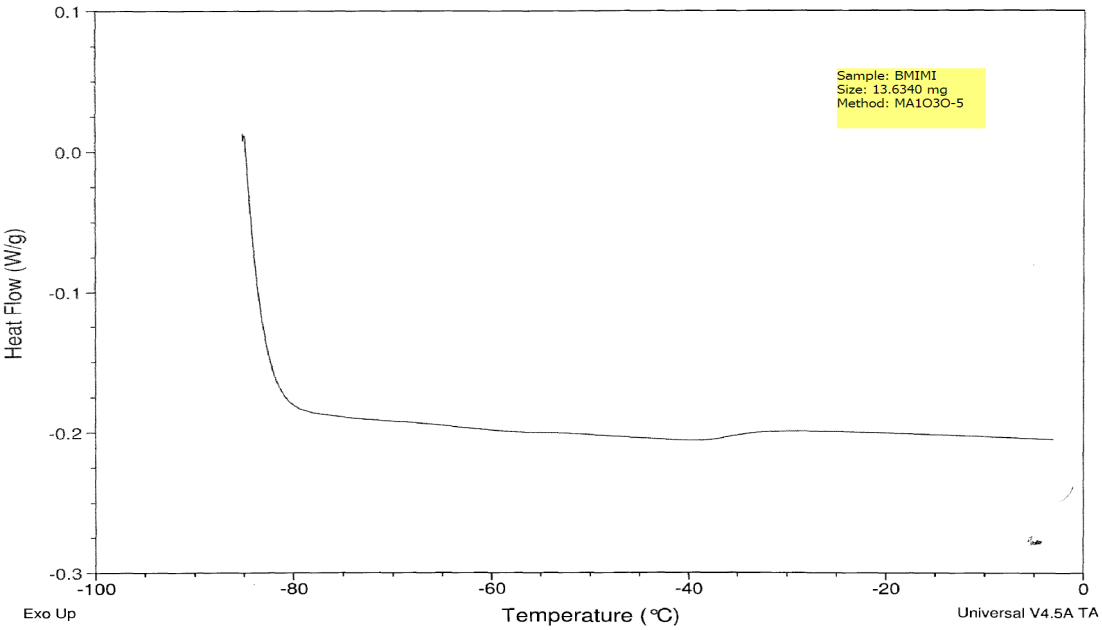

Figure 66. The DSC scan for $BMINTf_2$ ionic liquid.

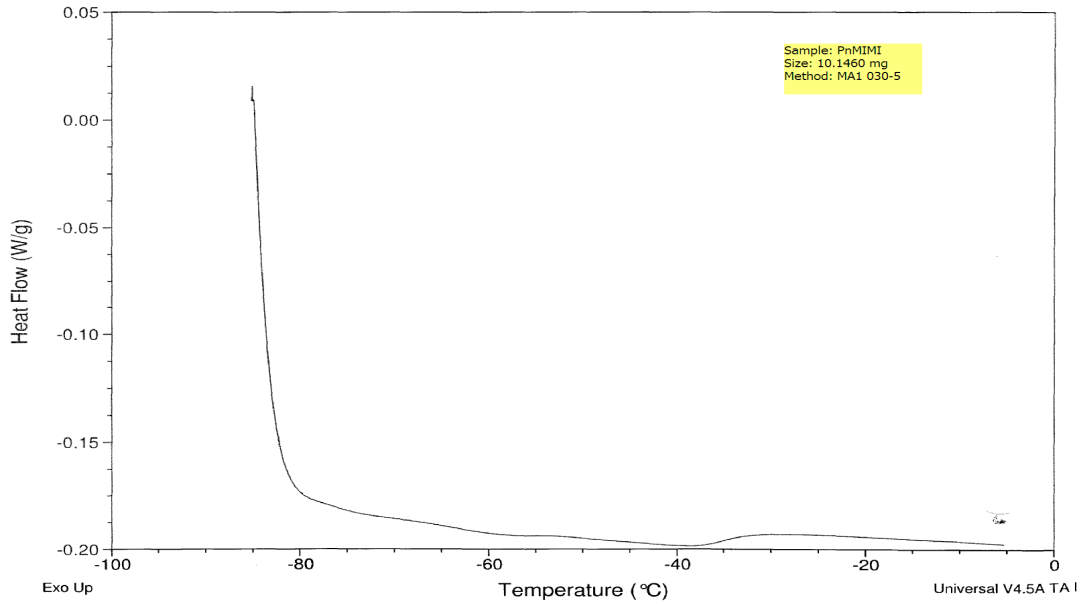

Figure 67. The DSC scan for $PnMINTf_2$ ionic liquid

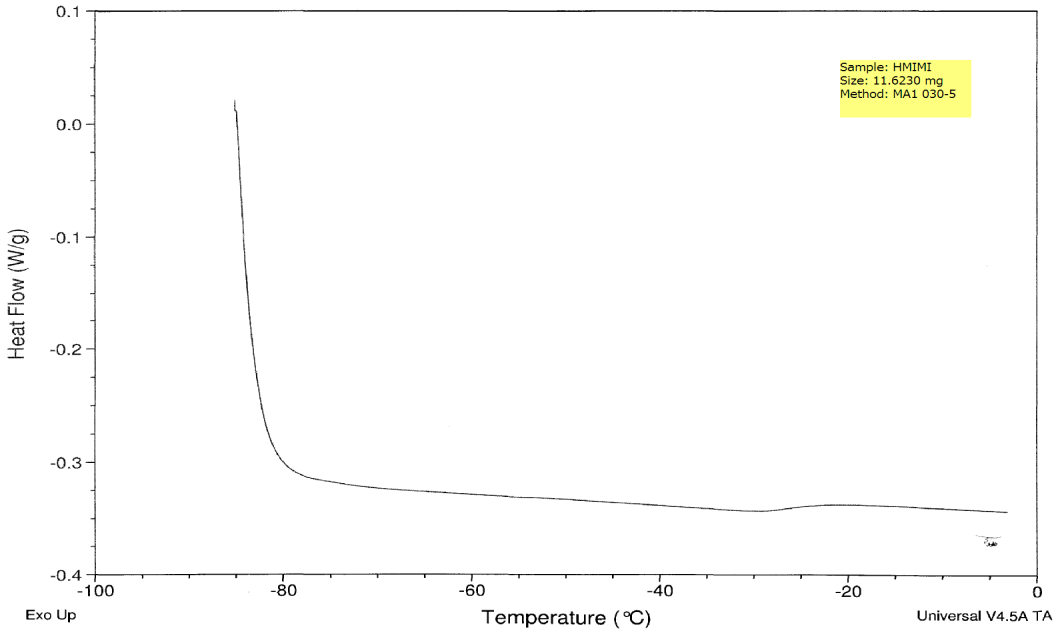

Figure 68. The DSC scan for $HMINTf_2$ ionic liquid.

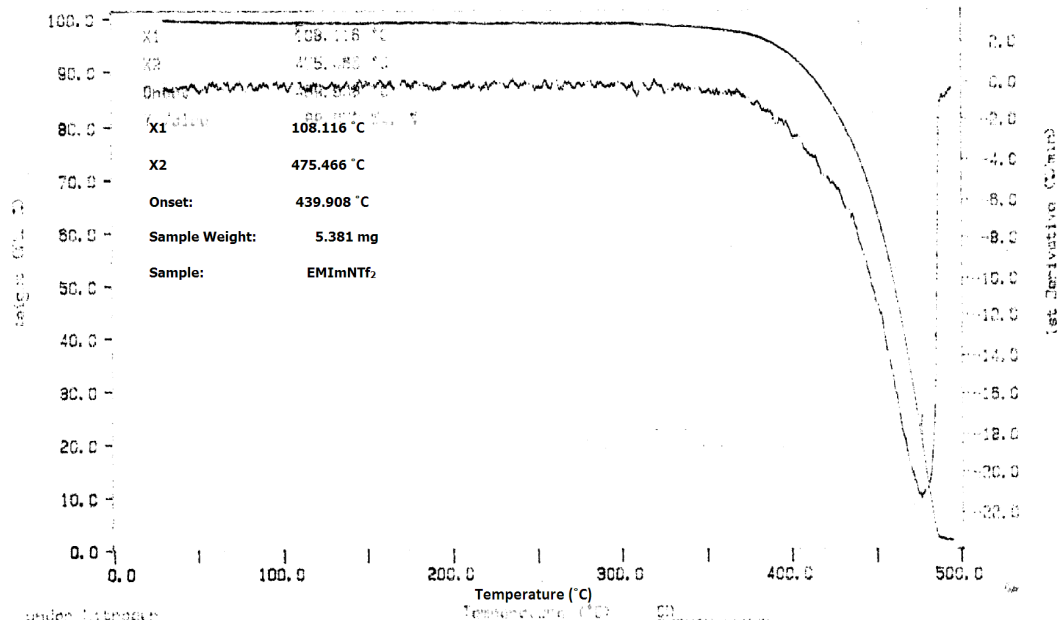

Figure 69. TGA scan 1 for $EMImNTf_2$ ionic liquid.

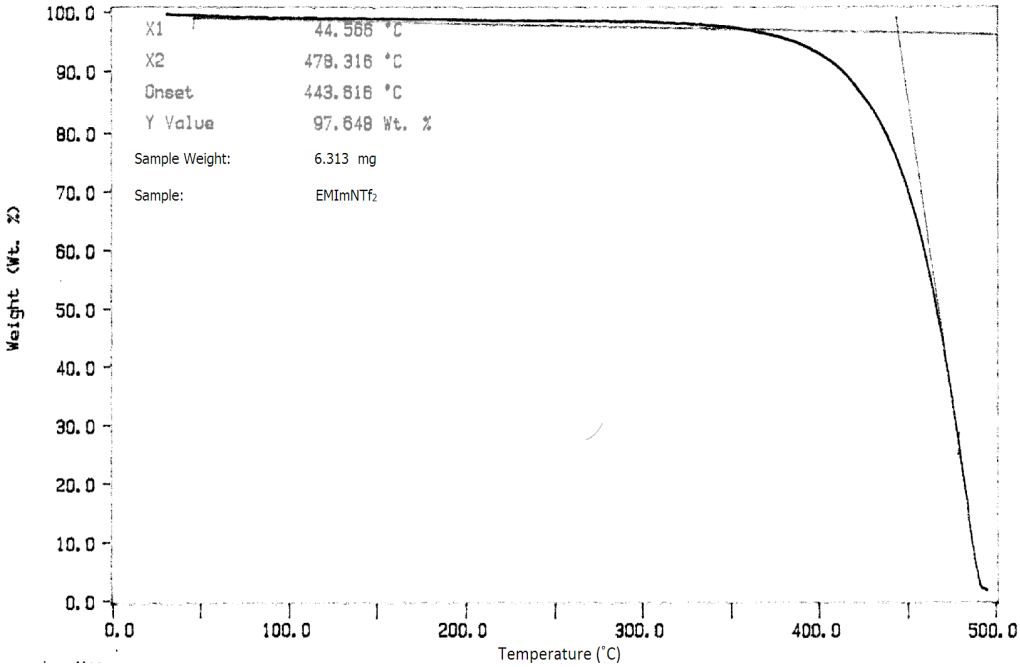

Figure 70. TGA scan 2 for $EMINTf_2$ ionic liquid.

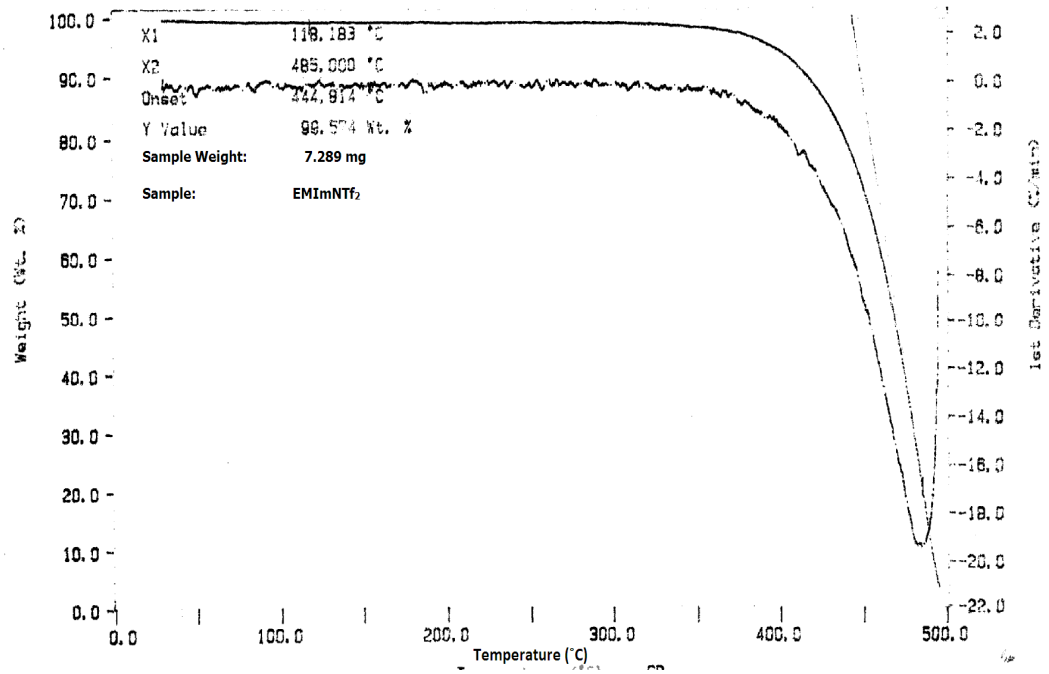

Figure 72. TGA scan 3 for $EMINTf_2$ ionic liquid.

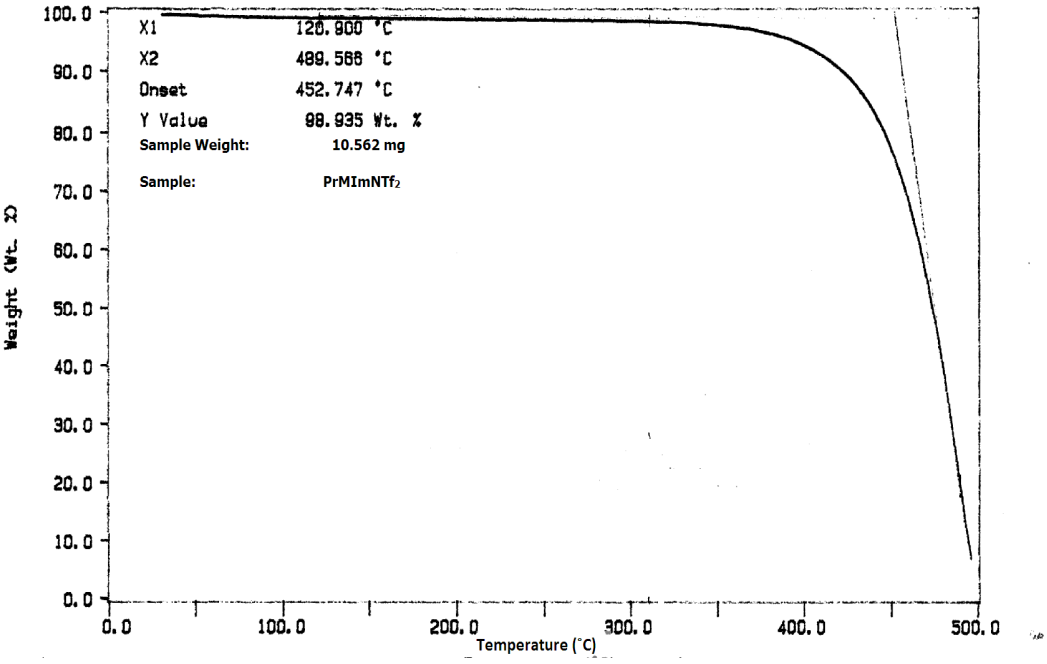

Figure 72. TGA scan 1 for $PrMINTf_2$ ionic liquid.

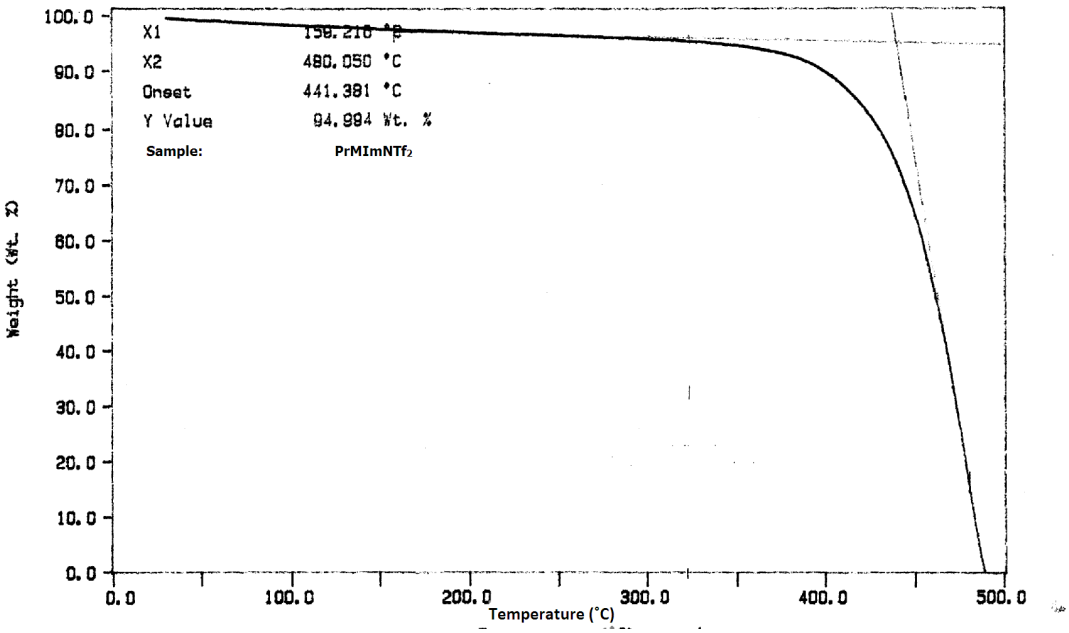

Figure 73. TGA scan 2 for $PrMINTf_2$ ionic liquid.

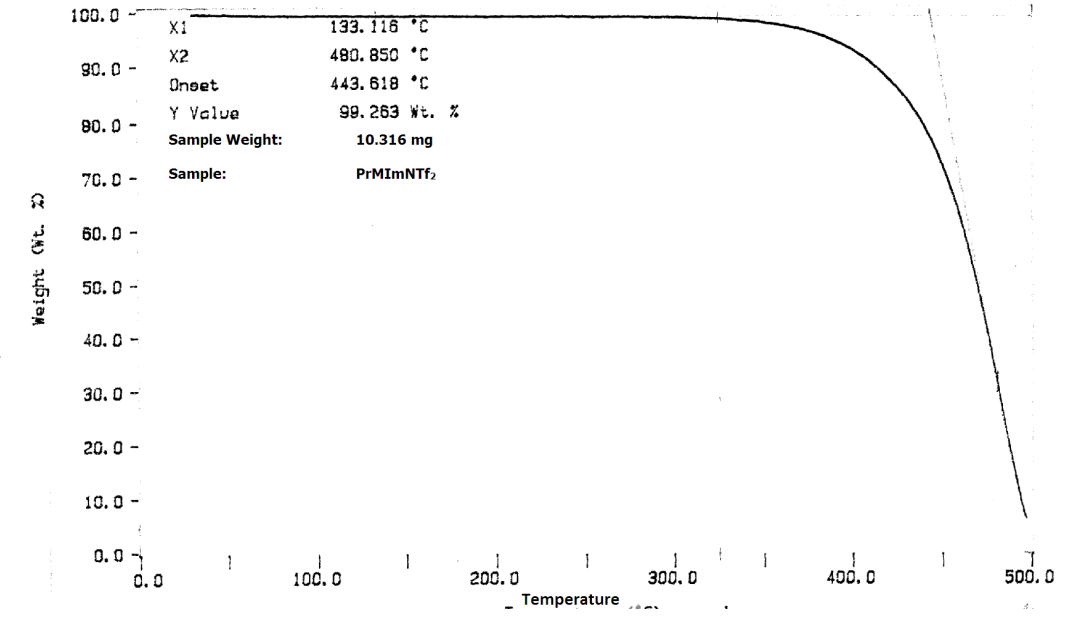

Figure 74. TGA scan 3 for $PrMINTf_2$ ionic liquid.

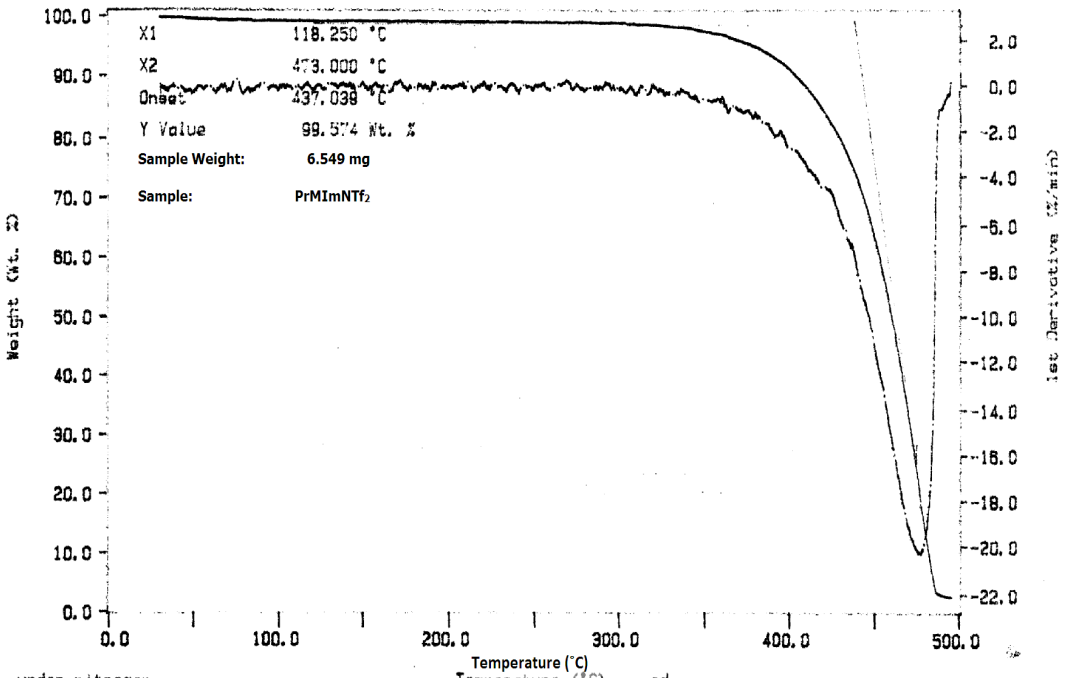

Figure 75. TGA scan 4 for $PrMINTf_2$ ionic liquid.

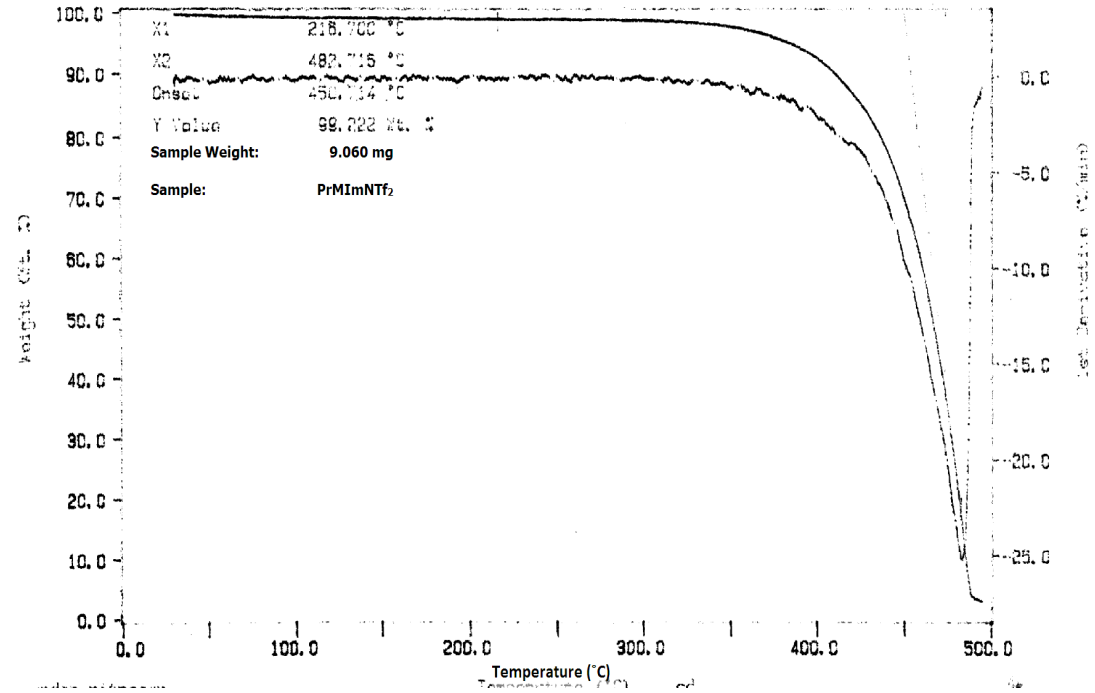

Figure 76. TGA scan 5 for $PrMINTf_2$ ionic liquid.

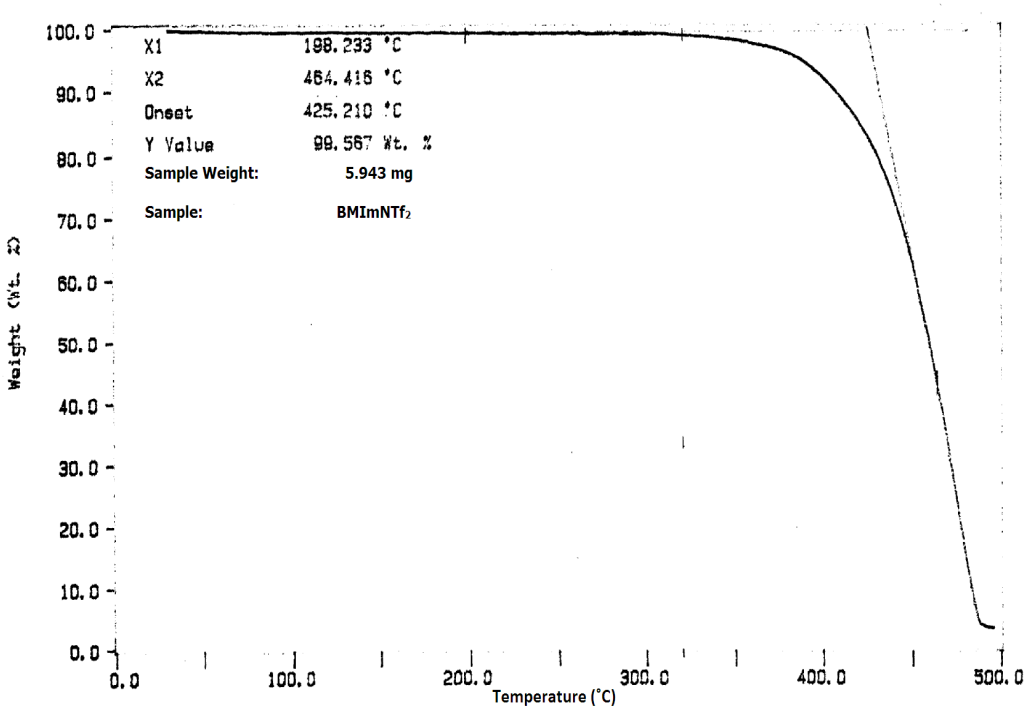

Figure 77. TGA scan 1 for $BMINTf_2$ ionic liquid.

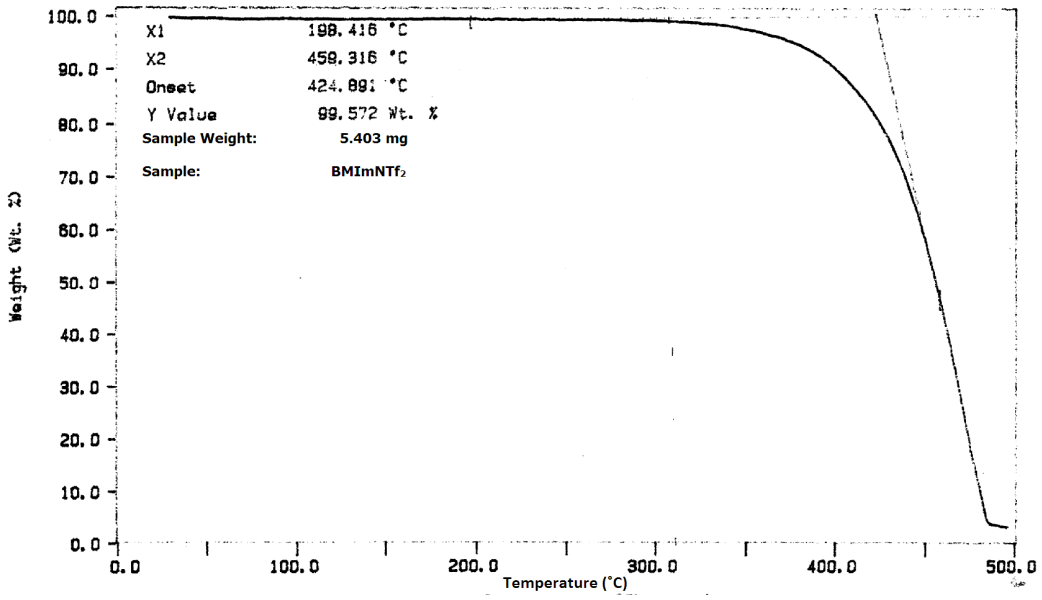

Figure 78. TGA scan 2 for $BMINTf_2$ ionic liquid.

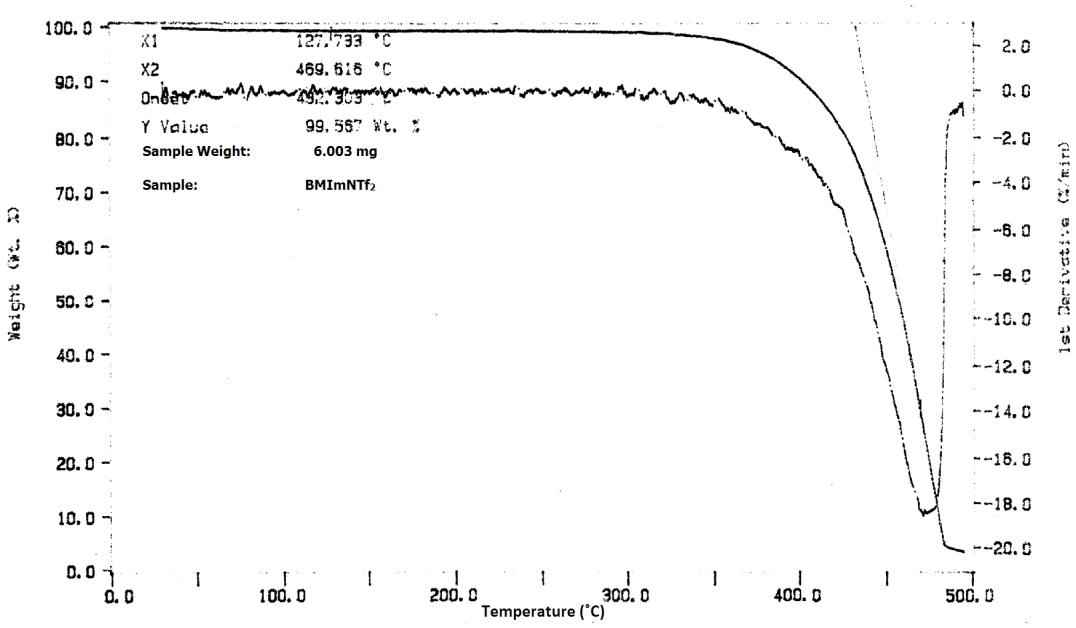

Figure 79. TGA scan 3 for $BMINTf_2$ ionic liquid.

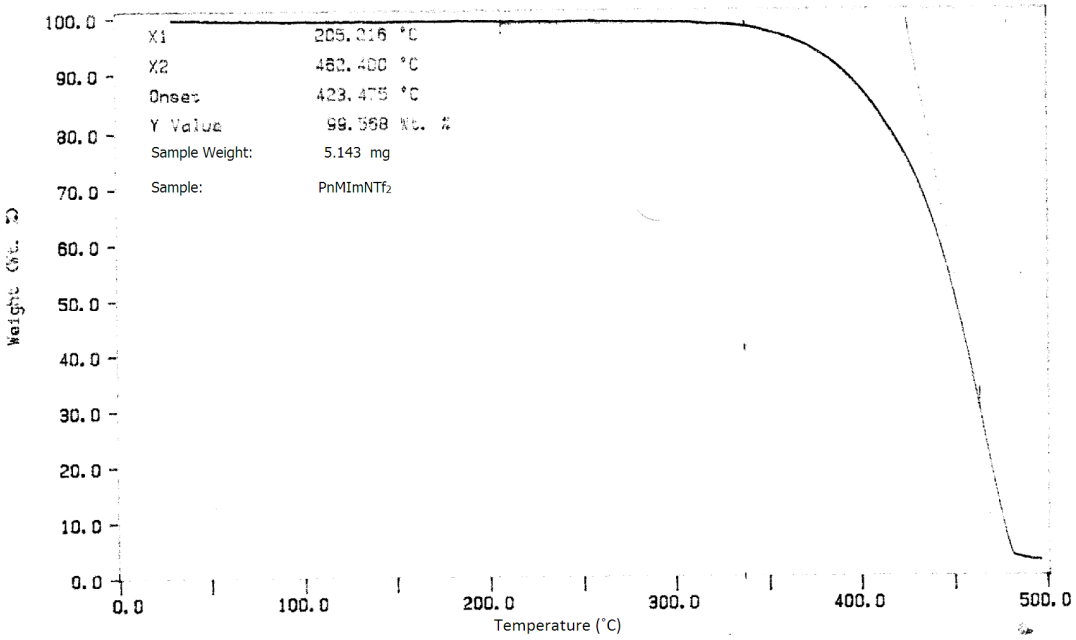

Figure 80. TGA scan 1 for $PnMINTf_2$ ionic liquid.

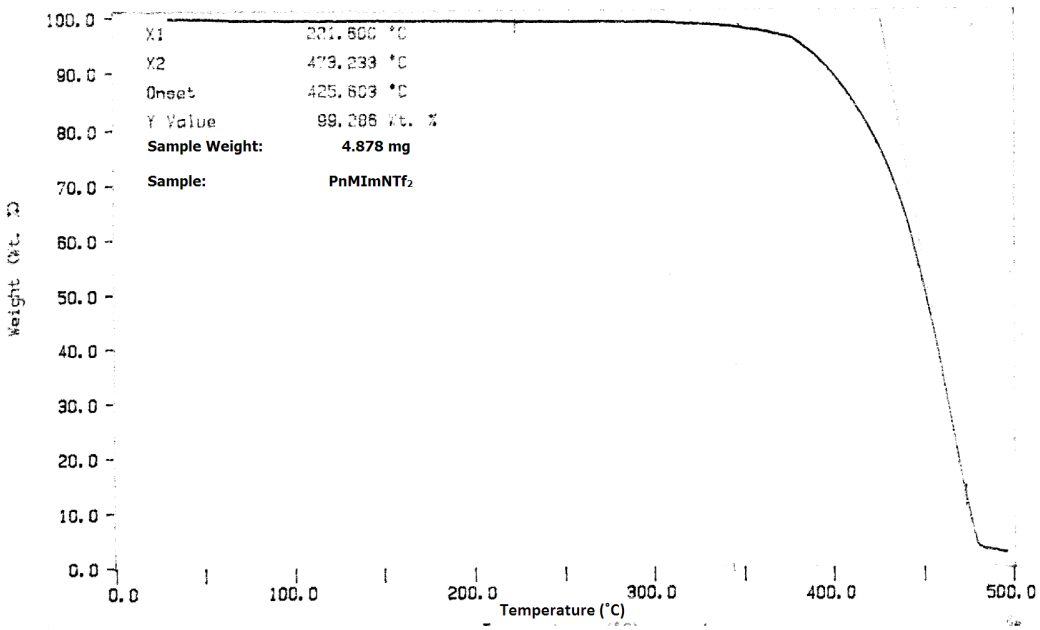

Figure 81. TGA scan 2 for $PnMINTf_2$ ionic liquid.

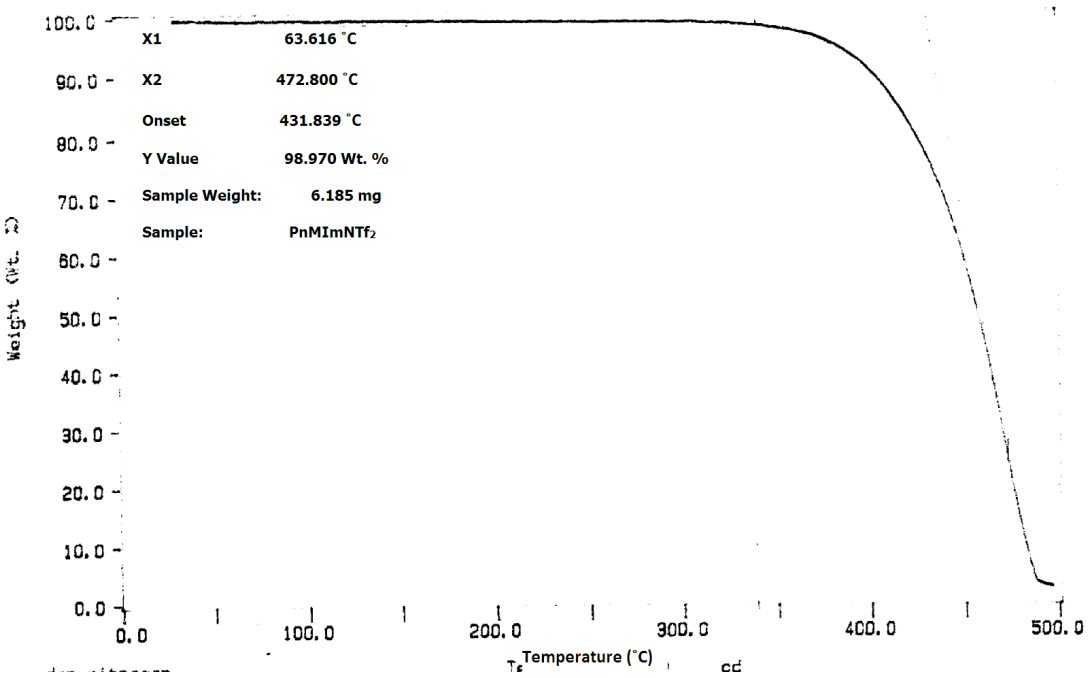

Figure 82. TGA scan 3 for $PnMINTf_2$ ionic liquid.

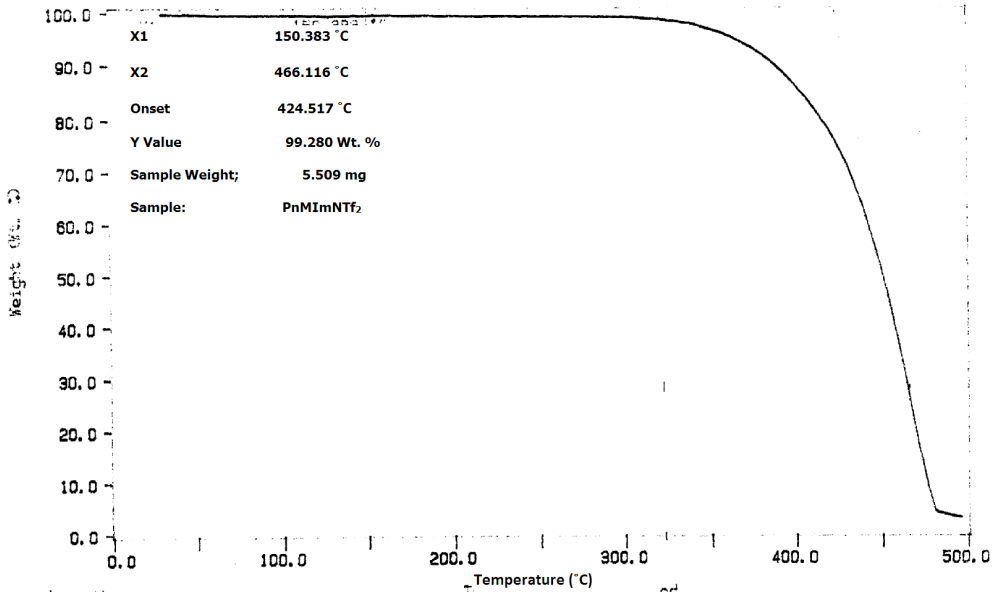

Figure 83. TGA scan 4 for $PnMINTf_2$ ionic liquid.

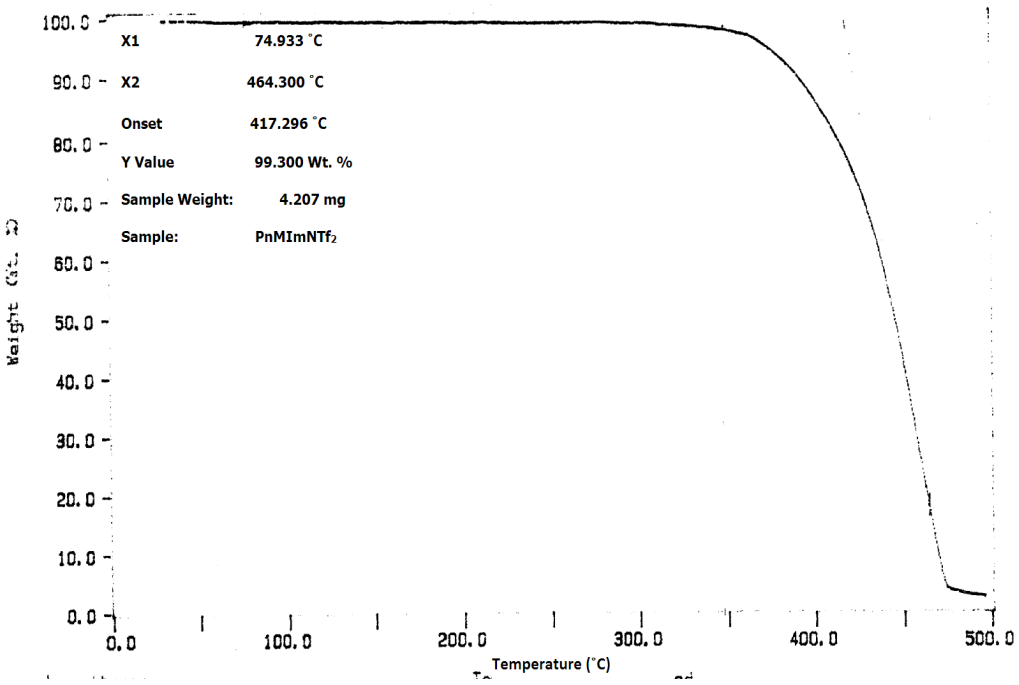

Figure 84. TGA scan 5 for $PnMINTf_2$ ionic liquid.

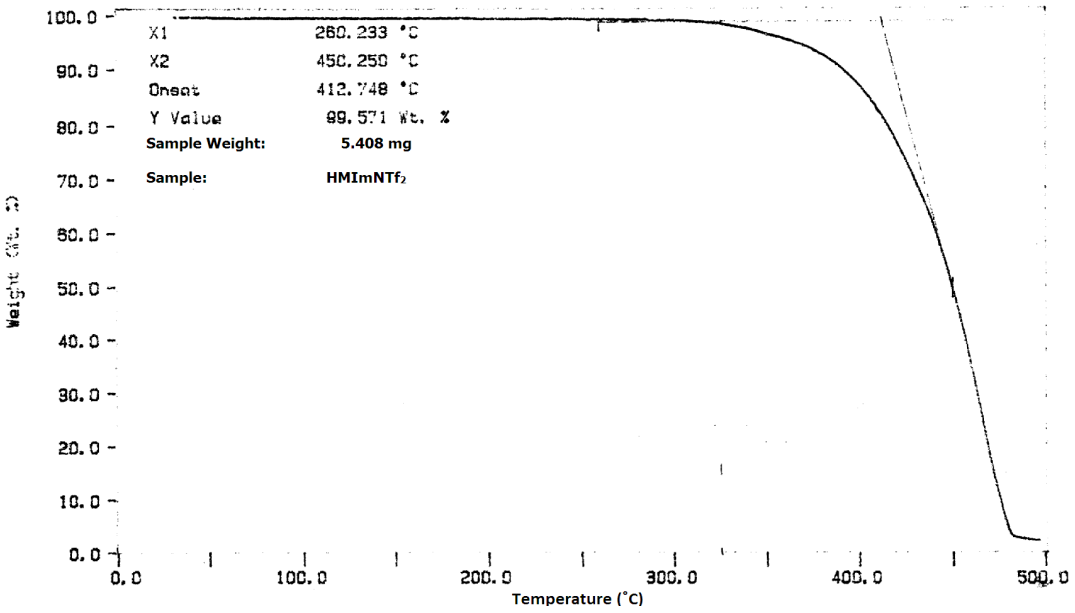

Figure 85. TGA scan 1 for $HMINTf_2$ ionic liquid.

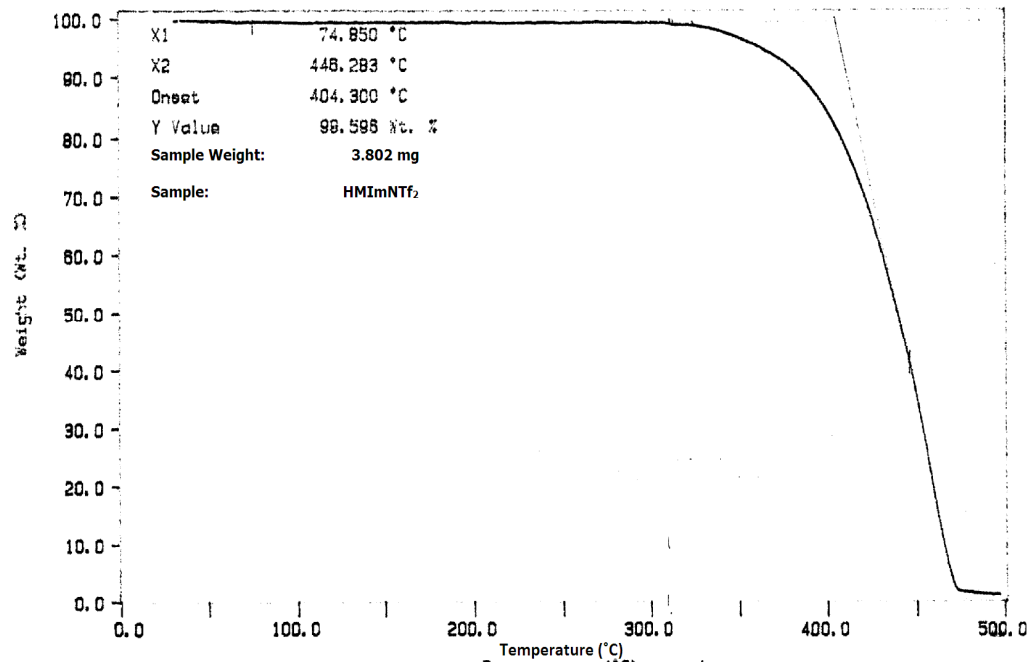

Figure 86. TGA scan 2 for $HMINTf_2$ ionic liquid.

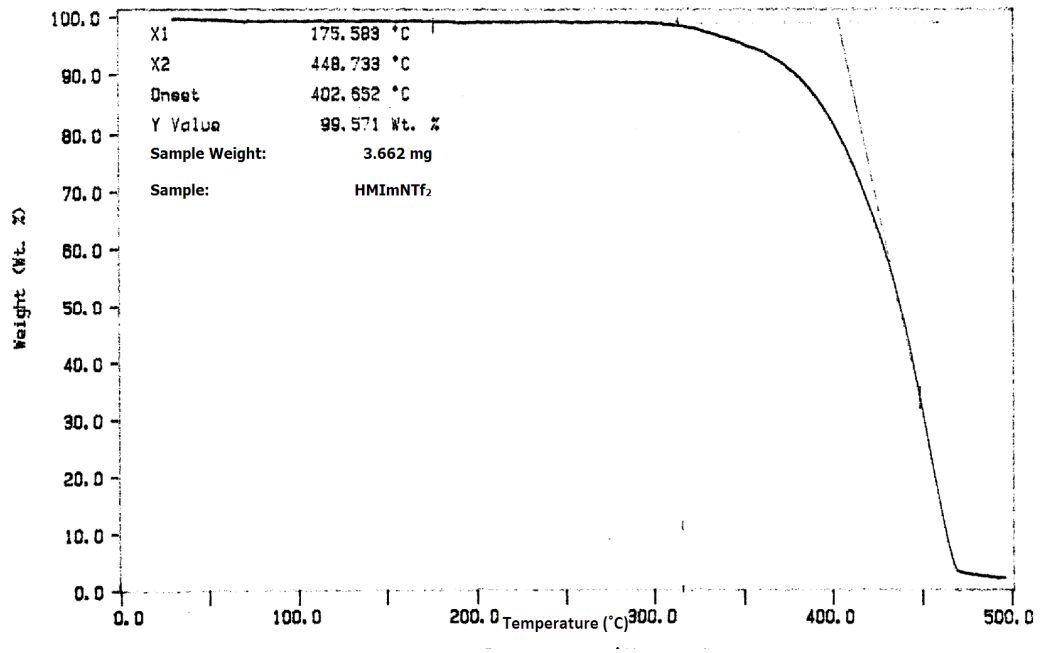

Figure 87. TGA scan 3 for $HMINTf_2$ ionic liquid.

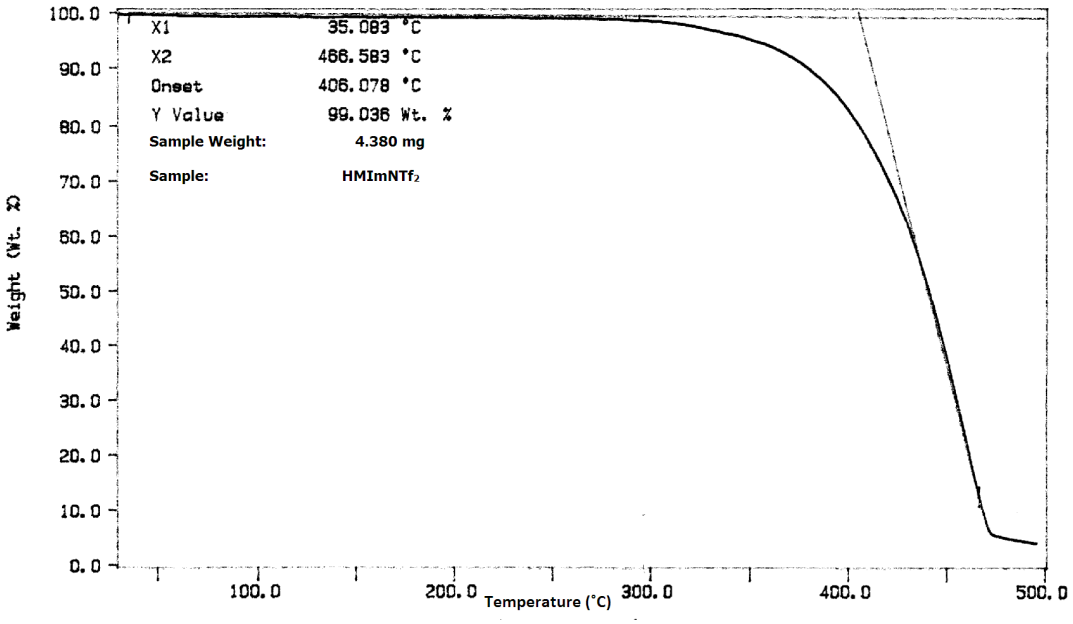

Figure 88. TGA scan 4 for $HMINTf_2$ ionic liquid.

Table 31. Conductitvity of $EMINTf_2$ at various temperatures (°C)

Temp(°C)	Measured Conductivity (mS)	Specific Conductivity (mS)		Temp(°C)	Measured Conductivity (mS)	Specific Conductivity (mS)
24.3	11.29	6.95		43.2	20.2	12.4
48.7	21.8	13.4		43.1	19.9	12.3
55.5	25.5	15.7		35.1	15.55	9.58
34.9	15.45	9.52		43	19.9	12.3
32.4	14.47	8.91		42.9	19.9	12.3
32.4	14.45	8.90		22	10.89	6.71
32.4	14.43	8.89		77.8	38.3	23.6
30	13.45	8.29		78.25	38.5	23.7
30	13.43	8.27		115.6	61.5	37.9
29.7	13.33	8.21		126.7	68.4	42.1
27.5	12.56	7.74		126.3	68.1	41.9
26.7	12.24	7.54		139.9	75.4	46.4
26.7	12.22	7.53		147.9	80.3	49.5
24.2	11.38	7.01		111.5	58.8	36.2
23.8	11.26	6.94		112.6	59.4	36.6
22.5	10.74	6.62		103.4	54.4	33.5
79.1	40.45	24.9		87.7	45.2	27.8
78.8	40.7	25.1		92.85	48.3	29.8
77.6	39.3	24.2		99	52.3	32.2
76.4	39.4	24.3		115.7	61.5	37.9

Table 31. Conductitvity of $EMINTf_2$ at various temperatures (°C) (continued)

Temp(^oC)	Measured Conductivity (mS)	Specific Conductivity (mS)		Temp(^oC)	Measured Conductivity (mS)	Specific Conductivity (mS)
69.4	34.8	21.4		115.8	61.5	37.9
69.15	34.7	21.4		115.9	61.5	37.9
72.9	36.7	22.6		139.7	75.4	46.4
74.55	37.6	23.2		111.4	58.8	36.2
75.4	35.5	21.9		111.2	58.8	36.2
58.4	27.1	16.7		111.3	58.8	36.2
58.1	26.9	16.6				

Table 32. Conductivity of $PrMINTf_2$ at various temperatures (^oC)

Temp(^oC)	Measured Conductivity (mS)	Specific Conductivity (mS)	Temp(^oC)	Measured Conductivity (mS)	Specific Conductivity (mS)
20.9	6.19	3.81	146	66.3	40.8
63.8	19.93	12.3	131.6	58.7	36.2
73	26.2	16.1	126.5	56	34.5
74.7	26.9	16.6	117	50.9	31.3
75.7	27.3	16.8	114	49.4	30.4
85.4	31.8	19.6	107	45.5	28.0
98.3	38.7	23.8	90.6	36.3	22.4
104.2	42	25.9	27.8	8.44	5.20
109.9	44.9	27.7	74	27.3	16.8
100.5	40.3	24.8	28	8.55	5.27
22.2	6.61	4.07	22	6.77	4.17
75.4	27	16.6	36.3	11.32	6.97
101.5	41.3	25.4	31.5	9.7	5.98
111.7	46.5	28.6	27.9	8.54	5.26
22.4	6.7	4.13	69.6	25.4	15.6
129.1	55.5	34.2	45.6	14.56	8.97
151.55	69	42.5	42.3	13.37	8.24
32.1	9.88	6.09			

Table 33. Conductitvity of $BMINTf_2$ at various temperatures (^oC)

Temp(^oC)	Measured Conductivity (mS)	Specific Conductivity (mS)		Temp(^oC)	Measured Conductivity (mS)	Specific Conductivity (mS)
22.2	5.02	3.09		91.5	29.7	18.3
57.8	14.15	8.72		23.1	5.3	3.26
58.3	14.23	8.77		58.1	14.41	8.88
69.3	18.24	11.2		71.8	19.5	12.0
71.6	19.08	11.8		22.1	5.06	3.12
70.6	18.75	11.6		88.6	28.5	17.6
83.3	25.7	15.8		39.6	9.4	5.79
88	27.8	17.1		38	8.96	5.52
90.2	28.8	17.7		30.9	7.06	4.35
102.7	35.1	21.6		22.5	5.15	3.17
106.8	36.5	22.5		22.4	5.12	3.15
110.7	38.8	23.9		71.1	19.25	11.9
125	46.2	28.5		26.1	5.46	3.36
142.4	54.9	33.8		38.2	8.44	5.20
21.4	4.91	3.02		42.1	9.56	5.89
84.3	26.3	16.2		42.3	10.1	6.22
37.5	8.81	5.43		36	8.4	5.17

Table 34. Conductitvity of $PnMINTf_2$ at various temperatures (^oC)

Temp(^oC)	Measured Conductivity (mS)	Specific Conductivity (mS)		Temp(^oC)	Measured Conductivity (mS)	Specific Conductivity (mS)
22.5	3.62	2.23		162	55.3	34.1
37.7	6.09	3.75		59.3	12.32	7.59
54.6	10.82	6.67		53	10.55	6.50
57.3	11.62	7.16		47.3	8.97	5.53
22.7	3.68	2.27		39.7	7.19	4.43
40.6	6.66	4.10		36.1	6.36	3.92
43.7	7.54	4.64		34	5.91	3.64
71.6	15	9.24		22.4	3.63	2.24
81.3	17.93	11.0		23.3	3.75	2.31
89.1	19.55	12.0		27.8	4.18	2.57
97.4	24.2	14.9		32	5.15	3.17
93.3	25.8	15.9		34.5	5.8	3.57
118.3	36.3	22.4		50.3	9.46	5.83
128.3	40.9	25.2		31.8	5.56	3.42
145.1	48	29.6		28.1	4.83	2.98
149.4	50.1	30.9				

Table 35. Conductitvity of $HMINTf_2$ at various temperatures (^oC)

Temp(^oC)	Measured Conductivity (mS)	Specific Conductivity (mS)		Temp(^oC)	Measured Conductivity (mS)	Specific Conductivity (mS)
22.7	2.83	1.74		60	9.3	5.73
26.3	3.24	2.00		61.8	9.5	5.85
27.7	3.31	2.04		64.5	10.16	6.26
29.1	3.44	2.12		81.4	14.86	9.15
33	3.89	2.40		83.2	15.38	9.47
33.7	4.05	2.49		84.1	15.66	9.65
34.3	4.16	2.56		97.4	19.82	12.2
35	4.27	2.63		109.1	26.3	16.2
38	4.68	2.88		22.6	2.9	1.79
40	4.96	3.06		60.8	9.07	5.59
43.4	5.45	3.36		87.3	16.66	10.3
45.7	5.93	3.65		89	17.68	10.9
49.3	6.42	3.95		91.4	18.58	11.4
49.5	6.55	4.03		96.2	21.8	13.4
49.9	6.66	4.10		101.9	23.9	14.7
50.8	6.89	4.24		106.4	25.7	15.8
53.1	7.13	4.39		113.6	28.7	17.7
53.3	7.18	4.42		133.9	37.3	23.0
54.5	7.5	4.62		135.7	37.7	23.2
56.5	7.96	4.90		145.4	42.5	26.2

Table 35. Conductitvity of $HMINTf_2$ at various temperatures (^oC) (continued)

Temp(^oC)	Measured Conductivity (mS)	Specific Conductivity (mS)		Temp(^oC)	Measured Conductivity (mS)	Specific Conductivity (mS)
58.4	8.52	5.25		156.6	47.5	29.3
58.8	8.65	5.33		150.2	44.2	27.2
22.6	2.89	1.78		122.6	32.6	20.1
29.9	3.67	2.26		117	30.2	18.6
89.4	18.22	11.2				

Table 36. Conductitvity of $EMIBF_4$ at various temperatures (^oC)

Temp(^oC)	Measured Conductivity (mS)	Specific Conductivity (mS)		Temp(^oC)	Measured Conductivity (mS)	Specific Conductivity (mS)
23.3	17.36	10.7		124.7	101.5	62.5
24	17.46	10.8		158.1	128.7	79.3
29.4	17.84	11.0		150.2	123	75.8
37.6	29.2	18.0		119.4	99	61.0
74.7	61.6	38.0		96.2	79.5	49.0
84.8	70.5	43.4		93.7	78.5	48.4
85.1	70.6	43.5		22.3	16.72	10.3
115.5	95.7	59.0				

Table 37. Water Absorption of $EMINTf_2$ at 60% RH

Time (Minutes)	Water Absorption (ppm)
0	211
1294	1090
2484	1900
4091	4480
6735	5770
10954	7140
15168	8440
23842	9290

Table 38. Water absorption of $PrMINTf_2$ at 60% RH

Time (Minutes)	Water Absorption (ppm)
0	244
937	2550
2101	3710
3109	5350
8706	6480
17473	8640
20218	8310
37218	8610

Table 39. Water absorption of PnMINTf$_2$ at 60% RH

Time (Minutes)	Water Absorption (ppm)
0	113
262	319
1432	1380
2936	2270
4436	2890
8777	3310
20226	4640
32683	6730
35507	6590
51424	6830

Table 40. Water absorption of $HMINTf_2$ at 60% RH

Time (Minutes)	Water Absorption (ppm)
0	76
200	382
510	592
1569	1120
3030	1680
4288	2600
5763	2960
8530	3870
10150	4420
13177	5100
18915	5300
40013	6650
42907	6470
58753	6700

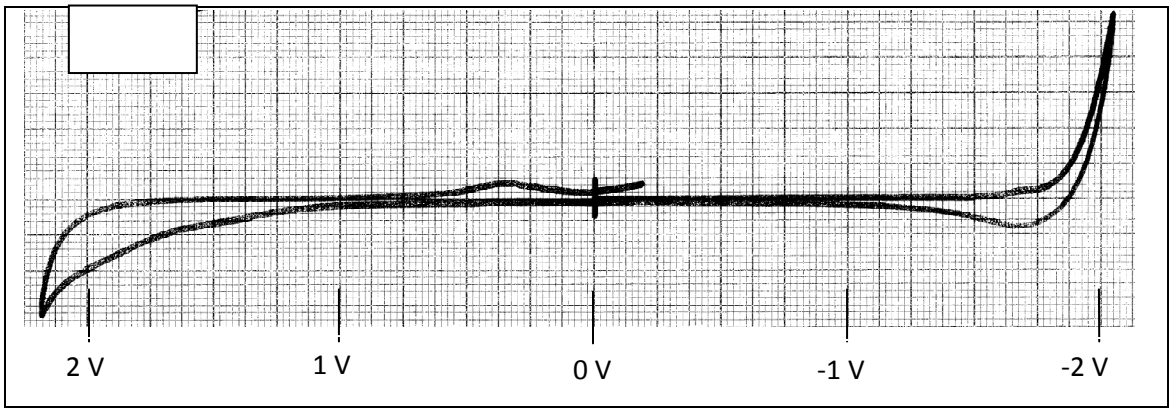

Figure 89. CV of $EMINTf_2$ ionic liquid using a platinum working electrode. (1700 ppm H_2O).

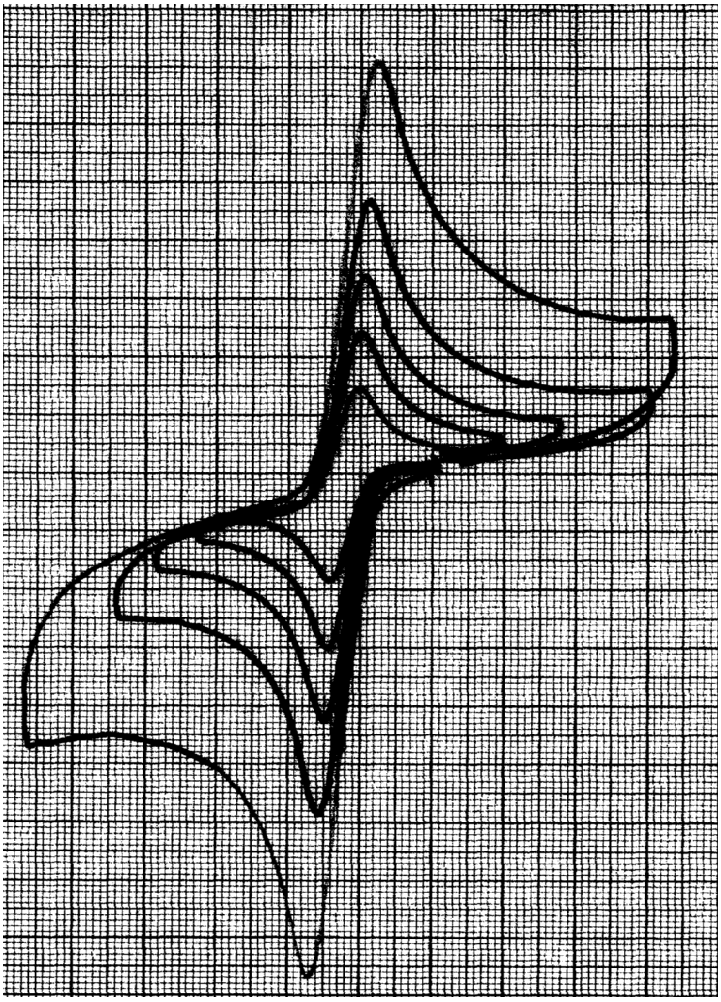

Figure 90. CVs of $PnMINTf_2$ ionic liquid using a GC working electrode. Solution contains 12.3 mg of ferrocene in 1.9712 g $PMINTf_2$. Scan rates are 20, 50, 100, 200, 500 mV/sec.

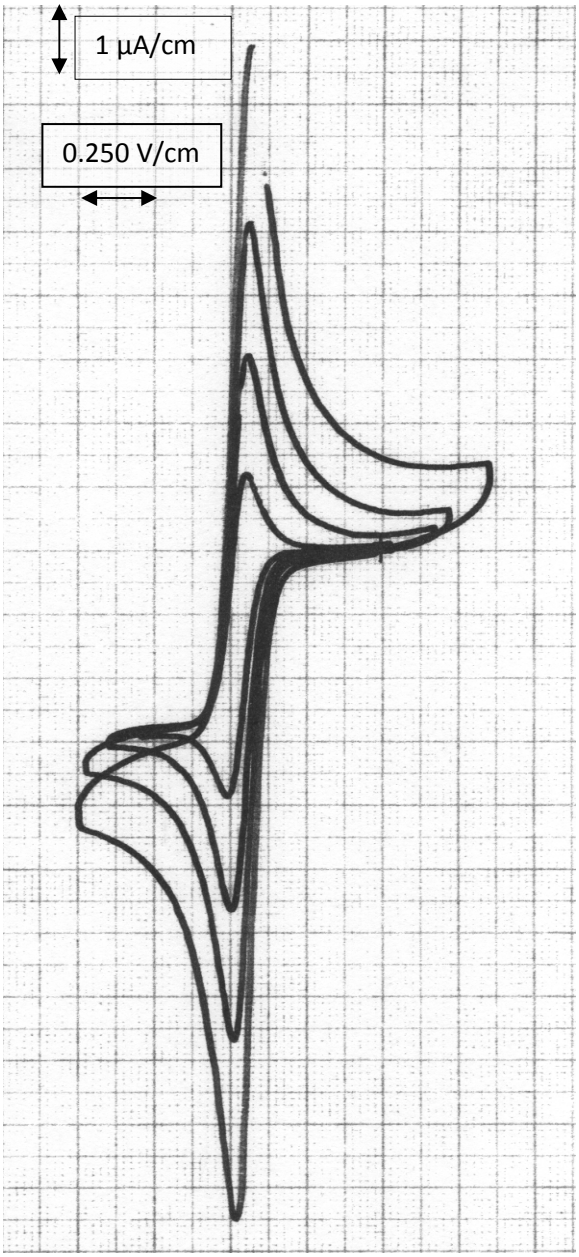

Figure 91. CVs ferrocene in acetonitrile using a platinum working electrode. Scan rates are 20, 50, 100, 200 mV/sec.

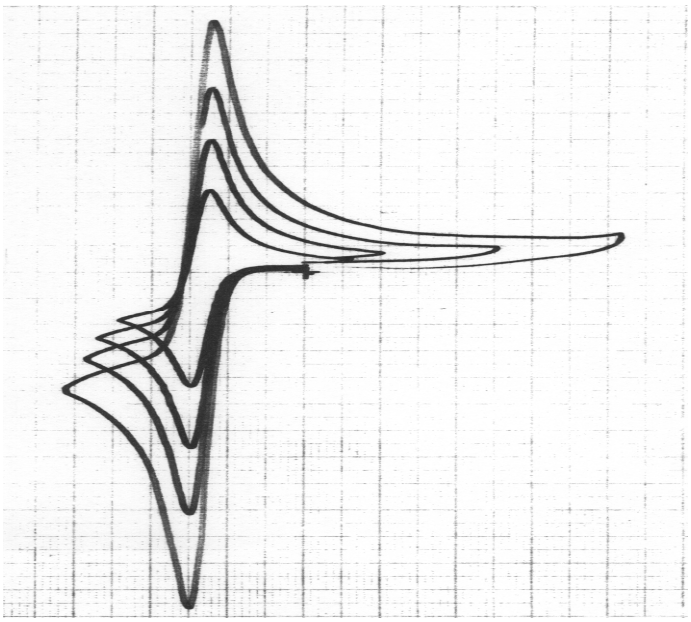

Figure 92. CVs of ferrocene in $EMINTf_2$ ionic liquid using a platinum working electrode. Solution contained 13.1 mg of ferrocene in 2.1326 grams $EMINTf_2$. Scan rates were 20, 50, 100, 200 mV/sec.

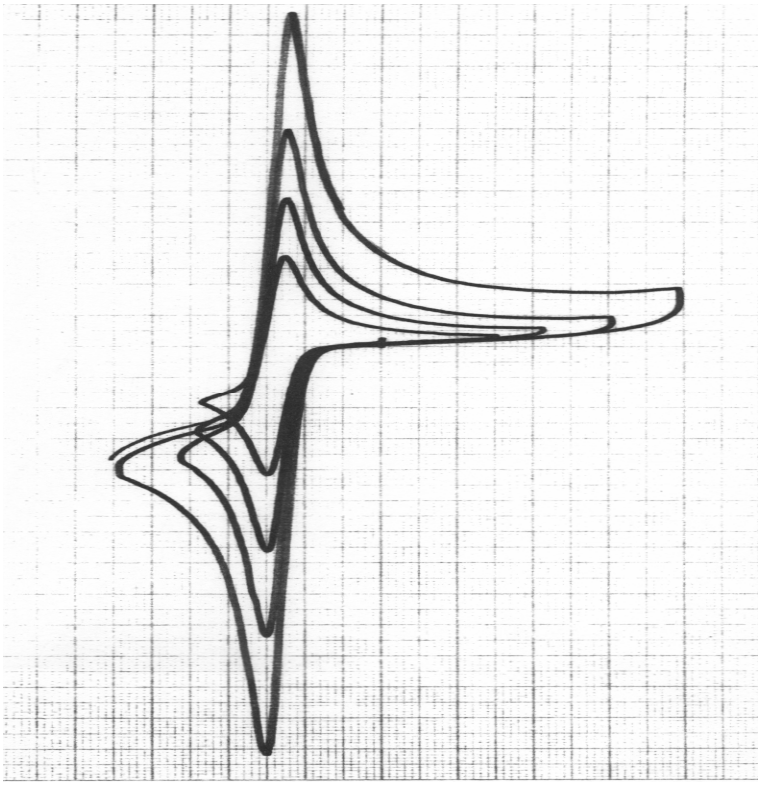

Figure 93. CVs of ferrocene in $EMINTf_2$ using a glassy carbon electrode. Solution contained 13.1 mg of ferrocene in 2.1326 grams $EMINTf_2$. Scan rates were 20, 50, 100, 200 mV/sec.

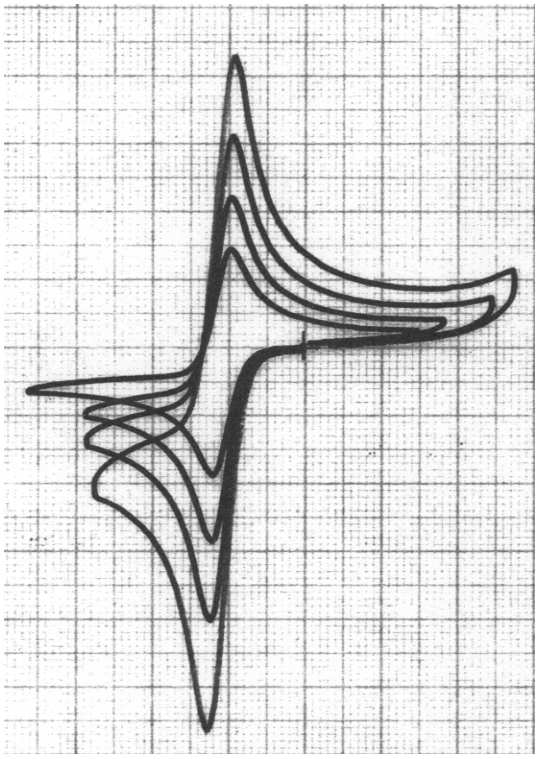

Figure 94. CVs of ferrocene in $BMINTf_2$ using a GC working electrode. Solution contained 11.2 mg of ferrocene in 3.0035 grams of $BMINTf_2$. Scan rates were 20, 50, 100 and 200 mv/sec.

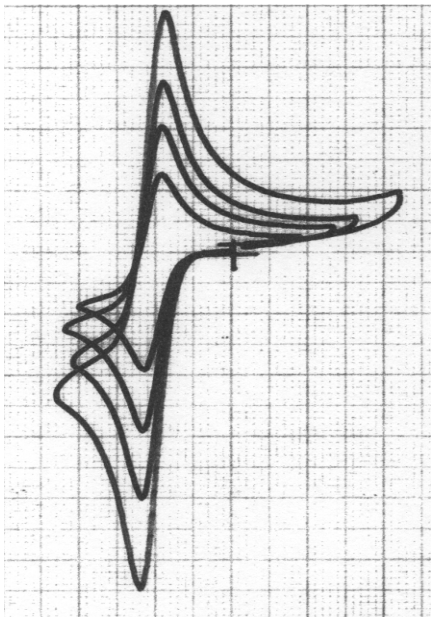

Figure 95. CVs of ferrocene in $BMINTf_2$ using a platinum electrode. Solution contained 11.2 mg of ferrocene in 3.0035 grams of $BMINTf_2$. Scan rates were 20, 50, 100 and 200 mv/sec.

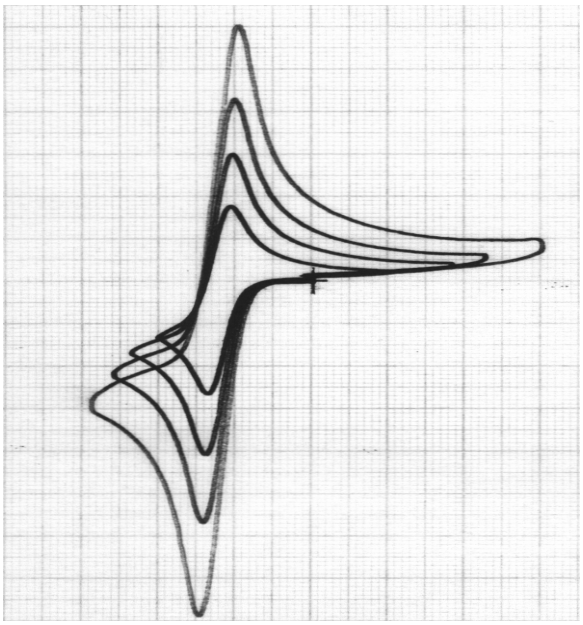

Figure 96. CVs of ferrocene in $HMINTf_2$ using a GC working electrode. Solution contained 15.4 mg of ferrocene in 2.3958 grams of $HMINTf_2$. Scan rates were 20, 50, 100 and 200 mV/sec.

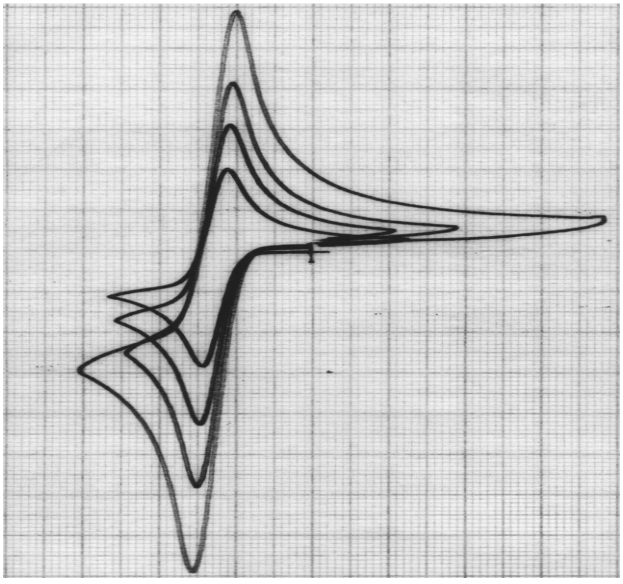

Figure 97. CVs of ferrocene in $HMINTf_2$ using a platinum working electrode. Solution contained 15.4 mg of ferrocene in 2.3958 grams of $HMINTf_2$. Scan rates were 20, 50, 100, 200 mV/sec.